Influence of surface waves on sand wave migration and asymmetry

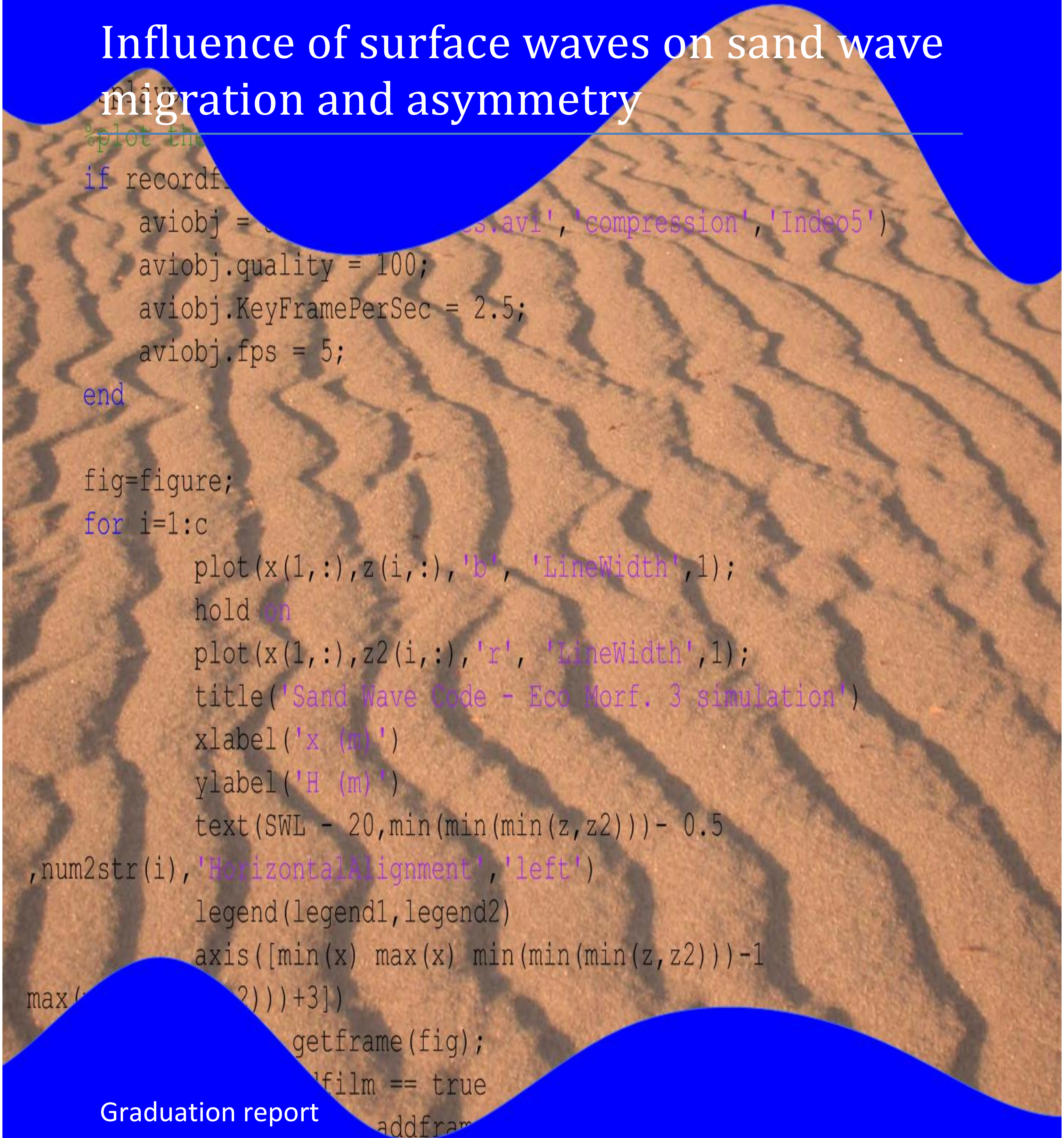

Graduation report
June 2010
Steven IJzer

Voor Lydia.

Zonder jouw aanmoediging, liefde en vertrouwen was het nooit gelukt.

Samen is echt beter!

Table of Contents

Voorwoord

Het werk dat voor u ligt is mijn afstudeerrapport. Het markeert het einde van mijn studie Civiele techniek en Management aan de vakgroep *Water Engineering and Management* van de Universiteit Twente. In deze laatste fase van mijn studie ben ik begeleid door het afstudeercomité bestaande uit:

dr ir F.M. Sterlini
dr T.A.G.P. van Dijk
prof. dr S.J.M.H. Hulscher

Bij deze zou ik Fenneke, Thaiënne en Suzanne graag willen danken voor hun begeleiding, ondersteuning, geduld, enthousiasme en kritische houding.

Verder wil ik Ad Stolk, werkzaam bij de Rijkswaterstaat, Directie Noordzee bedanken voor het meenemen van enorme bundels literatuur over de Middelkerke bank.

My gratitude finally goes out to Andrew Winterbottom, UK Hydrographic Office, for retrieving the bathymetry dataset of the area near the Varne Bank from backup tape and supplying it with excellent meta data.

Steven IJzer,
Juni 210

Summary

The seabed of shallow shelf seas is rarely flat. When sediment is in good supply and tidal flows are sufficiently strong, wavelike subaqueous sediment structures, called sand waves, may occur. As they may migrate up to several tens of meters each year and as their height may reach up to 1/3 of the local water depth, sand waves may severely influence human offshore activities, such as navigation. This makes it important to understand the physical processes that shape and change sand waves, in order to improve management strategies of expensive operations such as e.g. the dredging of shipping lanes.

Sand wave migration was until now explained as the result of interaction between a steady Z0 current with the oscillatory M2 tide, see e.g. Németh (2003) or as the result of interaction between higher harmonics of the tides with sufficient phase lags, e.g. M4 with M2. See Besio *et al.* (2004).

In field data, temporal variation in the direction of migration and the asymmetry of sand waves were found to be related to none tidal residual currents, such as a Monsoon-driven current found in the Adolphus Channel in Australia by Harris (1989). Surface wave action may also have an influence as Van Dijk & Kleinhans (2005) found that the dynamics of sand waves may depend on a balance between the relative influence of surface waves and currents. We found in a pre and post storm study that sand waves were lowered and that the asymmetry was changed.

In this study, a morphodynamic model and empirical wave and current data were used to investigate the relative importance of the waves with respect to the effect of the currents. It was found that an increasing angle of waves with respect to the residual current increasingly limits sand wave migration and increases the horizontal asymmetry. The effect increases for increasing height of surface waves.

In a pre and post storm study in the Varne area we find a lowering of the sand wave crest by a metre. Similar effects of a storm were also found by Houthuys *et al.* (1994) in a study of the Middelkerke Bank. When compared to the model output, it was found that these kind of changes in crests can occur due to wave action alone. However, the calculated timescale for these modifications (20 to 50 weeks under extreme conditions) is too long when compared to the length of storms in general. The morphological timescale in which the sand waves form in the modeling results is however realistic. It was also found that the effect sorted by wave stirring alone is limited (30 cm) with respect to the changes observed in the field (1 metre). The lowering effect in the stormy period, may therefore be caused by more than just higher surface waves. As a recommendation, it is suggested to also look at variations in the residual currents. This is further supported by the strong relation found in wave (and wind) direction and the direction of the residual flow. The lack in modeled lowering of the sand waves might be due to the fact that the sediment transport mode used is bed load transport, while Tonnon *et al.* (2007) show that under storms a suspended sediment transport mode is dominant and causes a lowering of the sand wave crests.

Finally, waves in the direction of the residual tide add to migration and sand transport in that direction. Waves opposing the residual current reduce the transport and migration. Higher waves increase this effect both ways. The waves were however never able to cause a migration against the direction of the residual current. Even the highest wave could only reduce the transport and migration rate. The waves and current combined however doe have a significant effect on the dynamics of the system as higher surface wave decrease the time in which e.g. sand wave grow and increase transport rates.

Chapter 1. Introduction

1.1 Background and rationale

The sea bed is rarely flat. In shallow parts of seas, where sand is in good supply and tidal currents are strong, dynamic wave-like features of bed material of different spatial scales may occur.
The smallest of these bed forms are classed as (mega)ripples and have heights that are in the order of centimetres to decimetres and wavelengths that are up to tens of metres. The largest bed forms are tidal sand banks, their wavelengths span several kilometres and their heights can be as large as the local water depth. The latter bed form migrates and changes its shape slowly. The timescale for these changes is in the order of years to decades.

In between these classes of bed forms are sand waves. Sand waves are up to several metres high (up to 1/3 of the water depth) and are up to several hundreds of metres long. See e.g. Van der Veen *et al.* (2007) and Knaapen & Hulscher (2002). Sand waves may migrate up to several metres per year, see e.g. Lanckneus & De Moor (1993), Van Dijk & Kleinhans (2005) and Buijsman & Ridderinkhof (2006).
Due to their considerable height and large migration rate, sand waves may have a significant influence on human activities. For example, they may lead to problems for shipping safety and/or cause exposure of pipes. See e.g. Morelissen *et al.* (2003). Furthermore, sand waves can be an important source for sediment mining activities.
From this interest in sand waves, we investigate offshore physical system processes and study how these processes affect sand wave behaviour.

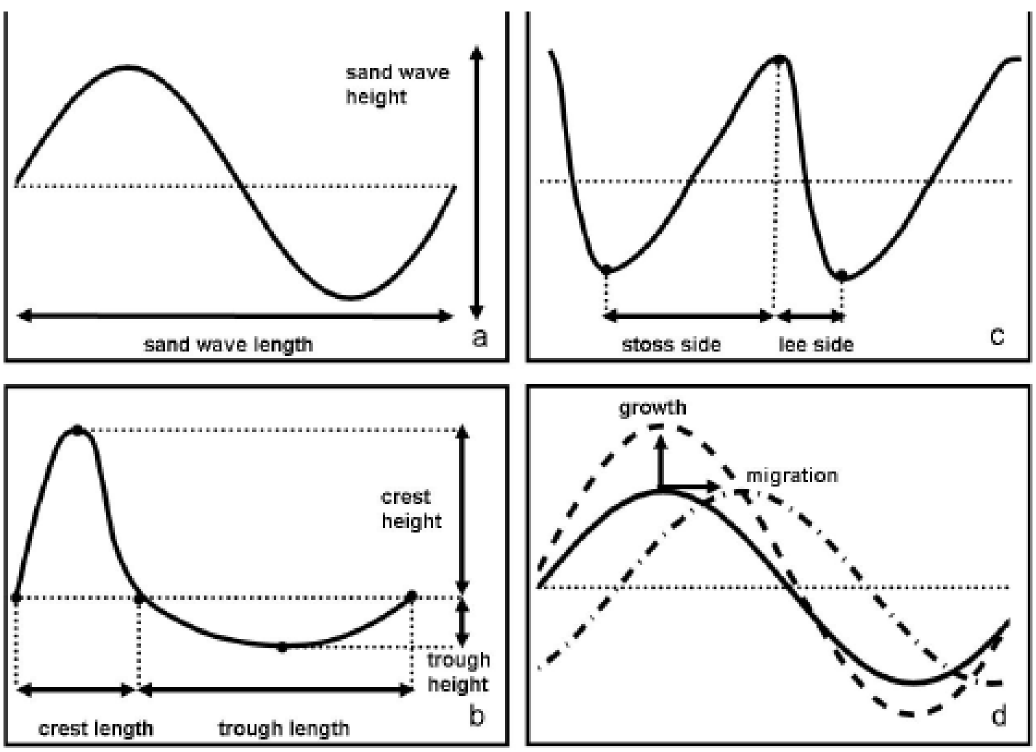

Figure 1.1: Sand Wave shape and asymmetry characteristics. The solid line represents the amplitude with respect to the mean depth (dashed line): a) wave length (m) and wave height (m). b) L_{crest} / L_{trough} asymmetry (-) and the H_{crest} / H_{trough} asymmetry (-). c) L_{stoss} / L_{lee} asymmetry. d) growth in volume (m^3 / m^2) and/or height (m) and migration (m/year). Figure taken from Sterlini (2009).

When we talk about sand wave behaviour, we mean a change in the characteristics as e.g. those shown in figure 1.1[a-c] or growth and/or migration as is illustrated in figure 1.1[d]. The figure, taken from Sterlini (2009), illustrates a 1D cross-section of sand waves normal to the crests.

Sand wave changes, and seabed changes in general, can be explained according to the morphodynamic feedback loop that is illustrated in figure 1.2. The figure illustrates that flow and sediment transport are linked to each other. In theory, the amount of sediment that a fluid can transport is related to the third power of the flow velocity. $q_b \sim u^3$. If for any reason the flow field is changed, this will have an effect on the amount of sediment that is transported. Any change in the amount of sediment transported will change the local bed level, as bed material is then locally eroded or accumulated. Changes in bed level change the local flow field, thus completing the cycle.
Furthermore, we have a theory about sand wave formation specific, namely that discussed in Hulscher (1996).

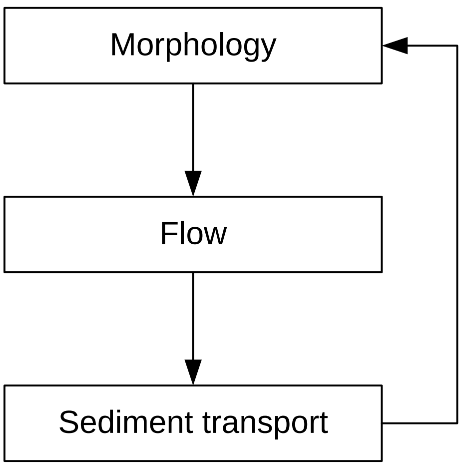

Figure 1.2: The morphodynamic loop

Hulscher (1996) showed in a three-dimensional morphodynamic model, using linear stability analysis, that sand wave growth can be explained as instability in the morphodynamic loop.
The process can be described as follows: Oscillatory tidal flow over small perturbations induces vertical, tide averaged, residual flow circulation cells that transport sediment. When the net displacement of the sediment is directed towards the crests of these perturbations, the seabed is unstable, meaning that the perturbations grow. The seabed is stable when (for all possible wave lengths) the net displacement is directed towards the troughs of the perturbations, resulting in a damping of these perturbation. By means of linear stability analysis, Hulscher finds which wavelength has the fastest growing mode (FGM). This is the preferred wavelength of the linear system. The results found by Hulscher correspond well with actual sand wave lengths. These theories were also transformed into several numerical models simulating sand wave growth.

The direction of migration
In a refinement of the work done by Hulscher (1996), Németh *et al.* (2002) show that the migration of sand waves may be explained by asymmetry in this vertical circulative motion. These asymmetries may be the result of interaction between a steady flow (Z0) and the main oscillatory tide (M2). In the model used by Németh *et al.* (2002) the direction of migration is always in the direction of the residual current. Besio *et al.* (2004) show in their morphodynamic model that the direction of the migration may even be against the residual current when appropriate phase shifts between the M4 and M2 tidal components exist.

The influence of currents on the direction of migration was also shown in empirical data.
Van Dijk & Egberts (2008) describe a seasonal seasonal back and forth migration of sand waves 50 km off the Dutch Coast. An example of asymmetry change due to current is given by Harris (1989), who found that Monsoon driven currents reversed the asymmetry and direction of migration of bed forms in the Adolphus Channel.

The influence of waves is also found in empirical data and shown with a model.
Van Dijk & Kleinhans (2005) find that the variability in dynamics between offshore and coastal sand wave sites can be explained by the relative contribution of current and wave action. The water depth is found to be an important parameter controlling the sand wave shape, since the stirring action by waves orbital velocity decreases with increasing depth. In coastal sites, were water depth is limited, the orbital velocities of surface waves frequently are high enough to flatten (compound) sand waves. This happens to such a level that the height of the sand waves can not be saturated by low frequent peak tidal velocities.
Houthuys *et al.* (1994) find an average lowering of the sand wave height of 1.2 metres in a pre- and post storm study of the Middelkerke Bank in the southern North Sea near Belgium. The effect increased with decreasing water depth on the flank of the sand bank where the sand waves were superimposed upon.

Sterlini (2009) showed that the relative rate of the M2 and the unidirectional tidal current has an influence on the bed form height and shape. And, by adding surface wave effects to the model based on Németh (2003), Sterlini (2009) showed that the theoretical sand wave model she used is able to predict increasingly lower bed forms for increasingly higher surface waves. The additional lowering thereby improved the predicted bed form height. The model outcomes also support the conclusion of Van Dijk & Kleinhans (2005) that the effect on the shape of the bed forms is a matter of the relative contribution of waves and current. Also, the surface waves were found to cause a higher migration rate for higher surface waves.

The hypothesis now is that variations in both currents as well as surface wave activity have a significant role in the sand wave shape and direction of migration. In this research it is aimed to quantify which part of the shown behaviour is sorted by the waves and which part must be attributed to other processes, such as variations in tidal currents.
In the previous study by Sterlini, surface wave were included, but their direction was always kept collinear with respect to the current. In reality, waves can come from a variety of directions. The secondary aim is to investigate the effect of the angle of the waves with respect to the current.

1.2 Aim

The aim is to find out whether, and if so to what extend, (the angle of) the surface waves has an influence on the shape of sand waves and the migration rate and direction.

1.3 Objectives

To accomplish the aim of research the following steps will be taken.

1. The relevant sand wave shape characteristics from empirical field data will be determined and their variation in time will be studied. The most interesting attributes are sand wave height, sand wave length, L_{stoss}/L_{lee} asymmetry and the sand wave migration rate.
2. Then, we will proceed in studying the environment data from the time of the recoding of the dataset. In this step we will look for relations between bathymetry changes and environmental conditions. We are interested in the surface wave height and direction, but also current data will be studied. This is done to compare the relative importance of the two physical processes for the sand wave shape and migration.

3. To further support any conclusion we might draw, we will finally simulate the environment in a morphodynamic model. The model we use is the model studied by Sterlini (2009). It will be modified to allow simulations with a variable wave angle. The model allows us to determine in which time span changes, if any, take place.

1.4 Research questions

By comparing the output of the theoretical model to the empirical dataset for the sand wave shape characteristics, the migration rate, migration direction and the rate of transport, we will try to answer our research questions:

1) How did the observed sand waves change shape and migrate over time?
2) What were the surface wave and flow characteristics during the recording of the bathymetry and how did these changes over the period prior to and in between recordings of the bathymetry affect the bathymetry?
3) What relations between the observed bathymetry changes and changes in environment data can be seen?
4) To what extend are the morphodynamic responses we see in the empirical dataset supported by our idealized model simulations?
5) Are the time scales in which the model predicts changes, if any, realistic compared to the changes we find in the bathymetry dataset?

These question will help answering our main research question: To what measure do the surface wave direction and height contribute to the sand wave migration rate, migration direction and sand wave shape?

Answering our main research question will help to improve sand wave models and will increase our knowledge about relevant offshore processes. This knowledge will help us to improve management strategies of the dredging of shipping lanes and/or help us assess the depth to which pipelines must be buried to prevent exposure.

Chapter 2. Methods: Empirical Analysis

This chapter explains the techniques and software that are used to help answer the questions posed in chapter 1 related to the study of the empirical data. Methods on the modelling part of the research are dealt with in chapter 3. In paragraph 2.1, the Kriging interpolation software used to transform the distributed x,y,z bathymetry data into regular grids is discussed. In paragraph 2.2, the cross correlation code is explained that is used to determine migration in the 2D plane. This technique tell us about the direction and rate a bathymetric pattern has moved in time. The third paragraph (2.3) deals with transects interpolated from the regular grid. Also, the methods of determining the values of the sand wave shape characteristics are shown. The definitions of these characteristics were given in chapter 1. The final paragraph (2.4) deals with how flow, wind and wave data were processed.

2.1 Bathymetry interpolation techniques

The bathymetry data is interpolated from spatially distributed points to regular grids, using a Kriging algorithm. The software used is named Gridsampler. Gridsampler is a java-based program supplied by Deltares that can - among other functions - be used to plot and interpolate bathymetry recordings. By means of Kriging interpolation, it can interpolate distributed data to a regular 2D grid and/or to a fixed distances transect (1D length profile).

Two exported regular grids of the same area with the same grid size are needed to determine the direction and migration rate by means of cross correlation (see paragraph 2.2). The transects are used to determine the height and shape characteristics of the bed forms by means of Fourier Analysis (paragraph 2.3).

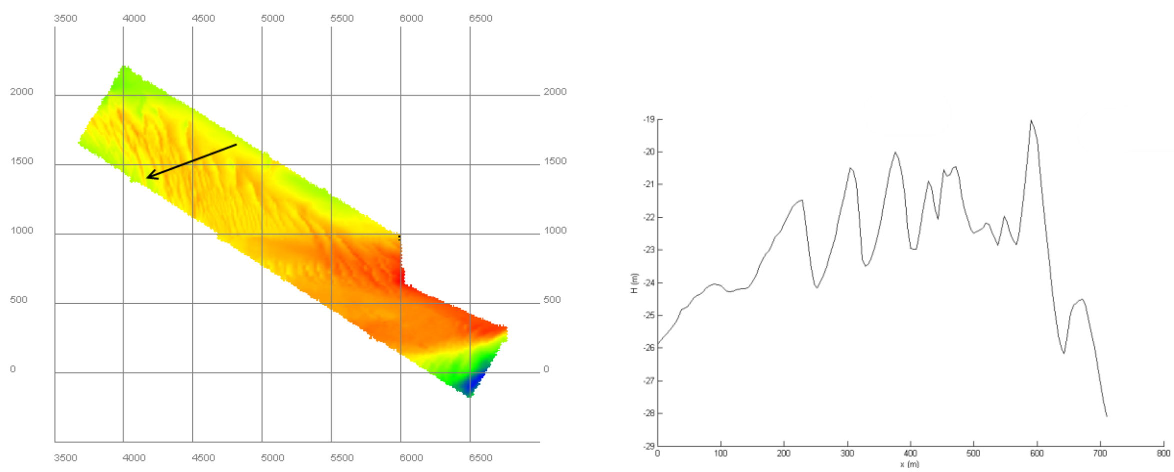

Figure 2.1: Example of the Gridsampler plot of bathymetry data (left) and a plot of the transect taken (right) from it. Start of the arrow (in the North East) is left on the transect plot. This example data is from the Bisanseto strait in Japan.

As an accuracy test, the Kriging process used in the Gridsampler program for the Varne area is evaluated. The area and its data are further discussed in chapter 4.

The depth difference between the Kriged approximation (1mx1m, 5m radius) are compared with the measured data points that the Kriged approximation is based on. (Also see figure 2.2).
For 40.000 data points the vertical distance between the interpolated and measured values, expressed as $z_{interpolated}$ - $z_{measured}$, is checked.

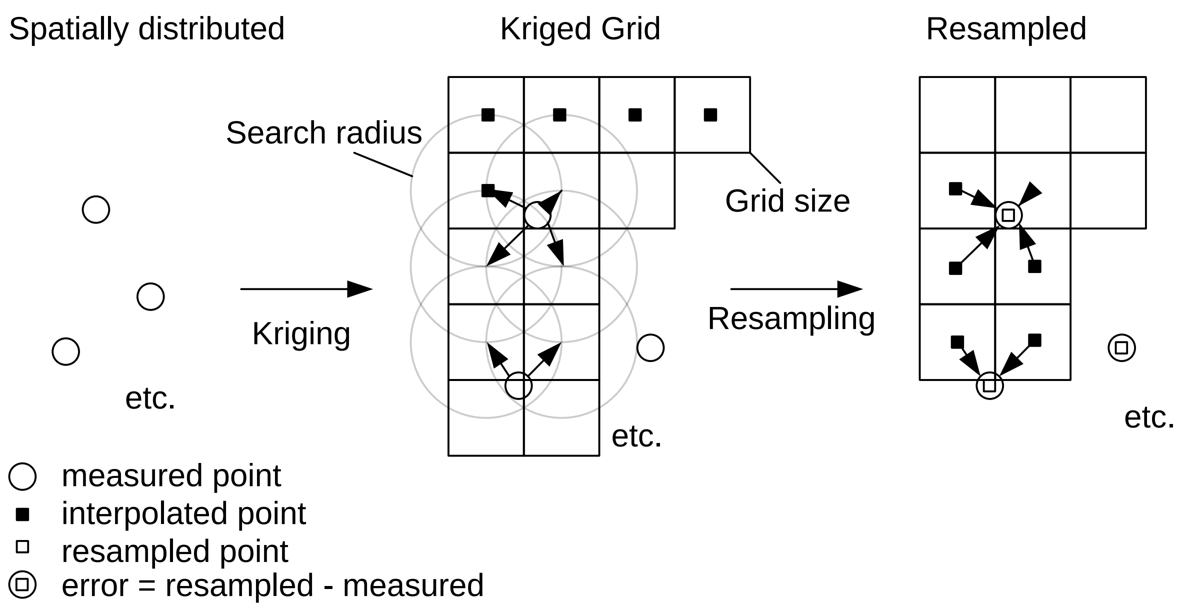

Figure 2.2: Calculation of the vertical error estimate of the Kriging procedure. The points represent a x,y-location with a certain depth value. The measure data point were resampled with the interpolated value and the difference in z coordinates tell us the error. For visual purposes the amount of measured points is illustrated a bit low compared to the resolution of the grid. In the kriging set, in reality multiple points (may) contribute to the value of a single cell.

The distributed dataset is resampled from the regular grid that is calculated in the Kriging interpolation step. The value at each (measured and spatially distributed) datapoint is recalculated from the interpolated, regular grid.

The differences in height between the interpolated and the measured z-coordinate value are put in a histogram with bin sizes of 1 cm. This histogram is shown in figure 2.3. The bin 0.05 thus shows the percentage of points for which the interpolation z coordinate was over estimated by 0.05 metres. 91% percent of the values are in the bins with an error between -0.05 and 0.05 metres difference between the measurement and the Kriging approximation. The accuracy may be considered to be better than or equal to the measuring error in offshore bathymetry measurements. E.g. Houthuys *et al.* (1994) determine that the absolute error in water depth in their research is of the order scale of 30 cm. The bed form features that can be distinguished in their studies (so relative water depth within a single recording) are below 15 cm in height and 10 metres in length.

The error introduced by the Kriging procedures, 0±0.05 metres is therefore about one to two orders smaller than the height of the bed forms under consideration. This gives confidence in the use of this procedure. The size or sign of the error did not show any relation with the location of the point (crest, trough, lee/stoss slope).

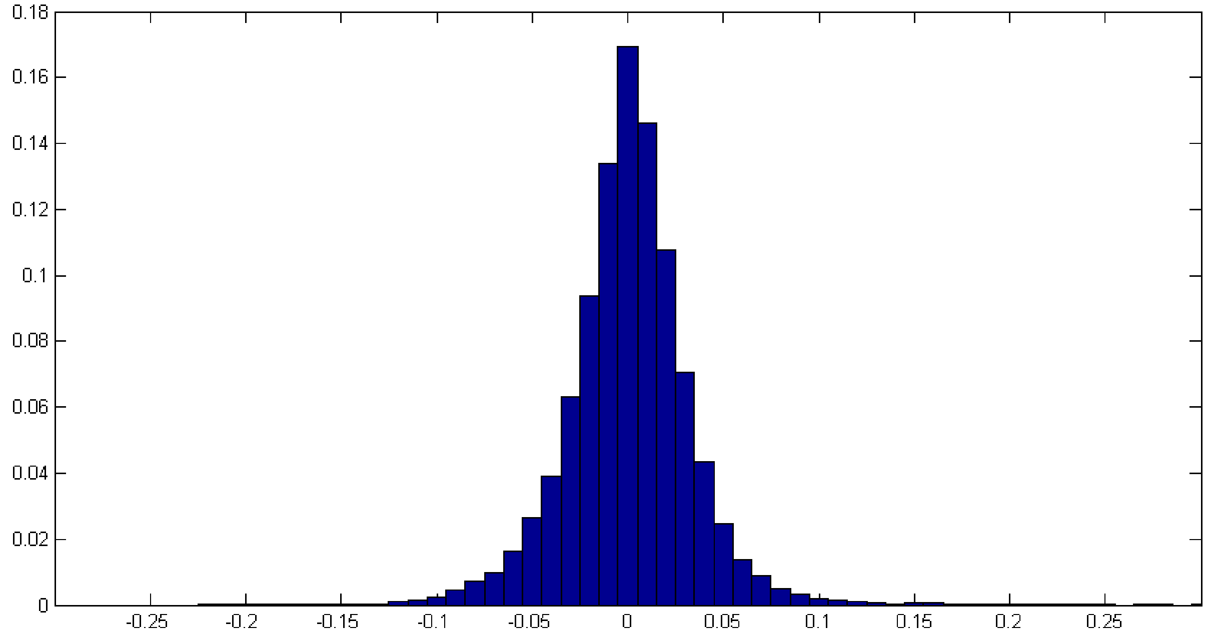

Figure 2.3: Kriging vertical error distribution. Horizontally: The 0.01 m bins, range -0.05 to +0.15m. Vertically: The percentage per bin. Total number of data point was 40000.

2.2 2D plain cross correlation

To determine the direction and rate of migration, a cross correlation technique is used. The software used is named Xcorr, it calculates the displacement of bathymetric patterns in two bathymetry recordings of the same location, recorded at different moments in time. The regular grids from the Gridsampler program described in paragraph 2.1 are the input for the software.
The output of the program is a direction vector (shift in x, and y position) in number of grid cells at which the highest correlation is found. By calculating the time difference in recordings and considering the x-y cell size of the data, this result can be extrapolated to a migration rate and a direction.
The process is illustrated in figure 2.4. Also see appendix 9.1 for an example on how the software works.

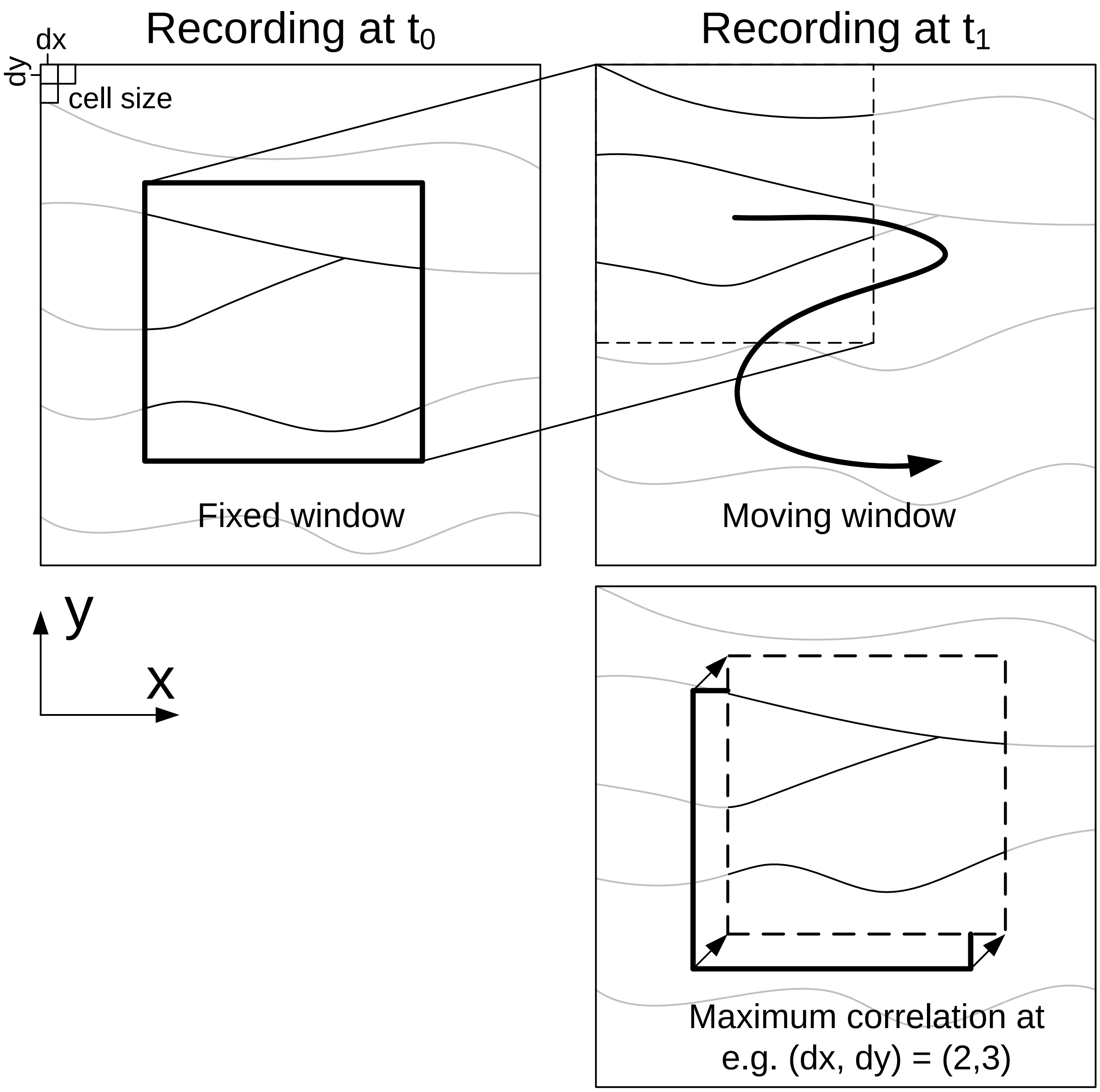

Figure 2.4: Illustration of the 2D plane cross correlation sequence. Two recordings (made at different times) of the same physical space are compared. In the time between recordings the bathymetry patterns has shifted and changed shape somewhat. The horizontal lines represent sand wave crests. At each iteration the sub area within the within the moving window is correlated (compared) with the sub area in the fixed window. The data outside the window in the first recording is therefore not used in the analysis. In this example the correlation is highest at (dx, dy) = (2,3). This means that the bathymetry pattern has shifted approximately to the North East.

The procedure in the software is as follows: Two datasets of water depth recordings of the same x,y bathymetry area are put into the software. The user defines a window smaller than the size of the area. The window contains the subset of both datasets that is used that iteration. The window over the first dataset is kept at the original (user defined) position. The window over the second dataset is shifted one position per iteration over the entire extend of the second dataset. Within each shift, the correlation of the points within the second window is calculated with the points within the first. The displacement of the window that results in the largest correlation is considered to be the displacement of the bathymetric pattern.

Distinct features such as bifurcations tend to persist in time and are therefore often recognizable in both datasets. These distinct features result in particularly high correlation when identified in the windows of both datasets. Absence of such distinct features results in high correlation along the crests of (rhythmic) bed forms and results in repetition of high correlation when the shift of the window approaches a multitude of the bed form wavelength perpendicular to the crests. Though no special attention is given to this in present study, selecting the location of the first in such a way that distinct feature are used in the analysis, limits both high correlation parallel to the crestlines and repetition after one wavelength perpendicular to the crestlines.
The maximum displacement under consideration in this routine is limited only by the extend of the dataset (larger is better) and the size of the window. A smaller window means a larger maximum displacement under consideration. As the choice for the size of the area was limited by the data availability, this meant the size of the window was reduced accordingly. Ideally, the size of the window is large enough to have enough distinct features in the correlation analysis to unambiguously identify the location with the best correlation. Preferably, the window contains multiple bed forms with, if possible, bifurcations. As the part of the data that lies outside the fixed window is not used in the analysis, keeping the size of the window as large as possible has the advantage that a larger part of the data is included in the analysis. The window should however also be kept small enough to prevent limiting the maximum displacement that could be considered.
In all analyses performed in this study, the window size was chosen in a way that allowed a displacement in all directions that was large enough with respect to known migration rates of sand waves. The time in between recording was also considered for this. The differences in the 1D transects of both datasets (see paragraph 2.3) provided the minimum possible displacement that had to be considered.

A strong point of the method is the fact that `no data`-point are neglected from the analysis. As a result the analysis can be performed independent of the direction in which the data is gathered by the vessel.

Additional visual inspections of differences in the contour plots of both areas, provided by the software, should be performed to see if the bathymetric pattern had not changed to such extend that the results are no longer trustworthy. A low maximum correlation (below 0.7) indicates when such visual checks are especially needed.

2.3 1D transect Fourier Analysis (FA)

The output of the Gridsampler program (see paragraph 2.1) is a transect that is resampled with a fixed interval from the interpolated grid. The spatially distributed bathymetry datasets for both case studies (see chapter 4 and 5) have an average dx, dy resolution of about 5 metres. Therefore, a sampling resolution of 1.0 m for the profile is considered to be fine enough to represent all the dynamics in the original dataset.
The Fast Four Transform (FFT) is used to determine the shape properties mentioned in chapter 1 as objectively as possible. The problem is that the sand waves may be superimposed on bathymetry with larger wave lengths, such as sand banks, or be superimposed itself by bed forms with smaller wavelengths, such as megaripples. In the first case, the correct height of the sand waves can not directly be determined. In the second case, the location of e.g. the crest may be drastically influenced by the crest positions of superimposed megaripples.

The FFT fits a discrete function through the x, y points of the transects in order to separate the signal of sand waves, from large and small scale morphology. The function is a (large) set of sinuses of different frequencies, at different phases and at different amplitudes that approximate the “real world” dataset.

The code is set with chosen minimum and maximum wavelengths that are included in the sand wave signal approximation, the so-called cut off frequencies.
The separated signal for which the sand wave properties are determined is illustrated in light blue in the bottom image of figure 2.5. To describe the images, samples of the z- values for the different bed form signals are given in table 2.1. In this table the columns Megaripple to Largerscale represent the FFT of the separated signals. These three numbers represent which part of the deviation from the mean depth (z_{mean}, col. 2) is assigned to which bed feature (col. 5 to 7).
Note that for presentational purposes only the first three values of an example FFT are given, while transects contain several thousand values depending on the length and the horizontal step size. The colours in the table indicate the same colours as in the figure.

The top figure
In the top figure, the fourier approximation (red) of the real data (blue) is determined.
The green line is z_{mean} + Largerscale
The red line is z_{mean} + Largerscale + Sandwave + Megaripple. This is the approximation of the real data, given in blue.

Bottom figure
The lime line is the full Fourier signal, minus the large scale morphology , minus the mean transect depth. This line represents the amplitude of the bed form signal as an amplitude to the mean transect depth, without the unwanted noise belonging to Megaripples (blue).

Example
At the first point (x=150.17 metres), the deviation from the mean depth is (-24.7581 - -21.2085 =) 3.54958 m. -0.06823 + 2.5485 + 1.069266 = 3.54958 m.

$x_{interpolated}$ [m]	$z_{transect}$ [m]	z_{mean} [m]	$x_{separated}$ [m]	Megaripple [m]	Sandwave [m]	Largerscale [m]
In plot:	Top plot, RD (Real data)			Bottom plot, RD - FA (365)	Bottom plot, FA (365) – FA (3)	Top plot, FA (Max. Freq 3)
150.17	-21.2085	-24.7581	150.17	-0.06823	2.548546	1.069266
151.17	-21.0596		151.17	0.0439	2.566531	1.088101
152.17	-20.7721		152.17	0.292014	2.587436	1.106585
etc.	etc.		etc.	etc.	etc.	etc.

Table 2.1: The breakdown of the transect data (column 2) into the separated signals (column 5 to 7), given as amplitudes to the mean depth of the transect (column 3). The mean depth for the entire transect + the amplitude for the separated signals for each discrete horizontal step (columns 3 + 5 + 6 + 7 = column 2) equal the depth of the interpolated transect for each step (Column 2).

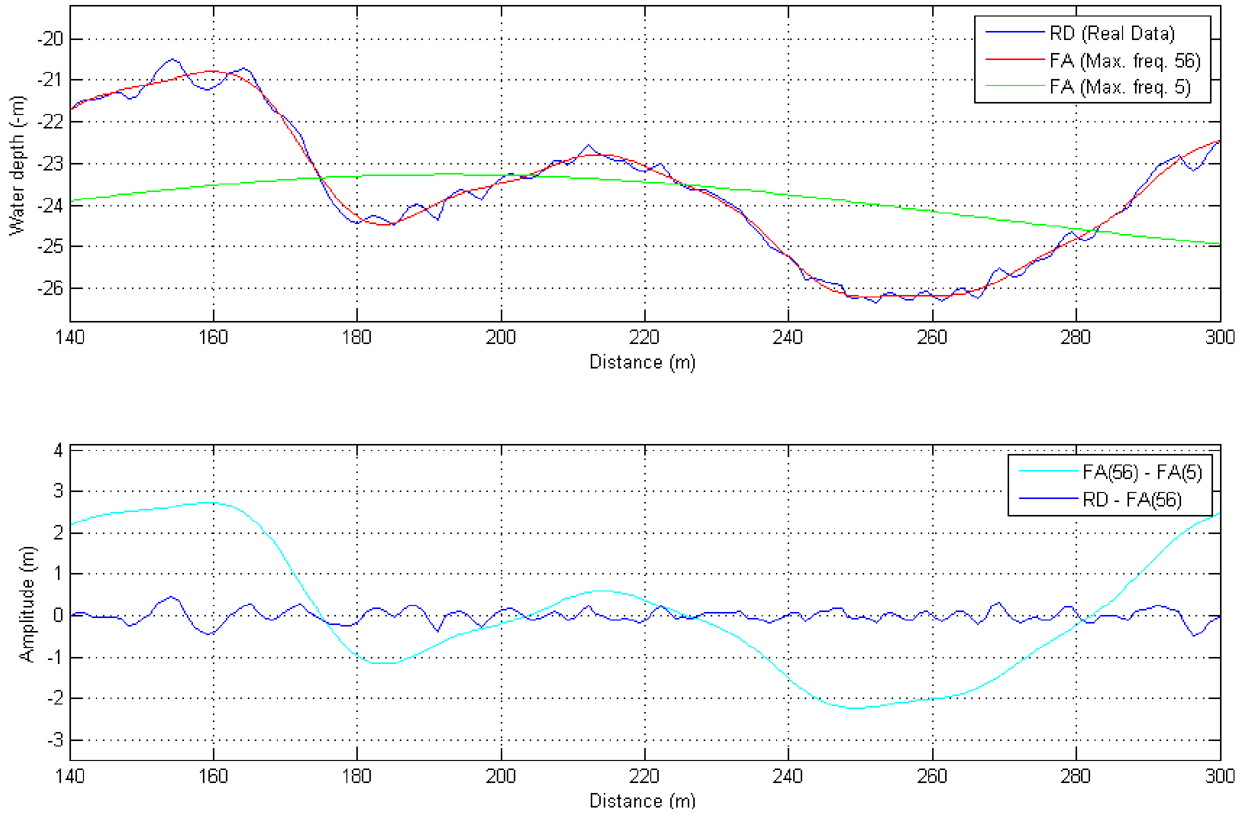

Figure 2.5: The breakdown of the real data into separated signal using Fourier analysis. In this example a good number of frequencies are included. The approximation is quite precise, but the signal belonging to megaripples is removed.

Shape characteristics

Once the sand wave signal is extracted, the shape characteristics of the sand wave can be determined. The zero derivatives of the sand wave signal represent the crest and trough points. The zero 2nd order derivatives (with negative first order derivative) of the signal represent the inflection points. The x- and y- coordinates of the points are selected automatically by the software to prevent user accuracy errors. The user is however still prompted to point out which points are the correct crests and/or troughs, the reason for this is shown in the sections below.

From the x and y coordinates of the (chosen) crest, trough and inflection points, the software calculates the length, height and L_{stoss} / L_{lee} asymmetry of the sand waves, as these characteristics are defined in chapter one. See figure 1.1 and figure 2.6.

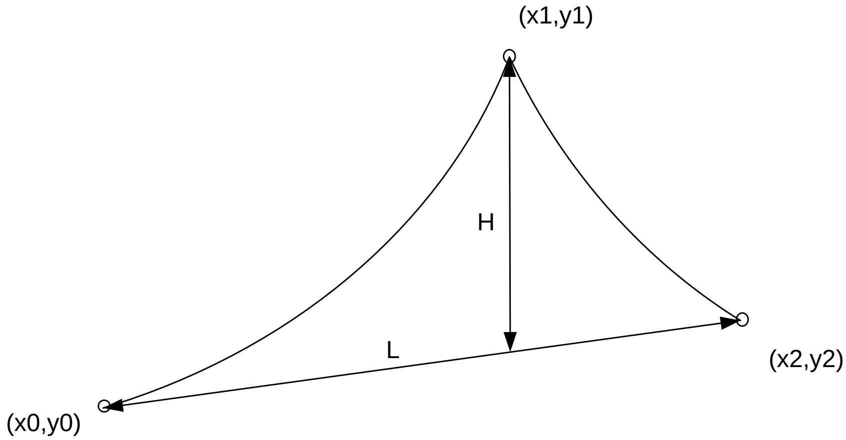

Figure 2.6: Height and Length of the sand wave as defined in the FFT code.

The next two sections "Selecting the right cut-off frequencies" and "Edge effect" deal with some specific issues that need to be considered in the analysis techniques.

Selecting the right cut-off frequencies

In the example shown in figure 2.7 the approximation is set too inaccurately, including not enough higher frequencies. The approximation shows noise/error peaks near the crests and troughs of the sand wave signal that in magnitude is close to 40% of the sand wave signal. Though peaks in the noise signal near the crests and troughs do occur to some extend, the direction and magnitude reveals that too much of the sand wave signal is dismissed as noise and is thus removed from the real height of the sand wave crest. See e.g. near 950 and 1200 m in the bottom figure. To overcome this, a larger number of frequencies must be included in the Fourier analyses. If more (higher) frequencies are added to the FFT, the approximation is able to follow even the small scale noise, resulting in a better approximation.

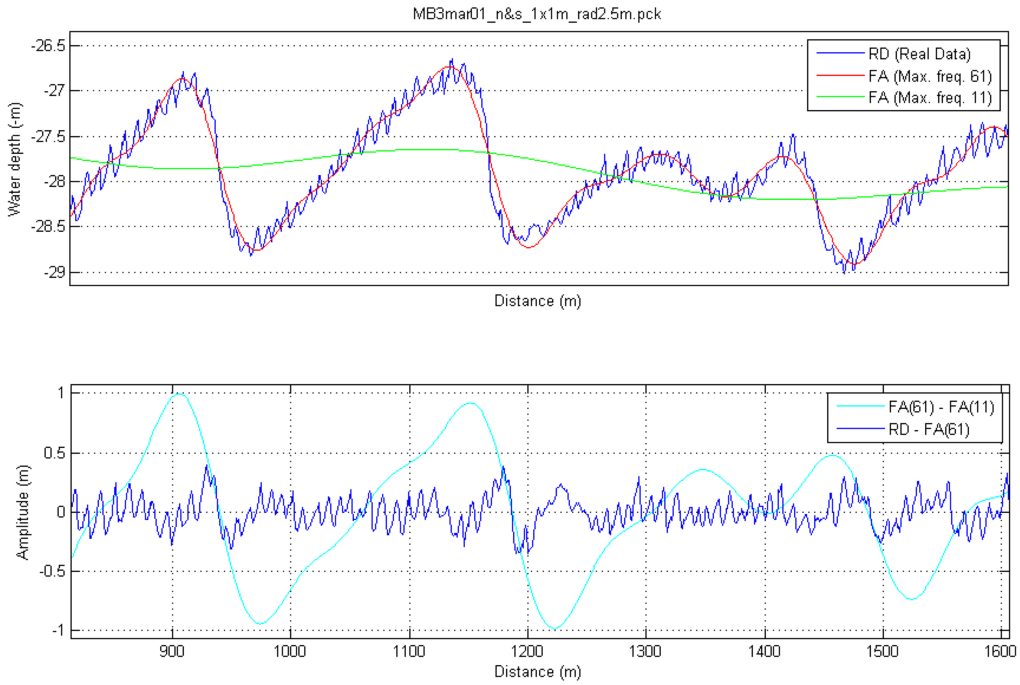

Figure 2.7: Example of including not enough frequencies in the FFT. Crest and trough positions are off and too much of the sand wave signal is removed as noise.

When a lot more frequencies are included, more frequencies are included as part of the sand wave signal and more zero first and second derivatives may be found. These are then (wrongly) pointed out as crests, troughs or inflection points. From these a (de)selection must be made. This issue is shown in figure 2.8.

In this example a lot more higher frequencies are needed to accurately follow the long troughs and short sharp crests of the bed forms. The green left and right troughs were selected (manually) over the red ones, since they are deeper. Should this procedure be done automatically, a change in depth of the megaripple could cause a jump in the selected trough point. Choosing a different point -e.g. in a later recording of the same location- would in this example result in a 40% decrease sand wave length and a 24% decrease in the L_{stoss} / L_{lee} ratio as the sand wave would become 22m shorter on a total length of 89 metres. At the same time, the length removed from the stoss side of the left wave would be added to the lee side of the wave to the right, thereby shifting the L_{stoss} / L_{lee} ratio to the same side for both bed forms.

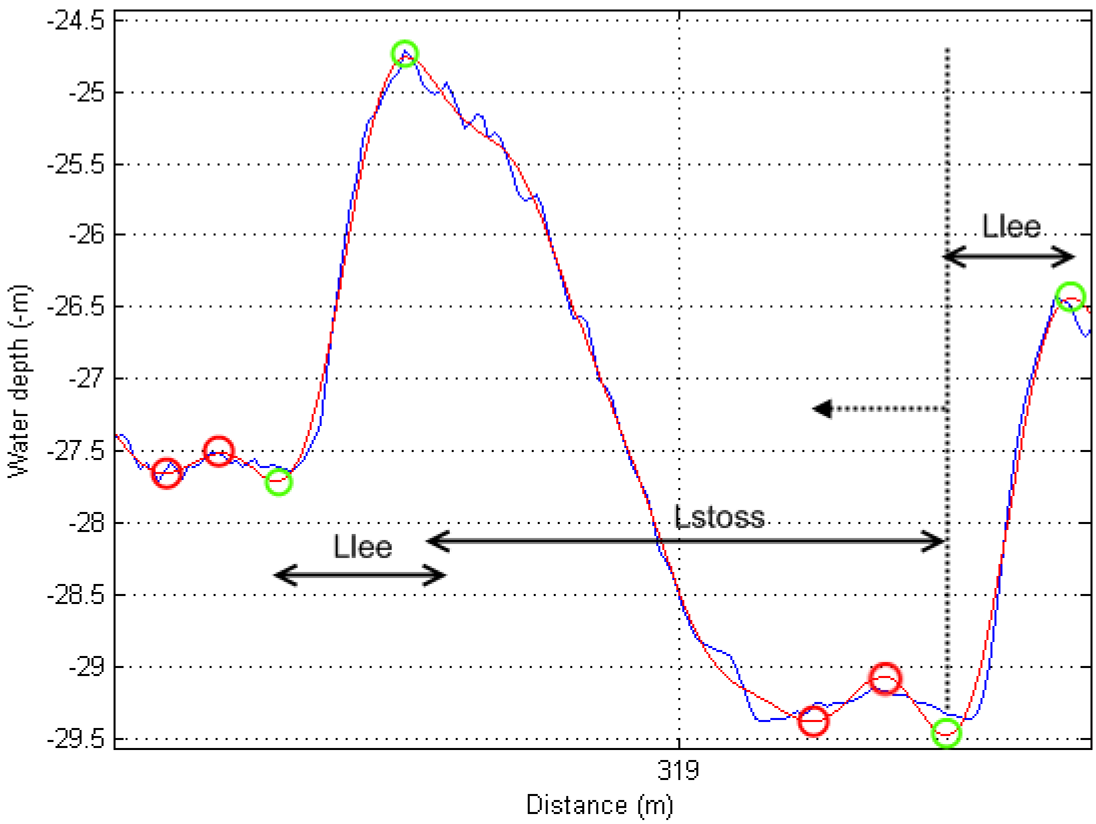

Figure 2.8: Extra zero derivatives result from including more frequencies in order to accurately follows sharp crested sand waves. Selecting a different trough point (in e.g. two different recording of the same location) influences the length of two sand waves and shifts the L_{stoss}/ L_{lee} ratio of both sand waves to the same direction.

Edge effect

The approximation method gives poor results on the edges of the transect. This has to do with the fact that the largest wave length the approximation handles is equal to the length of the transect. The effect is most apparent when e.g. the transect shows a general slope over the entire length of the transect. The approximation techniques will try to approximate that gradual slope with a large amount of small wavelengths instead of one very large wavelength (with a wave number corresponding to a length larger than the length of the transect). The resulting poor approximation (in red) of the real data (blue) is shown in figure 2.9. This edge effect fortunately disappears some metres into the transect. Therefore, leaving out the first and last metres from the transect is enough to overcome this problem.

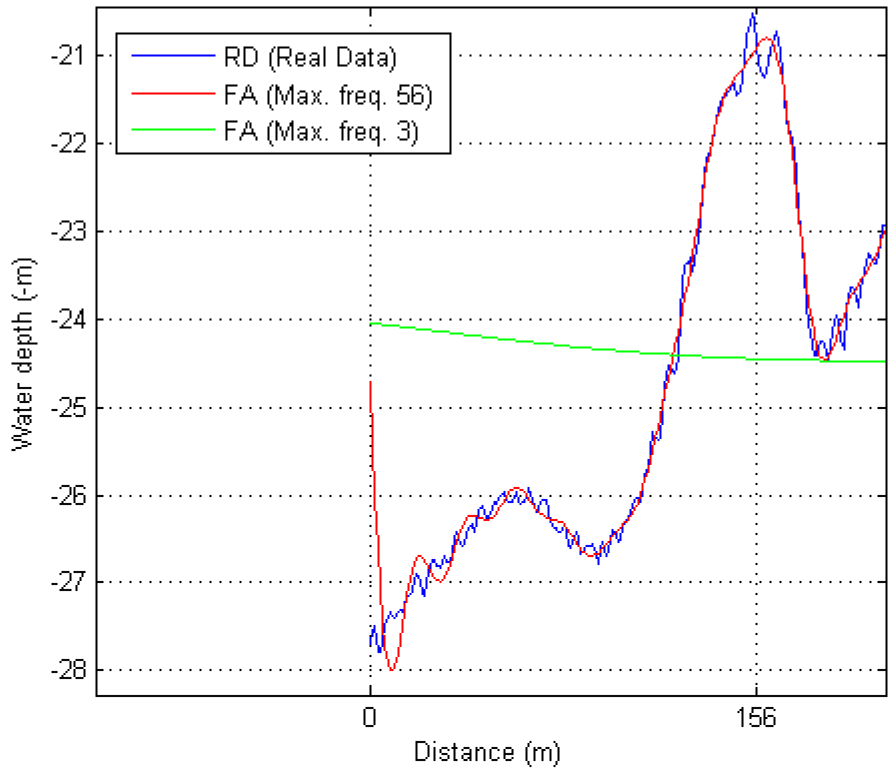

Figure 2.9: Fourier approximation problems may exist near the beginning and ending of transects.

These next four sections, "Migration", "Growth", "Volume" and "Transport rate" deal with the analysis of both the transect data as well as the analysis of the output of the model. The final section of chapter 3 shows that the output of the model is in effect the same as the separated sand wave signal as described in the previous sections. The only important difference is the fact that the sand wave signals contains multiple different sand waves, where the model calculates only one wavelength. This difference did not cause any problems.
The analysis of the transect data continues with the excel output of the FFT code. This output contains the separated signal and the Length, Height and Asymmetry of the sand waves.
The text file output of the model is read into Matlab and is further analysed with custom code.

Migration
Migration rates are determined by dividing the differences in x-coordinates of the same sand wave crest (or trough) by the time difference between recordings of the sand wave. The rates are extrapolated to yearly values for easier comparison. This is done by multiplying by 365/dt. dt is the time in days between recordings. dt in the model is 7 days or 35 days (by choice), dt in the measurements is between 66 and 192 days, depending on the data availability.

Growth
Growth of the sand wave is expressed as the change in crest height of trough depth. As the FFT transforms the sand wave signal into a distance with respect to the mean of the transect, comparing different recordings of the same transect must be done by adding the change in average waterdepth. The issue is explained in figure 2.10: In between recordings, the trough of the sand wave has moved right and down. To obtain the absolute change in trough depth, the difference in mean waterdepth must be added to difference in trough level (expressed as a distance to the transect mean).

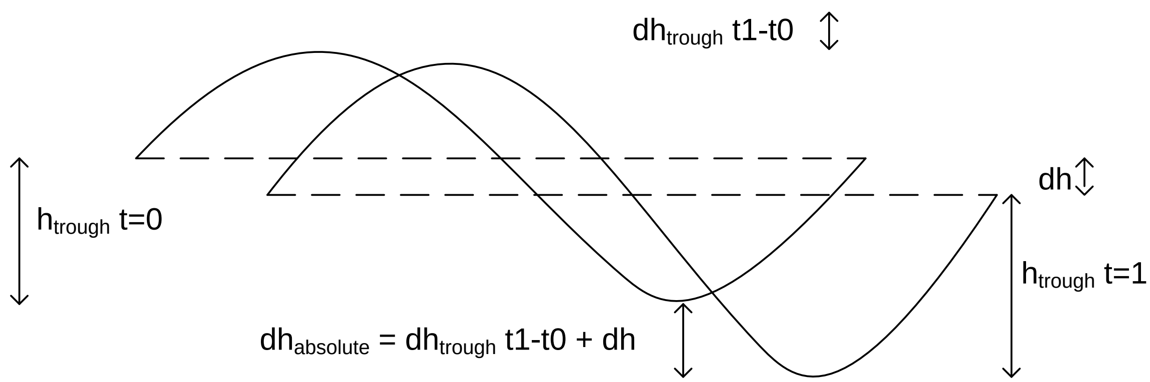

Figure 2.10: Explanation of the change in crests and through level with respect to a certain mean for two different measurements. dh_{trough} and dh_{crests} as the absolute difference in bed level.

The model has a constant means depth which is determined by the simulation settings. Crest and trough levels can be directely compared.

Sandwave Volume

The sand wave volume in [m^3 / m^2] is calculated with the following formula:

$$V = \frac{1}{2}\frac{dx}{L_{trans}}\sum_{1}^{n}|y_i| \qquad \textbf{Eq. 2.1}$$

In this formula dx represents the horizontal spacing, or transect resolution in metres. L_{trans} is the length of the transect in metres. y_i represents the amplitude for the separated sand wave signal at each x-coordinate. The factor 0.5 represents the fact that the volume in the crest is equalled by the (negative) volume in the troughs. The volume thus represents the average volume per m^2 that needs to be moved to create the sand wave shape from a flat bottom.

Example

In figure 2.11 we illustrate what we do by means of a simple geometry. Consider the domain of length L. The mean depth of the domain is equal to zero as $|y_2| = |-y_1|$. In order to go from a flat bed to the simple geometry, we need to move
0.5 * y_2 [m^3/m^2].

$$\frac{1}{2}\frac{dx}{L_{trans}}\sum_{1}^{n}|y_i| = \frac{1}{2}\frac{dx}{L_{trans}}(|-y_1| + |y_2|) = \frac{1}{2}\frac{dx}{2dx}(|2y_2|) = \frac{1}{2}|y_2|$$

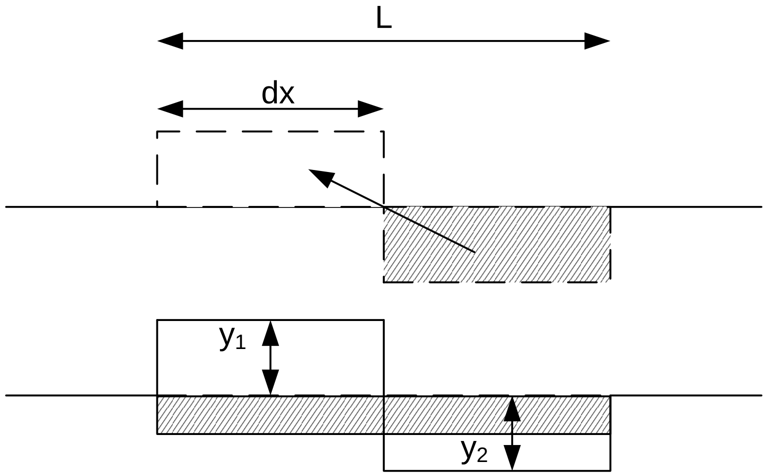

Figure 2.11: Illustration of determining the sand wave volume.

The procedure is similar for a more complex geometry:

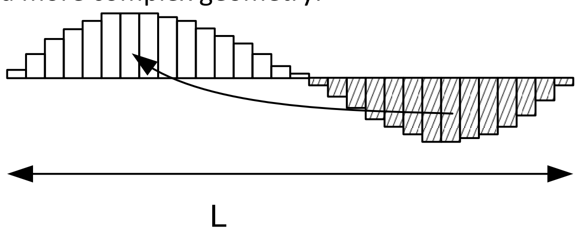

As the sand wave signal is given as an amplitude from the mean transect depth, this procedure also works for a series of sand waves.

The amplitude used must be the Sandwave (SW) signal and not the Sandwave signal + Larger Scale (LS) morphology because that would overestimate the volume. This is explained in figure 2.12.

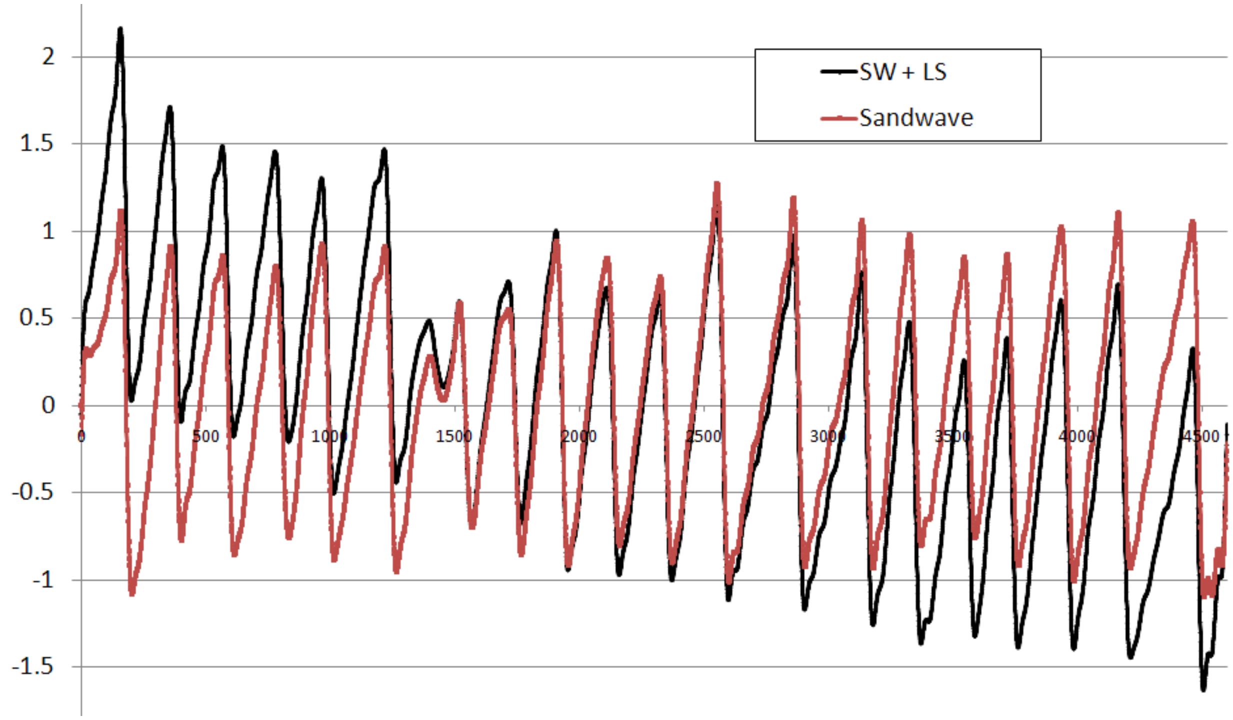

Figure 2.12: The large scale & sand wave (LS + SW) signal together accurately follow the transect. The separated sand wave signal is a bit off on the edges of the transect due to an underestimation of the LS morphology. The volume in the transect must be calculated with the SW signal in order to prevent overestimation as a result of underlying LS morphology.

Unfortunately the amplitude of the LS morphology is underestimated near the edges of the transect. And since the amplitude from the mean of the transect is approximated by Amplitude = LS + SW + ripples, this results in an overestimation of the sand wave signal and thus the volume. This can be solved by ignoring the first and last few metres from the volume analysis. The problem is addressed above in the section "edge effect". As the effect disappears some metres into the transect, the effect of this error is small if the length of the entire transect is sufficiently long.

Transport rate

The transport rate in the transect between recording [m^3 / (m^2*year)] is calculated similarly to the sand wave volume, see equation 2.2. dt is the time in days between recordings. $y_{i(t)}$ represents the height of a certain point i along the transect at time t. $y_{i(t-1)}$ is the same point a recording before.
Note that change in mean height is removed in order to only represent the change in shape and migration. This is partly also done in order to be able to compare the actual dynamics with those found with the model. The model uses the conservation of sediment and therefore does not show a change in mean depth over time.

$$dV\left[\frac{m^3}{m^2 year}\right] = \frac{1}{2}\frac{365}{dt}\frac{dx}{L_{trans}}\sum_{i=1}^{n}\langle\left|y_{i(t)} - y_{i(t-1)}\right| - \left(\overline{y_{\iota(t)}} - \overline{y_{\iota(t-1)}}\right)\rangle \qquad \textbf{2.2}$$

Example
The sand transport [m^3 / m^2] between two recordings (and between two time steps) in the modeling output) is equal to (or greater than):dV / L in figure 2.13:

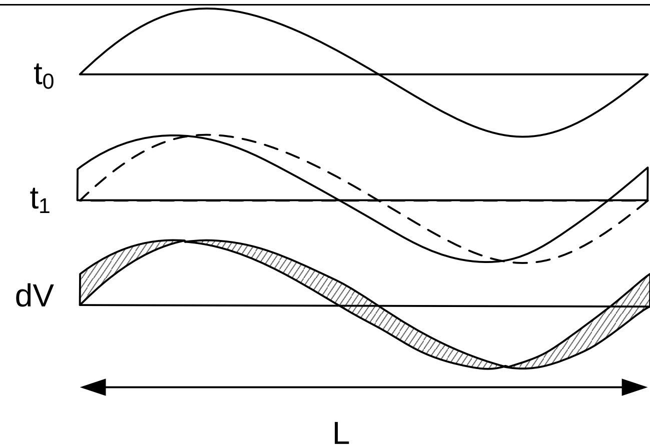

Figure 2.13: Volume transport example.

For the simple discrete geometry, the calculation of the volume transport is illustrated in figure 2.14:

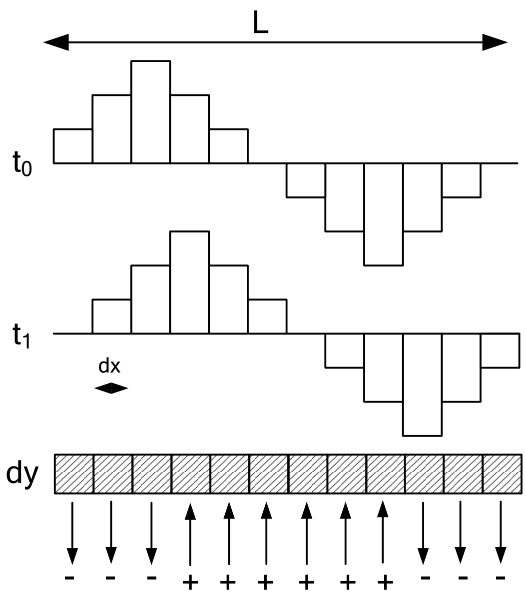

Figure 2.14: Transport in sand wave signal and model output.

In the example we have a domain of length L in which a sand wave moves one unit to the right between t_0 and t_1. Change in mean depth is not present / neglected.

$$\left(\overline{y_{\iota(t)}} - \overline{y_{\iota(t-1)}}\right) = 0$$

On average a Volume of 6 dy [m^3/m^2] was moved per 12 dx [m]. This is equal to 0.5 dy [m^3/m^2].
In formula:

$$dV = \frac{1}{2}\frac{365}{dt}\frac{dx}{L_{trans}}\sum_{i=1}^{n}\langle\left|y_{i(t)} - y_{i(t-1)}\right|\rangle$$

$$\sum_{i=1}^{n}\langle\left|y_{i(t)} - y_{i(t-1)}\right|\rangle = 12\ |dy|$$

$$dV = \frac{1}{2}\frac{365}{dt}\frac{12\,dx\,dy}{L_{trans}} = \frac{1}{2}\frac{365}{dt}\frac{12\,dx\,dy}{12\,dx} = \frac{1}{2}|dy|\frac{365}{dt}$$

Please note that the calculation this way only gives a trustworthy result if the migration of the sand wave in between recordings is not greater than half a sand wave length. This is not a real problem since for all our studied data: migration << L_{sw}.

2.4 Wind wave and current data

Current data: Matroos

MATROOS is a database in which modelled depth averaged flow velocities are stored for the Dutch coast. The model used to create the dataset accounts for the astronomical tide, wind effects, local water depths, temperature and salt gradients. The results are interpolated for any user specified location and can then either be presented or exported to e.g. excel.

The Northward and Eastward flow velocity are averaged separately over a 12 hour period to remove the M2 tidal signal. The remainder is assumed to be equal to the time dependent residual flow.

Wind and wave data

Wave height, wave period and wave direction were supplied by the UK Hydrographic office for the Varne studies (chapter 4) and were downloaded from the www.waterbase.nl website for the Eco Morf 3 area (chapter 5). Both datasets were recorded using measuring buoys. The buoys recorded the hourly average values for wave height, wave period and wave direction (this last one only if available).

Wave energy flux

To make a better distinction between the effective waves and less effective waves, and to visualize the direction the waves traverse, the wave height and angle are transformed into a wave energy flux. This also makes it possible to sum the fluxes over a period and determine for each period the direction in which the dominant flux was directed.

The wave height is transformed into wave energy through formula 2.3. To transform the wave height into wave energy flowing North, formula 2.4 is used. A negative value means the energy has a Southerly component. The same is done in formula 2.5, for the wave energy transported towards the East. A negative value means the energy is flowing in Westerly direction. In these formulae, E is the energy flux in Joules, the subscript denotes the direction, H is the wave height in metres, α is the angle of the wave in degrees with respect to the North (see figure 2.15), ρ is the density of water (1000 kg/m^3), g is the gravitational constant.

$$E = \frac{1}{8}\rho g H^2 \qquad \textbf{2.3}$$

$$E_{North} = \frac{1}{8}\rho g H^2 \cos\alpha \qquad \textbf{2.4}$$

$$E_{East} = \frac{1}{8}\rho g H^2 \cos(\propto -90^o) \qquad \textbf{2.5}$$

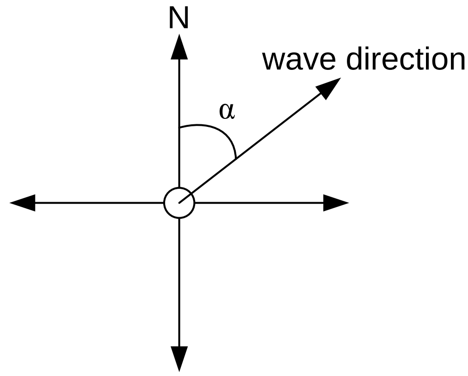

Figure 2.15: Definition of α (in degrees from UTM North)

Chapter 3. Methods: 2DV sand wave modelling: Sand Wave Code

The model used in this study is based on the model developed by Németh *et al.* (2006), further developed by Van den Berg & Van Damme (2006). Their work is based on analytical models such as made by Hulscher (1996) and Komarova & Hulscher (2000).

The model is a 2DV, non-linear, idealized, process-based model, named the Sand Wave Code (SWC).The latest refinement of this model was done by Sterlini (2009). In separate studies, she e.g. added surface waves and suspended sediment to the code.

This research focuses on the action of surface waves, so it continues with the version of the code that only described bed load transport with waves. A combination of waves and suspended sediment is not undertaken, as the time available is too limited to work out the complex re-suspension interactions between suspended sediment and surface waves. This is justified to some extend, as bed load transport is considered the dominant mode of transport in offshore tidal regimes, according to Németh *et al.* (2002).

Domain setup
The flow of the model is calculated using the hydrostatic shallow water equation for 2DV flow, as are shown in equations 3.1 and 3.2. The velocities in these equations are according to the domain setup shown in figure 3.1.
ξ is the surface water elevation in meters with respect to the mean water level. u represents the velocity in x – direction. w in the z-direction. Velocities in the y - direction are neglected as the model is 2DV. This is a fairly save assumption as the Coriolis force has a small effect on sand waves. The x-axis is chosen perpendicular to tidal forcing, F(t).

Boundary condition
The model uses periodic boundary condition, which means that values at the inflow and outflow boundary are equal. Physically this represents that the sand wave is in between identical sand waves. Equations 3.3, 3.4, 3.5 and 3.6 represent the boundary conditions. Equation 3.3 disallows flow perpendicular to the bottom. S is the partial slip parameter that is needed to compensate for the constant eddy viscosity A_v, which overestimates the shear stress at the bottom, see equations 3.4 and 3.9. $S = 0$ indicates perfect slip. $S = \infty$ indicates no slip. Friction at the free surface is 0 (3.5) and there is no flow across the surface (3.6).

Tidal forcing
In $F(t)$ (see eq. 3.7) the values for the parameters F_0, F_s and F_c depend on the unidirection tidal velocity (F_0) and the oscillatory velocity (F_s and F_c). ω is the angular frequency of the M2 tide. The forcing terms result in a M2 tide superimposed by a unidirectional residual current and no higher order harmonics. Hulscher (1996) shows that this is enough to catch most dominant physics is the formation of sand waves.

Shallow water equations:

$$\frac{\partial u}{\partial x} + \frac{\partial w}{\partial z} = 0 \qquad \textbf{3.1}$$

$$\frac{\partial u}{\partial t} + u\,\frac{\partial u}{\partial x} + w\frac{\partial w}{\partial z} = -g\,\frac{\partial \zeta}{\partial x} + A_v\frac{\partial^2 u}{\partial^2 z} + F(t) \qquad \textbf{3.2}$$

Boundary conditions:

$$w - u\frac{\partial h}{\partial x} = 0|_{\,seabed} \qquad 3.3$$

$$A_v\frac{\partial u}{\partial z} = Su|_{\,seabed} \qquad 3.4$$

$$\frac{\partial u}{\partial z} = 0\Big|_{\,surface} \qquad 3.5$$

$$w = \frac{\partial \zeta}{\partial t} + u\frac{\partial \zeta}{\partial x}\Big|_{\,surface} \qquad 3.6$$

Tidal forcing:

$$F(t) = F_0 + F_s \sin \omega t + F_c \cos \omega t \qquad 3.7$$

Typical values for the parameters are given in table 3.1. These values are chosen according to Németh *et al.* (2002) as typical parameters for the Southern North Sea.

parameter	unit	typical value
ω	[s^{-1}]	1.4e-4
A_v	[$m^2 \cdot s^{-1}$]	1.0e-2
S	[$m \cdot s^{-1}$]	8.0e-3

Table 3.1: Typical settings for the angular frequency (ω). The Eddy viscosity (A_v) and the Slip parameter (S).

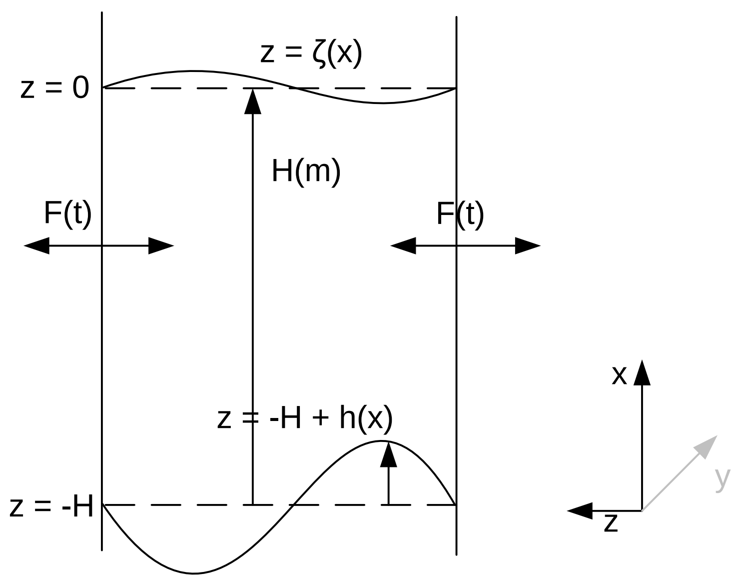

Figure 3.1: SWC domain setup with periodic boundary conditions.

As the flow velocities in the vertical direction are being calculated explicitly, bed load transport is modeled as a direct function of the bottom shear stress. The formula used is that of Komarova & Hulscher (2000), see eq. 3.9:

Bed load transport:

$$q_b = \alpha|\tau_b|^b\left[\tau_b - \lambda|\tau_b|\frac{\partial h}{\partial x}\right] \qquad 3.8$$

with $\boldsymbol{\tau_b}$ the shear stress at the sea bed:

$$\tau_b = A_v \frac{\partial u}{\partial z}|_{z=-H+h} \qquad \textbf{3.9}$$

Parameter α represents the proportionality constant that, among others, expresses sediment porosity and grain size, see Sterlini (2009). τ_b is the shear stress at the bottom. b is the power of transport. λ is the parameter that represents that sand is more easily transported downhill than uphill:

$q_b = 0$ if $\frac{\partial h}{\partial x} = \frac{1}{\lambda}$

For λ = 1.7 this means an angle of repose (β) of arctan(1/ λ) = 30°, see figure 3.2. Sand wave rarely attain slopes larger than 3° (or 5.2%), see Houthuys *et al.* (1994).

parameter	unit	typical value
α	[s^2m^{-1}]	0.3
$\lambda_{1,2}$	[-]	0.0 , 1.7
b	[-]	0.5

Table 3.2: Parameters: porosity constant (α), angle of repose (λ) and power of transport, based on Sterlini (2009)

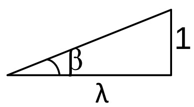

Figure 3.2: Bed form maximum angle of repose is a function of λ

The flow and the bottom are coupled through a continuity of sediment; eq. 3.10. As the SWC is a numerical model, the SWC uses a grid. The grid is a uniform rectangular grid in the horizontal direction; the vertical direction is non-uniform in order to have more resolution near the bottom and to save computation efforts at the same time.

Continuity of sediment:

$$\frac{\partial h}{\partial t} = -\frac{q_b}{\partial x} \qquad \textbf{3.10}$$

Including the wave angle

The influence of waves is added as an additional bed shear stress that is caused by the wave induced, orbital velocities near the bed. The relation between shear stress by the flow and by the current is shown in Sterlini (2009, eq. 3.9). Some changes had to be made to the code to represent the variable wave angle uses in chapters 4 and 5. Up to this point the wave - current system is approximated by the SWC as is displayed in figure 3.3, with φ equal to zero. Flow velocity is represented by the letter u, σ represents the wave period. φ is the angle between the (sinusoidal) waves and the current.

When the waves are placed under a non-zero angle, the wave orbital velocities in the component perpendicular to the direction of the tide under consideration become non-zero. This is done in this research. The next section shows that the orbital velocity perpendicular to the tidal direction adds to the orbital velocity in the component parallel to the direction of the tide.

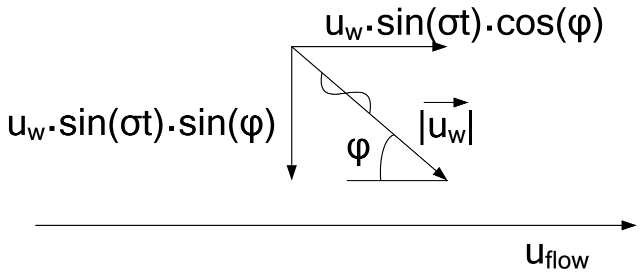

Figure 3.3: (Top view schematization of the system) Non collinear surface wave angle with the tide.

Considering that the tidal velocity is stationary during the surface wave period the set of equation for the depth average flow velocities become as in equations 3.11 and 3.12:

$$u = u_{\text{flow}} + u_{\text{wave}} \cdot \sin\sigma t \cdot \cos\varphi \qquad \textbf{3.11}$$

$$v = \qquad u_{\text{wave}} \cdot \sin\sigma t \cdot \sin\varphi \qquad \textbf{3.12}$$

The sediment transport in x and y direction is:

$$\left(q_x, q_y\right) = \alpha\left(u_x, u_y\right)^3 = \alpha(|\vec{u}|^2 \cdot \vec{u}) = \alpha\left((u^2 + v^2) \cdot (u, v)\right) \qquad \textbf{3.13}$$

For the 2DV simulation ignore the transport in the y-direction. The combined wave – current velocity in the x-direction averaged over the wave period is:

$$\langle {u_x}^3 \rangle = \langle (u^2 + v^2) \cdot u \rangle \qquad \textbf{3.14}$$

Working this out with equation 3.11 and 3.12 yields:

$$\langle (u_{\text{flow}} + u_{\text{wave}} \cdot \sin(\sigma t) \cdot \cos\varphi)^2 + (u_{\text{wave}} \cdot \sin(\sigma t) \sin\varphi)^2) \cdot (u_{\text{flow}} + u_{\text{wave}} \sin(\sigma t) \cos\varphi) \rangle \qquad \textbf{3.15}$$

Integrating over the surface wave period, using: $T = \frac{2\pi}{\sigma}$, gives:

$$\frac{1}{T}\int_0^T \langle {u_x}^3 \rangle dt = {u_{flow}}^3 + \left(\frac{1}{2} + cos^2(\varphi)\right) {u_{\text{wave}}}^2 \cdot u_{\text{flow}} \qquad \textbf{3.16}$$

Using ϕ = 0 rad (mod π) this formula transforms into Sterlini (2009)-(eq. 3.15). If you define $\gamma = \left(\frac{1}{2} + cos^2(\varphi)\right)$, it indeed has a value between 1/2 and 3/2. Sterlini (2009) takes the value of γ for simplicity equal to 1, which means the waves have an angle of ±45° (mod π radials).
The formula physically means that even if the waves are perpendicular to the tidal current the stirring action of the wave induced velocities still adds to the sediment transport in the x direction, due to non-linear wave – current interactions.

Doppler effect

Taking a non-zero angle between the waves and the current causes changes in the Doppler effect described by Sterlini (2009) after Mei (1999). Using the same approximation, Sterlini (2009, eq. 3.1) changes into:

$$\omega = Uk * \cos(\varphi) + \sqrt{gk \cdot \tanh{(k \cdot h)}} \qquad \textbf{3.17}$$

Sterlini (2009, eq. 3.2), representing the conservation of wave action, changes into:

$$\frac{d}{dx}\left(\left[U \cdot \cos(\varphi) + C_g\right]\frac{E}{\sigma}\right) = 0 \qquad \textbf{3.18}$$

The physical meaning of this is explained in Mei (1999). For $\varphi = \pm\frac{\pi}{2}$ the current does not influence the waves. For $U\cos(\varphi) < 0$ the current is opposing the waves. In this case, if $-\mathrm{U}\cos(\varphi) > \sqrt{gh}$, no waves of any length are possible. For $-U\cos(\varphi) = \mathrm{C_g}$ wave energy is held in place, although crests appear to move upstream. Depending on the size of $-U\cos(\varphi)$ with respect to Cg wave energy is moved up- or downstream. For $\mathrm{U}\cos(\varphi) > 0$ the wave crests and wave energy are swept along by the current.

Wave assumptions/simplification

- Surface waves are presumed not to break (as the water is relative deep compared to the amplitude of the wind driven surface waves at locations were sand waves occur). As a result, linear wave theory is considered to be valid.
- It is assumed that the currents influence the wave characteristics, while the waves do not influence the currents.

Simulations

The simulations are based on the assumption of weak non-linearity, which assumes that the wavelength chosen in the linear regime is maintained for the non-linear regime. For small initial perturbations, 3 time steps were simulated for a range of domain lengths. The length that showed the fastest growth, the fastest growing mode (FGM), is chosen as the length for the full simulation. This technique is similar to the linear stability analysis performed by Hulscher (1996).
An example of determining the FGM is shown in figure 3.4. For wave lengths larger than 130 meter the growth rate is positive and sand waves develop. The FGM is at about 280 metres.
Saturation of the sand waves is reached when sediment transport uphill balances with sediment flux downhill due to the angle of repose of the sand wave. This is the $\lambda|\tau_b|\frac{\partial h}{\partial x}$ term in equation 3.8.
The chosen parameter settings and simulation results are discussed in chapters 4 and 5.

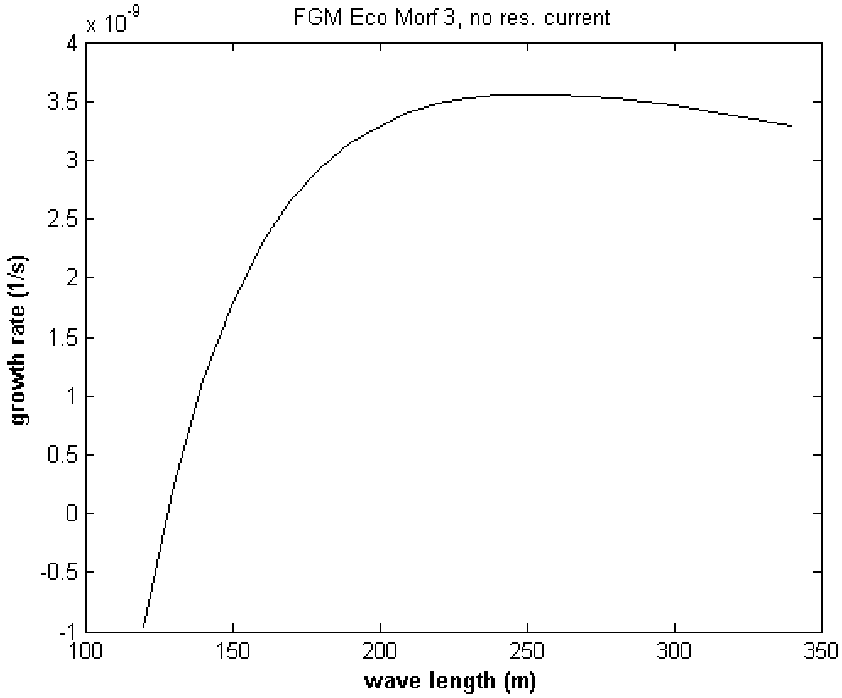

Figure 3.4: Example plot of the calculation of the Fastest Growing Mode.

Processing the simulation results

The results for the sand wave code are analyzed exactly the same as the shape attributes of the transects are, see chapter 2. The difference is that the output of the model is by itself a “transect” for each time step. E.g. the model has sediment continuity and predicts for just one wave length, so there is no need to separate the larger scale morphology from the sand wave signal with a Fourier analysis.

The output of the SWC is illustrated in figure 3.5. The crest and troughs are selected as being the highest and lowest points at each time step. The horizontal step size is the sand wave length divided by the number of step in the horizontal direction (Npx). As the model gives the height for Npx discrete x coordinates, the maximum error in the crest and trough location is equal to the length of the domain divided by Npx. The maximum error as a result of this limited numerical precision in the L_{crest} / L_{trough} ratio is equal to (4 / Npx). In case of 30 horizontal steps, the error is ±15%.
The location of the up and downward crossings are interpolated linearly between the first and last positive / negative value of the sand wave code output. The error in this is neglect able.

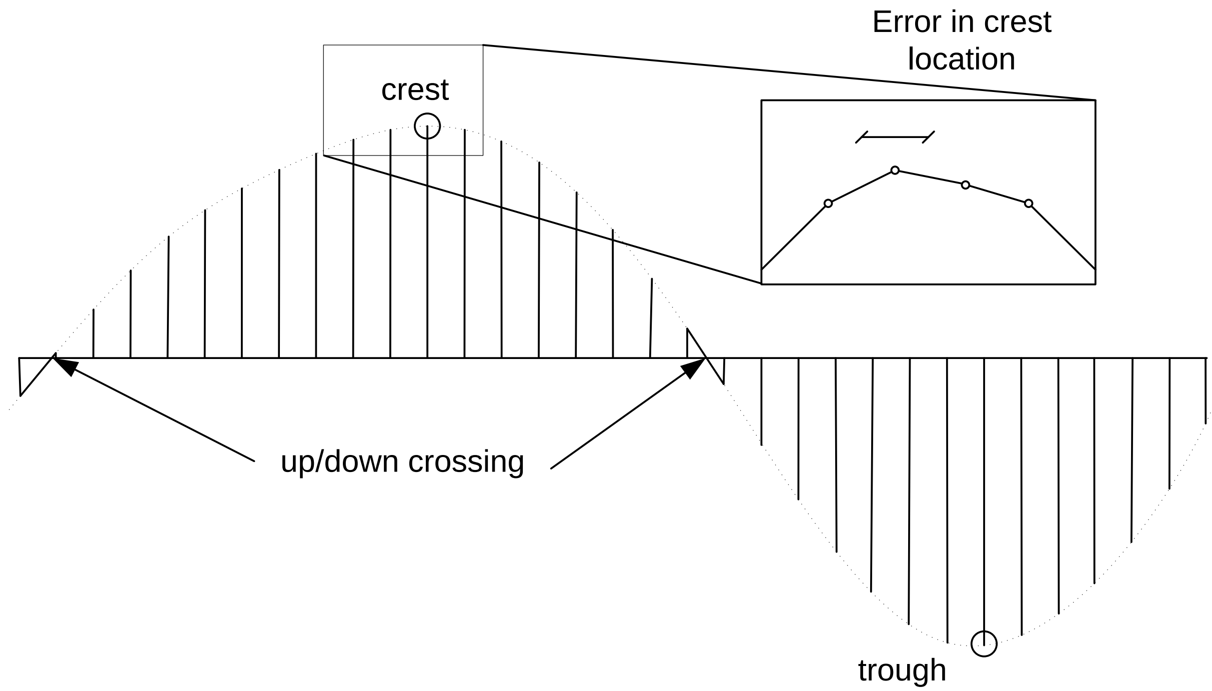

Figure 3.5: Illustration of the SWC output for Npx horizontal steps. Choice of the crest, trough and up/down crossing points of the SWC simulations

Chapter 4. Results: Varne area

Chapter summary
Bathymetry measurements at the Varne bank near the UK show that fair weather sand waves with tall and narrow crests collapse under stormy situations. The sand waves that were built up during a long period of fair weather are reduced about 1 meter in height over the period of 66 days with multiple storms that have waves higher than 2 metres, reducing the volume in the sand wave by 10-20%.
One of two transect shows a reversal of the horizontal asymmetry (expressed as the ratio L_{stoss} / L_{lee}).

Simulations with the Sand Wave Code, an idealized model that is accurately able to predict sand wave height, migration and net transport rate, show that differences in the angle of surface waves with respect to the tide are by themselves not enough to explain the back and forth migration of sand waves.
The stirring action of sufficiently high waves is however able to change the L_{stoss} / L_{lee} ratio of the simulated bed forms within time scales of several weeks. The model shows the change in asymmetry is almost instantaneously with respect to the wave height forcing and is comparable with the asymmetry in the post storm empirical data set. The reduction in bed form height can not be entirely explained by wave stirring alone as the simulated height reduction is a lot smaller than the reduction in the empirical dataset. Furthermore, the timescale for height adjustments is, with 20 to 50 weeks, significantly (and unrealistically) longer than the duration of storms in general and particularly those shown in the empirical data set.
Recommended is to update the model to be able to run simulations in which the residual flow is varied according to as a function of the wind speed and/or wave forcing.

Introduction
This chapter presents the morphodynamics and geometric properties of the bathymetry and the surface wave climate at the Varne bank (UK) in the Dover Strait. The last section shows the modelling results. This is done to see if and how temporal variations in the surface wave climate attribute to bed form changes.

The Varne bank is located in the Dover strait near the UK, see figure 4.7 (4). The bathymetry data under investigation was gathered just north of the sand bank. Here, sand waves cover the bottom with their crests orientated perpendicular to the main direction of the tidal current, which has a residual in the north-eastern direction. This is approximately parallel to the geometry of the channel.

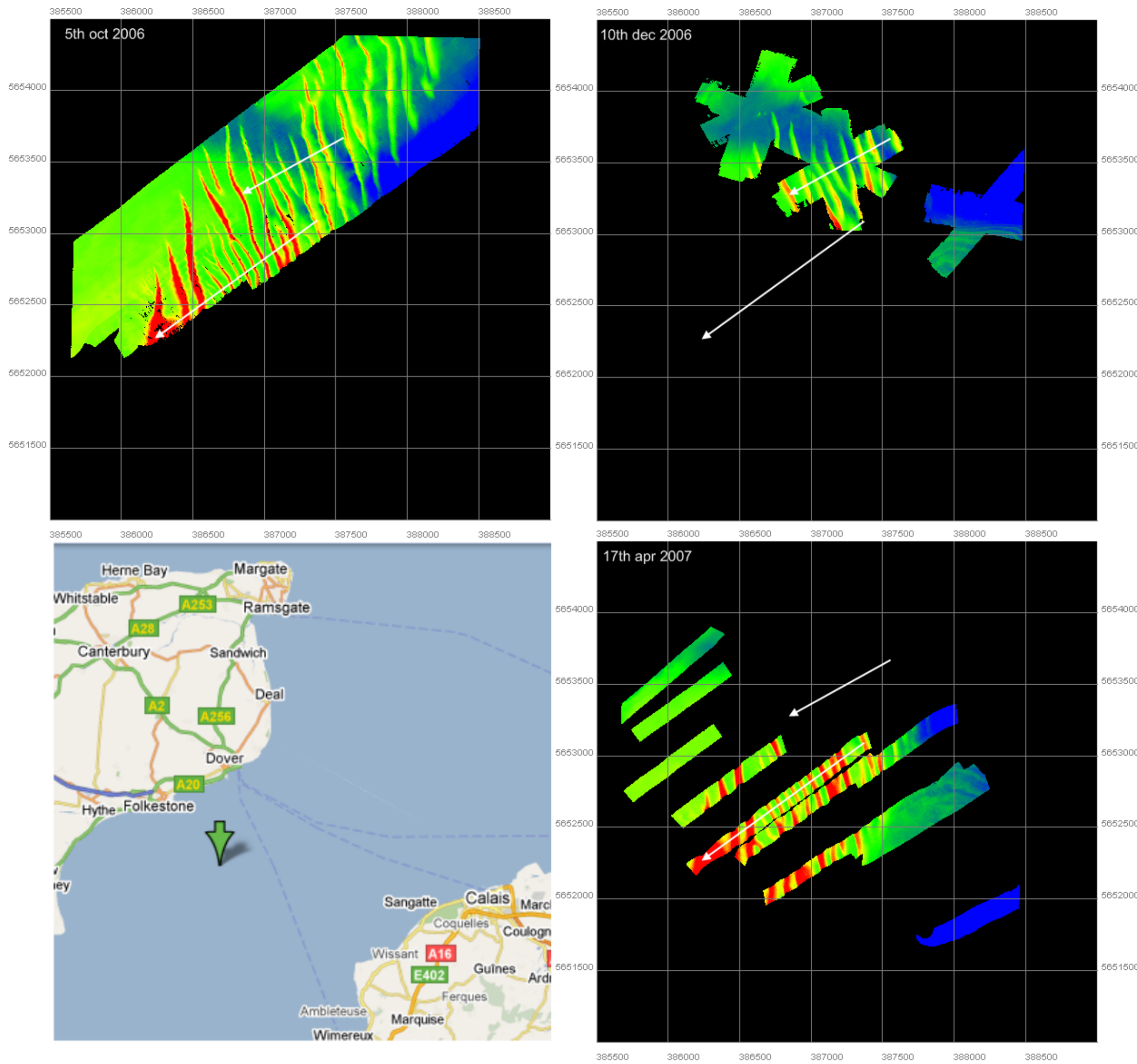

Figure 4.1: (clockwise) 1-3: Plot of the measurements taken at the 5th of October 2006, the 10th of December 2006 and the 17th of April 2007. The two arrows indicate the locations and direction (left to right) of the two transects analysed. These are displayed in figure 4.2 and figure 4.3. The grid scale is 500 metres. The colours indicates the local depth, blue to red corresponds with a depth of 30 to 21 metres. 4: Google maps plot of the Varne bank location in the Dover Strait.

The location of the two transects that were studied are shown in white arrows in figure 4.1 (1-3). The amount of available, overlapping data points with sand waves was limited. The transects were taken almost perpendicular to the crests. Transect 1 lies most northerly of the two transects. This transect was taken with an angle of 240° to the North. The second transect was taken with an angle of 233° to the North. The interpolation settings and coordinates are given in table 4.1.

sampling parameters	
radius (m)	2.5
start x	385500
start y	5651000
dx (m)	1.0
dy (m)	1.0
nx	3500
ny	3500

Transect 1	start	end	length (m) / angle (deg)
x	387588	386763	956
y	5653713	5653229	240°

Transect 2	start	end	length (m) / angle (deg)
x	387318	386443	1091
y	5653091	5652439	233°

Table 4.1: (Left) Interpolation sampling parameters. (Top right) Transect 1 coordinates, length and direction of the profile in degrees from the North. (Bottom right) Similar for transect 2. X and Y are in UTM coordinates.

4.1 Morphodynamics

The bed forms that were found are about 80 metres in length and 4 metres in height. The transects are plotted in figure 4.2 and figure 4.3. Please note that the vertical scale is different for the two plots. In general both transects display short and tall crests at the initial measurement on the 5th of October 2006. They show broad, flatter crests with shorter troughs at the second recordings. The second recordings were made on the 10th of December (2006) and the 17th of April 2007 for the first and second transect respectively.

The characteristics and their dynamics of the first transect are summed up in table 4.2 and table 4.4. The definition of these characteristics are given in chapter 2.1 and the methods used to obtain their values are described in chapter 2.3.

The first transect

The first transect shows the sand waves reverse their horizontal asymmetry in the period October 2006 – December 2006. The L_{lee} / L_{stoss} ratio changes from 2.7 to 0.5 and thus inverts effectively. At the second recording the longest and shortest side on average still had the same length, 66 meters versus 30 metres. The mega ripples are no longer present at the North East side of the bed forms. These can now be seen on the South West side. An example of the asymmetry change can also be clearly seen in the shape of the bed forms that are displayed around x coordinate 200 and 300. The steep side of the sand wave at the first measurement is opposite to the steep side of the same bed form at the second measurement.

In the same period the bed form heights are reduced by 26%, corresponding to about 1 meter. In table 4.4 we see that this is only a result of a lowering of the crests and not a change in the depths of the troughs. The absolute change in crest and trough depth is -1.48 m and -0.35 m. If we subtract the mean change in bed level of the entire transect of -0.31 m, we see that the change in bed form height is only a result of a change in crests height.

The crests on average migrated 25 metres to the North East, while the troughs on average migrated 12 metres to the South West. A change of (-)25 to (+)12 metres in 66 days corresponds with a migration rate of (-)139 to (+)66 m/year. This is a huge migration rate and a very large spread in rates. Part of this high migration rate is caused by a large shape change and not so much a displacement of the entire bed form.

The bed form indicated with number 3 is considered a separate sand wave in the FFT analysis. Due to its small height and length, compared to the rest of the bed forms, it is considered to be an outlier and it is left out of the analysis.

The second transect
(See table 4.3) The bed forms in the second transect are a lot less asymmetrical than the bed forms in the first transect. The L_{lee} / L_{stoss} ratio changes from 1.2 to 1.9 in the period between the 5th of October and the 17th of April 2007. In between recordings the L_{lee} and L_{stoss} adjusted to each other (L_{stoss} +17%, L_{lee} -18%).
The sand waves that can be seen between x=800 and x=900 are ignored in the shape comparison as the first recording displays two bed forms that have formed into one at the second recording. Mega ripples are not present at the first recording, but they can be seen on the North East side of the bed forms in the second recording.

The height reduction of the sand waves is again 1 metre, see table 4.3. It is shown in table 4.4 that this again is predominantly a change in crest level: -0.49 – 0.47 = -0.96 m. The troughs have changed +0.40 m, this almost completely the result of a change in average bed level. 0.40 – 0.47 = -0.07 m.
The migration is in North-Easterly direction for both the crests and the troughs. On average the displacement of the crests is -11 metres, versus -17 metres for the troughs. Given the time interval of 192 days between recordings, the migration rate is thus between -22 and -32 metres / year. The maximum migration rate of 260 m/year rate of migration is a result of the drastic shift in trough position between bed forms 8 and 9. (See Figure 4.2) The L_{stoss}/L_{lee} ratio susceptible to the lowest point of the (long) trough. The lowest point in the trough of the first recording (black) of the first transect between bed form 8 and 9 is considerably closer to wave 8 than it is in the second recording (blue).

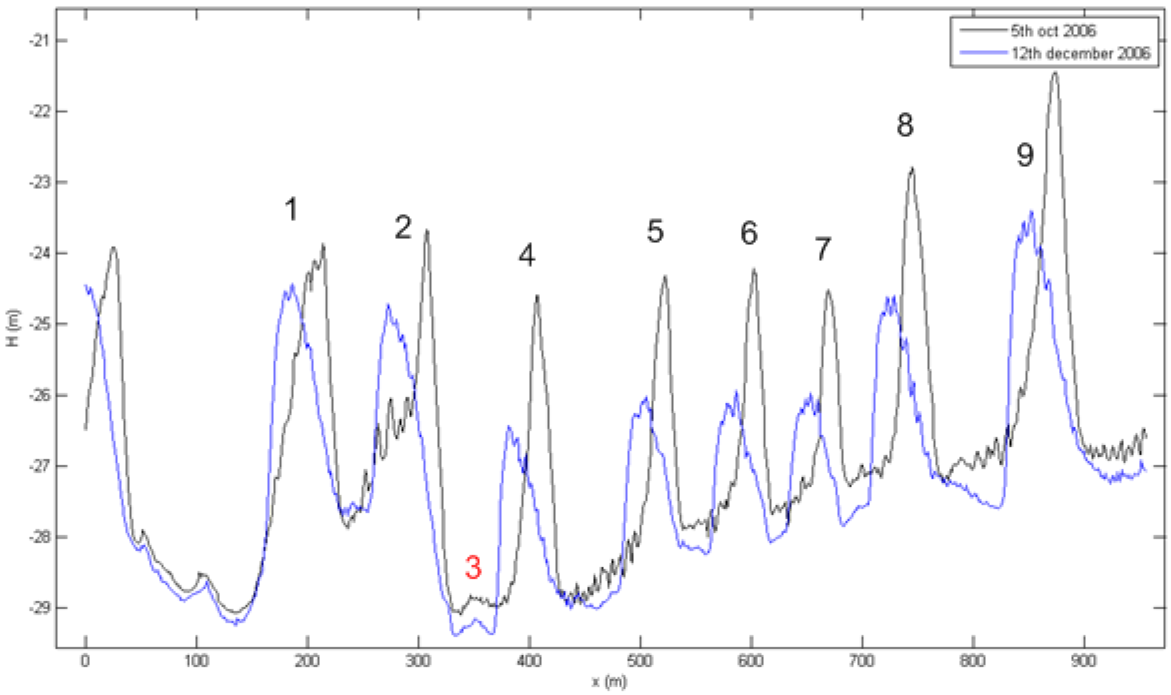

Figure 4.2: The first transect displayed in figure 4.1. To the left is the North East, to the right is the South West. Vertical scale is not equal to figure 4.3. The area pointed out by bed form 3 was left out of the shape analysis.

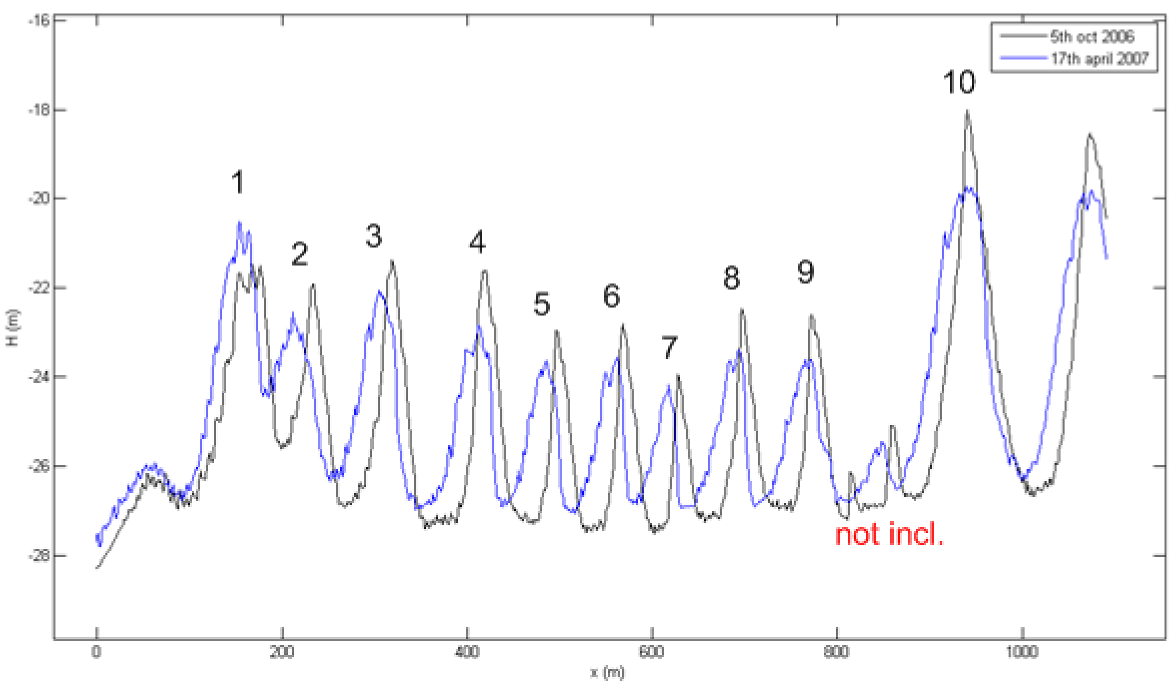

Figure 4.3: The second transect displayed in figure 4.1. To the left is the North East, to the right is the South West. Vertical scale is not equal to figure 4.2. The two bed forms between 9 and 10, that were merged into one in the second recording were not included in the analysis.

Transect 1

5th of October 2006	L (m)	H (m)	L_{stoss} (m)	L_{lee} (m)	L_{stoss} / L_{Lee} (-)
min	64	2.85	39	18	1.5
mean	92	4.10	67	25	2.7
max	136	5.41	98	38	4.3
st dev	23	0.80	19	7	0.8

10th of December 2006	L (m)	H (m)	L_{stoss} (m)	L_{lee} (m)	L_{stoss} / L_{Lee} (-)
min	60	1.99	21	33	0.3
mean	96	3.05	30	66	0.5
max	138	4.11	47	99	1.1
st dev	34	1.16	12	27	0.3

differences	L (m)	H (m)	L_{stoss} (m)	L_{lee} (m)	L_{stoss} / L_{Lee} (-)
absolute	4	-1	-37	41	inverted
%	4%	-26%	-55%	161%	

Table 4.2: The changes of transect 1 over the period October 2006 until December 2006. Note the bed forms have become about a meter lower, which is a height reduction of 25%. The Llee / Lstoss ratio has inverted.

Transect 2

5th of October 2006	L (m)	H (m)	L_{stoss} (m)	L_{lee} (m)	L_{stoss} / L_{Lee} (-)
min	55	3.19	23	27	0.7
mean	86	4.89	47	39	1.3
max	137	8.52	86	70	3.3
st dev	26	1.47	19	13	0.7

17th of April 2007	L (m)	H (m)	L_{stoss} (m)	L_{lee} (m)	L_{stoss} / L_{Lee} (-)
min	56	2.45	30	21	0.8
mean	86	3.85	55	32	1.9
max	143	6.58	80	63	3.0
st dev	24	1.13	15	14	0.7

differences	L (m)	H (m)	L_{stoss} (m)	L_{lee} (m)	L_{stoss} / L_{Lee} (-)
absolute	1	-1	8	-7	Increased 50%
%	1%	-21%	17%	-18%	

Table 4.3: The changes of transect 2 over the period October 2006 until April 2007.

dx_{crest} (m)	5 October 2006 - 12 December 2006	5 October 2006 17 April 2007	dx_{trough} (m)	5 October 2006 - 12 December 2006	5 October 2006 17 April 2007
min	-34	-21	min	-6	-29
mean	-25	-11	mean	12	-17
max	-20	-4	max	47	3
stdev	5	5	stdev	17	11

dx_{crest} rate (m/y)	5 October 2006 - 12 December 2006	5 October 2006 17 April 2007	dx_{trough} rate (m/y)	5 October 2006 - 12 December 2006	5 October 2006 17 April 2007
min	-189	-39	min	-35	-55
mean	-139	-22	mean	66	-32
max	-112	-7	max	260	6
stdev	25	10	stdev	95	22
dt (days)	66	128	dt (days)	66	192

dh_{crest} (m)	5 October 2006 - 12 December 2006	5 October 2006 17 April 2007	dh_{trough} (m)	5 October 2006 - 12 December 2006	5 October 2006 17 April 2007
min	-2.06	-1.34	min	-0.53	-0.10
mean	-1.48	-0.49	mean	-0.35	0.40
max	-0.51	0.75	max	0.16	1.17
stdev	0.54	0.57	stdev	0.23	0.35

dh_{mean} (m)	5 October 2006 - 12 December 2006	5 October 2006 17 April 2007
	-0.31	0.47

Table 4.4: Change in crest and trough location and the change in depth of the crests and troughs for the two transects (1. left and 2. right). Row (1) indicates the change in coordinates (min, mean, max and standard deviation). These were extrapolated to yearly values in row (2). A negative sign for the change in x coordinate means a migration in North Eastern direction, a positive sign means a migration towards the South West. In row (3) the dh_{trough} and dh_{crest} are given. These indicate the absolute change in crest and trough depth. A negative sign for dh_{trough} means the troughs have become deeper. In order to compare the relative changes, dh_{mean} must be subtracted from dh_{crest} and dh_{trough}. dh_{mean} is the average change in bed level over the entire profile. A negative sign means the transect is deeper on average. This is further explained in the text describing figure 2.10 in chapter 2.

Sand wave Volume and transport

The volume of the sand waves is listed in table 4.5. The volume of the sand waves is about 2 to 4 times larger than the volume of the sand waves in the Eco Morf 3 area, see table 5.5. This has to do with the fact that the sand waves are higher. The rate of transport is 17 to 24 times larger, interpreted as a result of the higher dynamics in the Varne area.

	transect 1		transect 2	
	5 October 2006	12 December 2001	5 October 2006	17 April 2007
V [m^3/m^2]	0.53	0.48	0.80	0.72
	5 October 2006 - 12 December 2006		5 October 2006 17 April 2007	
dV [$m^3/(m^2 \cdot year)$]	2.44		1.18	

Table 4.5: Volume of the transect in m^3/m^2 and Volume change of the transect in m^3 / (m^2 .year). The rate represents the rate with which the height changes averaged over the length of the transect.

Regional migration

The cross correlation studies were performed on the areas shown in figure 4.4. The results are shown in table 4.6.

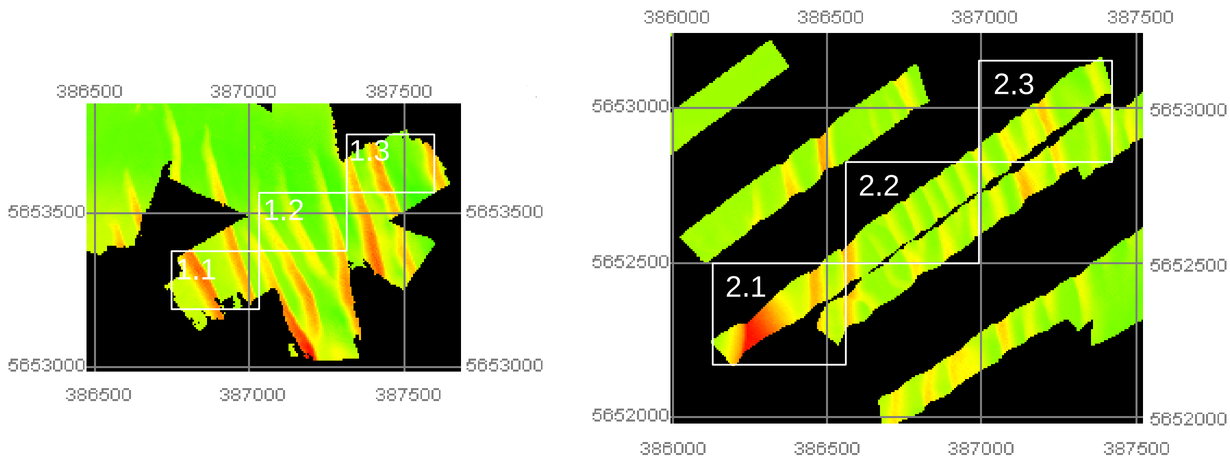

Figure 4.4: Cross correlation areas. The numbering is according to the corresponding transect number (1 – 2) and sub area (1-3). The subareas are 280 m by 193 m (areas 1.1-1.3) and 413 m by 307 m (areas 2.1-2.3).

October 2006 -	December 2006			
area 1.1		dx [m]	20	xcorr
angle [deg]	81	dy [m]	3	0.88
direction name	E	rate [m/year]	**112**	
area 1.2		dx [m]	10	xcorr
angle [deg]	25	dy [m]	21	0.87
direction name	NNE	rate [m/year]	**129**	
area 1.3		dx [m]	15	xcorr
angle [deg]	111	dy [m]	-6	0.93
direction name	ESE	rate [m/year]	**89**	
Fourier analysis	direction*			
crests	ENE	rate [m/year]	**139**	
troughs	WSW	rate [m/year]	**66**	

*direction
+ = 60 to 240 (WSW)
- = 240 - 60 = (ENE)

October 2006 -	April 2007			
area 2.1		dx [m]	5	xcorr
angle [deg]	22	dy [m]	12	0.97
direction name	NNE	rate [m/year]	**37**	
area 2.2		dx [m]	22	xcorr
angle [deg]	118	dy [m]	-12	0.88
direction name	ESE	rate [m/year]	**71**	
area 2.3		dx [m]	9	xcorr
angle [deg]	39	dy [m]	11	0.93
direction name	NE	rate [m/year]	**41**	
Fourier analysis	direction**			
crests	NE	rate [m/year]	**22**	
troughs	NE	rate [m/year]	**32**	

**direction
+ = 53 to 233 (SW)
- = 233 to 53= (NE)

Table 4.6: Cross correlation results compared with the Fourier results. The first three rows show the cross correlation results. The angle [deg.] is the migration angle with the North, given displacement dx [m] and dy [m]. A positive dx corresponds with a migration towards the East. dy is the migration towards the North. The angles were transformed to named wind direction for easier comparison. The rate is the displacement extrapolated to yearly values, given the dt of 66 and 192 between recordings of areas 1 and 2 respectively. xcorr [-] shows the correlation between the two recordings. The last row is the rate and direction of the Fourier analysis, see table 4.4. A positive number in that table corresponds with a approximately SW migration (towards 240 and 233 degrees), a negative number is a migration towards the NE (approx.)

The rate and direction of migration shown in the 2D plain correlation compare well with the rate and direction found in the Fourier analysis. The cross correlation is not able to distinguish between the different directions of migration of the crests and troughs shown in the FFT analysis of the first transect. The high rate shown in the first area (dt = 66 days) are shown not to be maintained over the longer period that is between the recordings of the second area. All cross correlations showed high along crest correlation.

The results for the cross correlation method show larger rates than the results for the Fourier analysis. This is because the FA method considers migration normal to the sand wave crests, while the cross correlation method looks at the direction and rate of maximum migration.

4.2 Wind, wave and flow data

Weather data was analyzed to see if and how the found morphodynamics might be attributed to temporal variation in the surface waves.

For the Varne area the surface wave climate was measured at the nearby Sandetti buoy. The dataset is taken from January 2006 until May 2007. The wave height, wind speed and wind direction are plotted in figure 4.5, figure 4.6 and figure 4.7. The red lines indicate when the bathymetries, displayed in figure 4.2 and figure 4.3, were recorded.

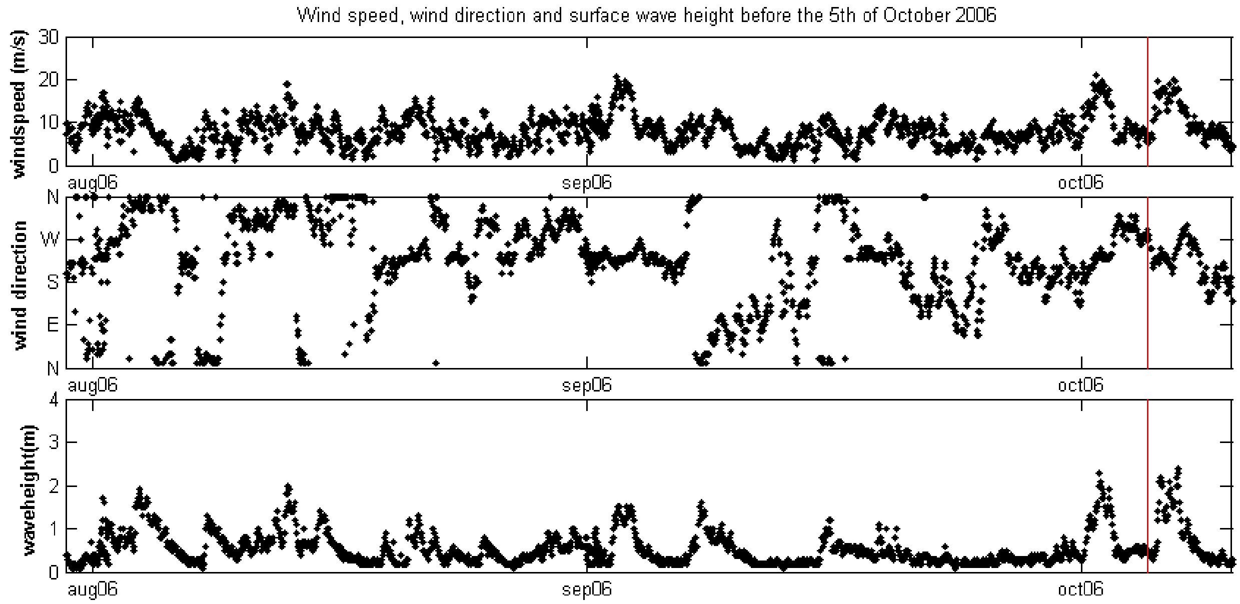

Figure 4.5: The Sandetti measured wave height (m), wind speed (m/s) and wind direction. Dataset August 2006 – April 2007. The red lines indicated when the bathymetry was recorded. The wind direction was measured in degrees from the North. E.g. 180 degrees corresponds with S in the plot, meaning the wind comes from the South. 0 and 360 are the same direction; the North.

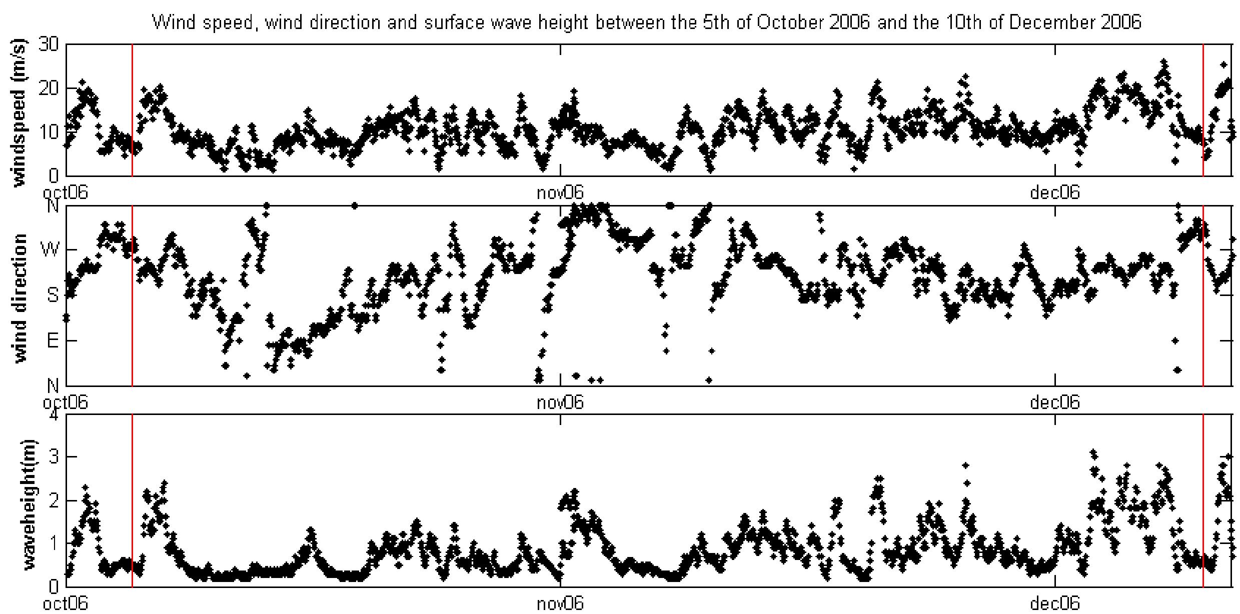

Figure 4.6: See caption at figure 4.5

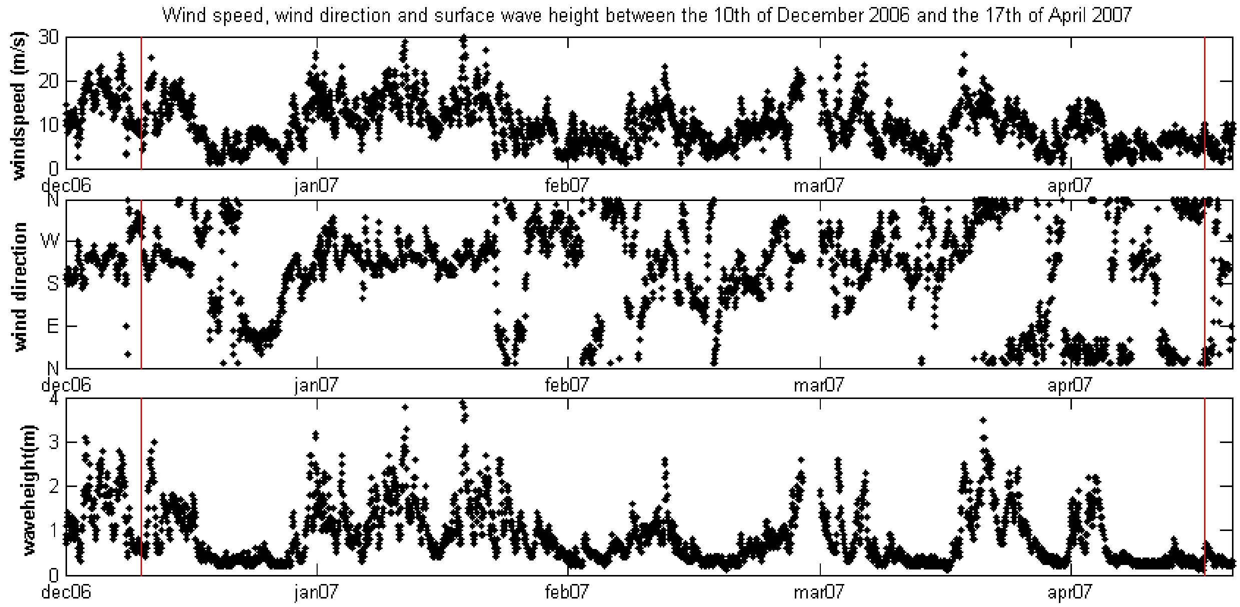

Figure 4.7: See caption at figure 4.5. Note this plot has a different horizontal scale from the first two as it displays a longer period.

The period before each recording was chosen the same for each plot: 66 days. This was the smallest period in between recordings.

The strongest winds and highest waves can be seen in the period before the second recording of the second transect. In general, wind and wave come from the South-West. In the third period a period with wind from the North East is also seen.

To assess to the relative contribution that waves from each direction might have on the sand wave migration, the wave height and wave angle are transformed into a wave energy flux according to the methods described in chapter 2. The results are shown in figure 4.8 and are quantitatively per general direction given in table 4.7.

period		(N) 310^o – 30^o	(SW) 180^0-270^o
July 30th 2006 -	Oct 05th 2006	0.4	0.4
Oct 05th 2006 -	Dec 12th 2006	0.2	0.7
Dec 12th 2006 -	April 17th 2007	0.2	0.6
July 30th 2006 -	April 17th 2007	0.2	0.6

Table 4.7: Wave energy transport from the NE (310^o – 30^o) and the SW (180^o - 270^o) in percentage

In the period before the first bathymetry was recorded, shown in figure 4.8 [a], the peak in wind that accounts for 40% of the transported wave energy is from the South West. A second order peak describing also 40% of the total wave energy is from the North. This peak is however more spread out over the directions. The remaining 20% is spread out over the directions. In the second period (b) 70% of the wave energy is from the South West and 20% from the North – North West. The third period (c) shows approximately 60% of the wave energy is from the SW and 20% of the wave energy is from the North East. The rest of the wave energy transport is spread out over the wind directions.

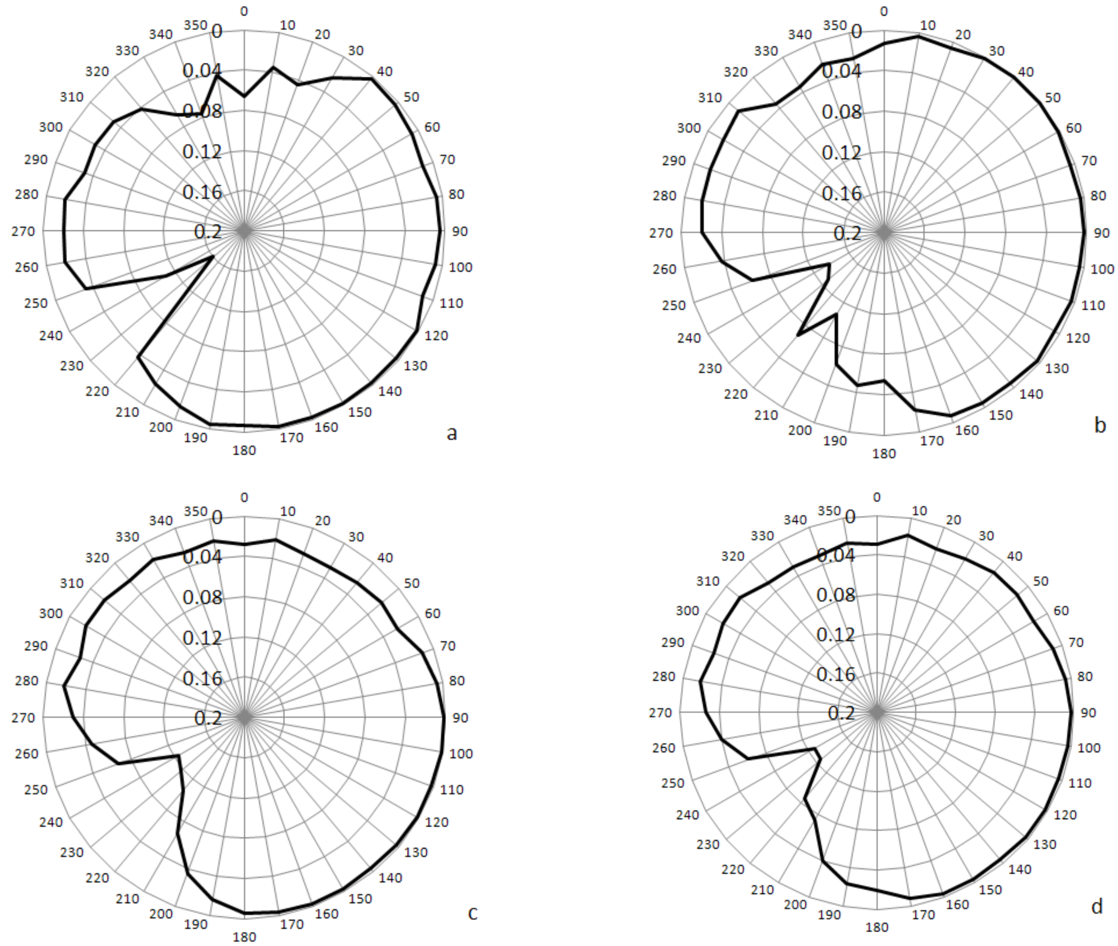

Figure 4.8: Direction the waves come from - Wave energy frequency distribution. [a] Period 30th of July 2006 – 5th of October 2006. [b] 5th of October 2006 – 12th of December 2006. [c] 12th of December 2006 – 17th of April 2007. [d] (all data) 30th of July – 17th of April 2007.

Bathymetry and weather data results

In figure 4.5 it can be seen that the initial recordings of transect one and two in October 2006 were made after a period of calm weather, with only one small, 2 day lasting storm with waves higher than 2.0 metres just prior to the recording. Before that a period of 8 weeks passed without waves higher than 2 metres. The high, narrow crests with long troughs that are shown in the initial recording of both transects are therefore interpreted as the fair weather state of the system. This recording was made after a long period of fair weather with just one small storm just prior to the recording.
Figure 4.8-a shows that wave energy in this period came predominantly from the South West.

The second recording for the first transect was done after a period of two months with multiple storms that had waves higher than 2.0 metres. Wind direction in this period is again predominantly from the South West, but also has a great part with wind from the North East and North West. Figure 4.6 shows that the wind from the North (so directed towards the South) was more in the beginning of this period and wind towards the North East more to the end.
In this period the bathymetry (see table 4.4) moved its crests to the North East and its troughs to the South West.
It could well be that the sand waves in this period moved back and forth, hence explaining the difference in change of location of the crests and the troughs. The megaripples on the second recording of the first transects indicate that the last direction that the system migrated in indeed was towards the North East. Unfortunately, no in between recording exists to support this.

The migration rate shown at the first transect is not continued in the long period between the recordings of the second transects. However, the migration of the second transect can be seen in both crests and troughs, meaning the sand waves were moved more as a whole in this period.
The second recording of the second transect also shows a period with storms from the South West in the period January 2007 – February 2007 and in March 2007. This period was followed by a short period with waves from the North East just before April 2007. The high migration rate seen at the first transect are not maintained over the longer period between recordings of the second transect even though the storms were stronger and the surface waves were higher.

In figure 4.9 we summarized the result of the bathymetry analysis and the wave data into a single image. Migration found by the cross correlation method was found to be predominantly in North Eastern direction. The wave direction is towards the North East.

The L_{stoss} / L_{lee} ratio of the bed forms of the second recording of transect two is not as large as the second recording of the first transect. This is interpreted as a possible reduction of the asymmetry by the South West going wind and waves just before April 2007. Unfortunately no recording of the bathymetry prior to this South West oriented storm just before April 2007 was available to support this conclusion. The period between bathymetry recordings for the second profile, 192 days, might be too large to decisively conclude anything.

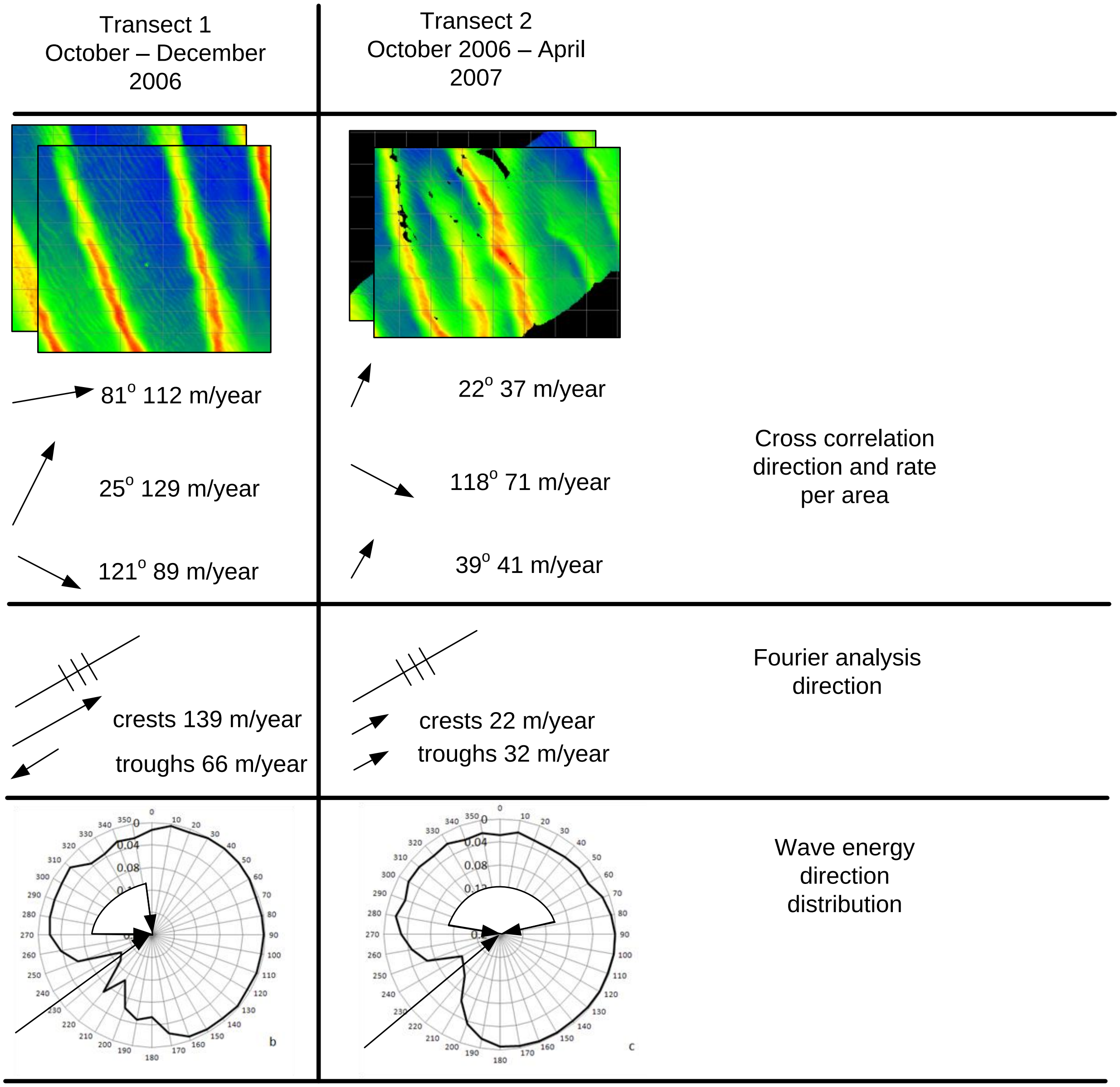

Figure 4.9: Summary of the change in bathymetry, and the forcing by the waves.

The question we need to answer is if the wind direction can indeed be used for the wave direction. If so, the second question we need to answer is if wind speed is independent from the time dependent residual flow.

Wind direction versus wave direction

This section discusses if assuming wind direction and wave direction are interchangeable is just or not.

Wave directions were not measured by the Sandetti buoy, but were measured by the vessel that recorded the bathymetry. These measurements were recorded in the hourly weather log and show a correlation between wind direction and the wave direction that is better than 0.8. A comparison between the two datasets is made in figure 4.10. Figure 4.10-[1] shows the wind direction of the vessel and buoy dataset compare very well. Figure 4.10-[4] shows the direction in wind and wave both recorded by the vessel compare very well also. The good correlation gives confidence in using the wind direction measured by the buoy as the direction for the local waves. Figure 4.10-[2] shows a good resemblance between the wind speeds measured at the buoy and the wind speed measured by the vessel.

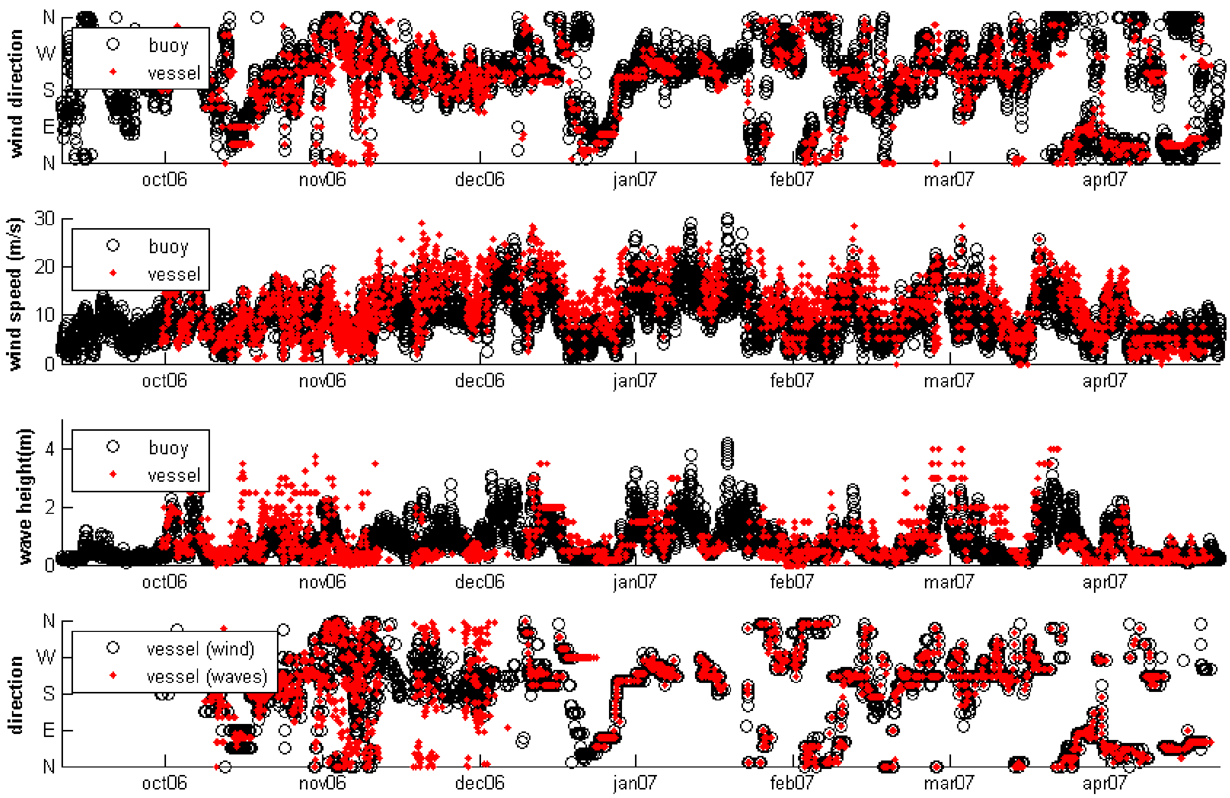

Figure 4.10: Comparison of weather datasets. Buoy versus vessel data. 1) The winddirection compared. 2) The wind speeds recorded. 3) The wave height. 4) Direction in wind versus waves. Note that plot [4] only contains vessel data and that the correlation in the period between December 2006 and May 2007 is unnaturally high.

The vessel recordings are however not as extensive and continuous as the recordings from the buoy. E.g. figure 4.10-(3) shows not all high waves were recorded as the ship was docked at night and during storms. The vessel data also gives not insight in the weather prior to the first bathymetry measurement. Other than that, the vessel will have moved over the area in different directions with respect to current and waves and required the personnel to actually write down the recording. Small errors in dates on the weather log forms suggest this process was not automated. Also the unnaturally high correlation in figure 4.10-(4) suggests the wind direction and wave direction might have even been mixed up. For these reasons, only the weather data from the buoy is used for analysis purposes.

The conclusion from this image is that wind speed and wave height, as well as wind direction and wave direction compare very well.

Wind induced residual flow

No data is available on the actual tidal flow during the measurement period. The residual tidal flow is therefore estimated based on a relation found by Bowden (1956).

Bowden defines a relation between the non-tide related part of the flow through the English Channel, the surface gradient and wind speed. He accomplishes this by measuring the potential difference that occurred in submarine telephone cables as a result of the flow of salt (conductive) sea water across the earth's magnetic field. Bowden finds a maximum daily variation in the residual flow of 0.8 m/s. This is about the same order as the largest, M2, tidal component, which accounts for a tidal ellipse amplitude of about 1.0 m/s. A recording during neap-tide shows the wind and surface gradient were capable of preventing any South-Westerly flow on two consecutive ebb tides. The long term mean residual current averages 0.05 m/s towards the North East. This was found by Carruthers (1930), according to Bowden.

Using a modified version of formula (6) of Bowden (1956) a potential wind induced residual flow was estimated using the wind velocity data.

$$V = 0.37\, W^2 \cos\phi + 0.70\Delta\zeta \qquad (6)$$
$$\phi = (\theta - \alpha)$$

In this formula, V is the residual flow in cm/s. W is the wind speed in m/s. α is the angle of the channel with the North. θ is the angle of the wind with respect to the North. Δζ is the difference in water level between the English Channel and the Southern North Sea. This change in water level is thought to be setup by non-local winds. As this data was not available, the residual flow was estimated by using formula 4.1. This formula is the first part of formula (6) in Bowden (1956), and effectively ignores Δζ.

$$V = 0.37\, W^2 \cos(\theta - \alpha) \qquad 4.1$$
$$\alpha = 60^{o}$$

The results are shown in figure 4.11-(3). The wind direction is subtracted by 180^0 to transform the direction the wind came from to direction the wind was flowing towards.

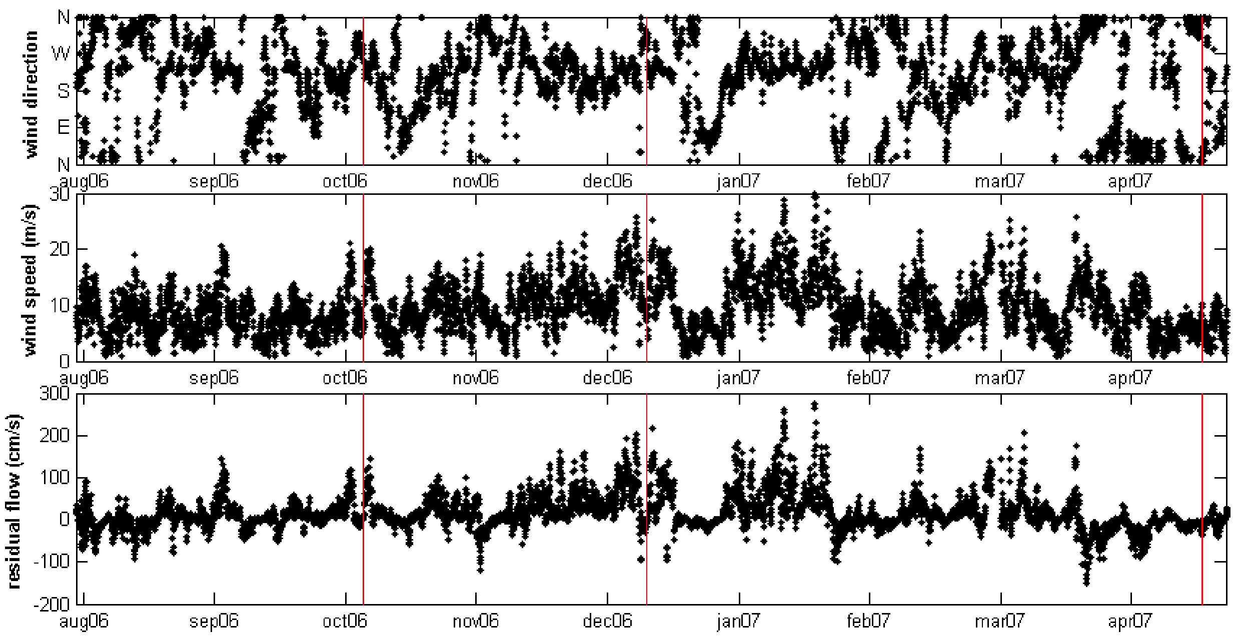

Figure 4.11: 1) Wind direction. 2) Wind speed. 3) Residual flow estimate using formula 4.1. A negative value means flow into the South West. A positive value means flow towards the North East.

The results estimate the local winds also introduce a significant flow velocity besides the waves. This flow can be of the same order as the magnitude of the M2 component of the tidal ellipse, 1.0 m/s, see Prandle *et al.* (1992). Just before the second recording of the second transect a small period with flow to the South West can be distinguished. Together with the surface waves this might be the reason why the second recording of the second transect is not as asymmetrical as the second recording of the second transect.

The maximum residual flow in the period of our studies is calculated at 3 m/s. This is very large compared to the maximum value of 1 m/s fond by Bowden. The factor $W^2\cos\theta$ did not surpass 200 in the studies of Bowden, which means the maximum wind speed in his studies were 14 m/s or more. The wind speeds in this study often surpassed that velocity (speeds up to 30 m/s were recorded, which are very severe storms) and it might be unlikely that the relation found by Bowden still hold at these extreme wind speeds.

Nonetheless, the relationship between wind speed and direction and flow rate and direction is explicitely made in this paper and it is therefore worth considering in the modelling efforts.

We can proceed in asking what part of the total effect we see is caused by waves and what part is caused by e.g. by the flow or other processes not yet discussed. To do this we modified the Sand Wave Code to include varying wave height and angle, as discussed in Chapter 2.

4.3 Varne SWC simulations

To understand the timescale of the change in bathymetry as a result of a change in surface waves the following model setup is made:

Parameter settings

The parameter settings are given in table 4.8. The symmetrical tide amplitude was set to 1.0 m/s. The asymmetrical residual tide was estimated to be 0.05 by Carruthers (1930). The tidal velocity amplitude is expressed in the F[3] term in the table. For further explanation I refer to chapter 3. A_v and S are set according to Németh (2003).

Parameter	Value
F[3]	{0.05*3.0*S*A_v/(H*(3.0*A_v+H*S)) 0.3692034217259848e-4 0.1584482984479147e-3}
H(m)	30
A_v	1.0e-2
S	8.0e-3
Npx	60
SWL (m)	180 & 210
D50 (m)	2.5e-4
l1 l2	0.0 1.7

Table 4.8: Parameters settings for the Varne simulations.

The SWC was run with a time step size of 1 week for 700 weeks. Roughly this equals a period of 14 years. The length of the domain was chosen 210 m, this equals the length of the FGM. The plot for the FGM is shown in figure 4.12. A slightly shorter length (180m) was chosen as well to see if the results are influenced greatly by the domain length not equal to the FGM. Furthermore the two different lengths help determine which changes might be caused by temporal numerical instabilities in the model itself and which might be attributed to the changes in the surface wave environment.

The wave settings used are derived from the wave buoy dataset described in paragraph 2, these settings are given in table 4.9. The wave height of 0.5 is surpassed 50% of the time and is therefore considered representative for the background or fair weather equilibrium wave conditions.

wave height (m)	wave period (s)	> frequency wave height surpassed
0.5	6	0.50
1.4	7	0.10
2.8	8	0.01

Table 4.9 Wave height - Wave period combination used in the SWC simulation. The third column shows the frequency with which the corresponding wave height is surpassed.

To help see which change may have been caused by the choice of wave angle, a second experiment is done with a constant 0 degrees wave angle. The wave height of 0.5m is set to 0 to see the effect of our choice for the fair weather situation. Domain lengths and other parameters in this second experiment are chosen the same as in the first experiment.

At t = 0, a sinusoidal bed form with an initial amplitude of 2.0 m is given 300 time steps (6 years) to reach a equilibrium state (shape, height) before changes in the surface wave climate environment are added. The first 200 time steps are not shown in the results to remove the effect of choice for the initial sinusoidal profile. All changes were implemented for a duration of 50 weeks to see the rate with which the bed form reacted and/or time until the bed form returned to it equilibrium state. The wave direction is altered after the change in wave height to be able to compare the relative effect. The changes throughout the simulation for experiment one are listed in table 4.10. Experiment two is roughly the same, only the fair weather waves were set to zero and no angle is simulated between waves and tide. See table 4.11.

time steps	surface wave height (m)	surface wave period (seconds)	surface wave direction (degrees from res. current)
0 – 300	0.5	6	0
300 – 350	1.4	7	0
350 – 400	1.4	7	180
400 – 450	0.5	6	180
450 – 500	0.5	6	0
500 – 550	2.8	8	0
550 – 600	2.8	8	180
600 – 650	0.5	6	180
650 – 700	0.5	6	0

Table 4.10: Surface wave environment in first Varne simulation. The wave height, wave period combination was derived from a measuring buoy, see table 4.9.

time steps	surface wave height (m)	surface wave period (seconds)	surface wave direction (degrees from res. current)
0 – 300	0.0	-	0
300 – 350	1.4	7	0
350 – 400	1.4	7	0
400 – 450	0.0	-	0
450 – 500	0.0	-	0
500 – 550	2.8	8	0
550 – 600	2.8	8	0
600 – 650	0.0	-	0
650 – 700	0.0	-	0

Table 4.11: Surface wave environment in second Varne simulation. Wave angle was kept zero in this simulation and the height of the fair weather waves was set to zero.

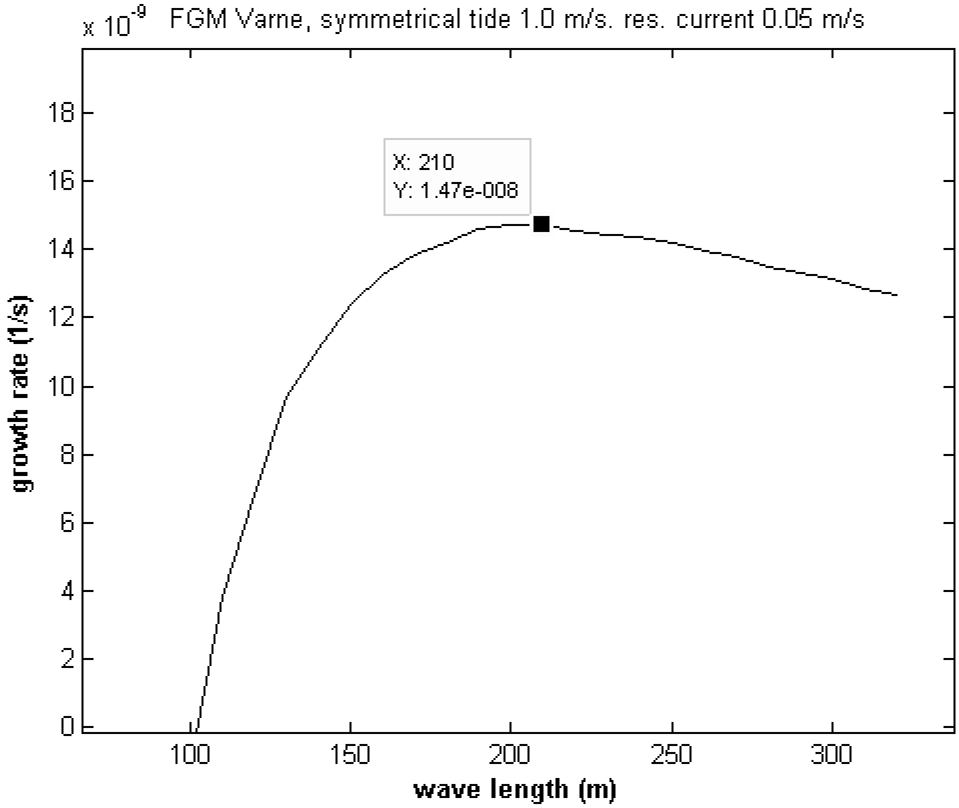

Figure 4.12: The fastest growing mode for the Varne simulation equals 210 metres. The systems shows a positive growth rate for domain length greater than 100 m.

The results of the first experiment are shown in figure 4.13, figure 4.15 and figure 4.17. The L_{SW} 210m simulation crashes at t = 657 weeks, so results for experiment one are shown until this step.
The results for the second experiment, without a wave angle and the fair weather waves reduced to 0 m height, are shown in figure 4.14, figure 4.16 and figure 4.18. These simulations made it through all 700 time steps.
Significant differences in result between setting the fair weather waves at 0.5m or at 0m was not found.

H_{crest}

In figure 4.13 and figure 4.14 is shown that the height of the crests and depth of the troughs are not influenced by the surface waves of 1.4 metres height (t=350 – 450), but are by the waves of 2.8m height (t=500 – 600). Due to the fact that the crest is more affected than the troughs, the bed forms become less asymmetrical in vertical direction under influence of surface waves. The L_{SW} 210m simulation shows a higher crest and a deeper trough than the L_{SW} 180m simulation.
Both the height of the crests and the depth of the trough show temporal instabilities that are undone in between 5 to 30 weeks. These changes are not always correlated with changes in the environment. E.g. the change in H_{trough} simulation L_{SW} 180m just before t=325 (figure 4.13) and the change in both H_{crest} and H_{trough} of simulation L_{SW} 180m just before t=500 (figure 4.14) are such events.

<u>Experiment one:</u> Under influence of the higher surface waves (t=500 – 600) the crests become lower: A downward trend starts when the wave height is changed- and ends about 40 to 50 weeks later. The effect is a reduction in height of the crest of the bed form of about 0.5 metres.
The reduction of the wave height is not maintained throughout the duration of the higher surface waves as this trend is followed by an upward restoring of the sand wave height when the wave angle is changed to 180 degrees and continues until after the surface wave height is reduced, but stops before

the wave angle is set back to 0^o again. The trend correlates with a change in volume (see **Volume**, below) and can be seen in both simulations for both lengths; L_{SW} 180m and L_{SW} 210m. The effect might be considered a combined wave height and angle effect.

Experiment two, L_{SW} 180m simulation: The simulation shows a significant numerical instability just before the wave height is adjusted. The crest height does not restore before the end of the simulation.
Experiment two, L_{SW} 210m simulation: The effect of the forcing by the higher waves lasts until the forcing is removed. The timescale for adaption to the storm situation and restoration back to the fair weather situation is about 50 weeks.

H_{trough}
Both experiments: Under a change of the surface wave height, the depths of the troughs deepen in a period of 30 to 40 weeks and restore in a period of 5 to 30 weeks. The troughs deepen about 0.4 metres under the higher surface waves.

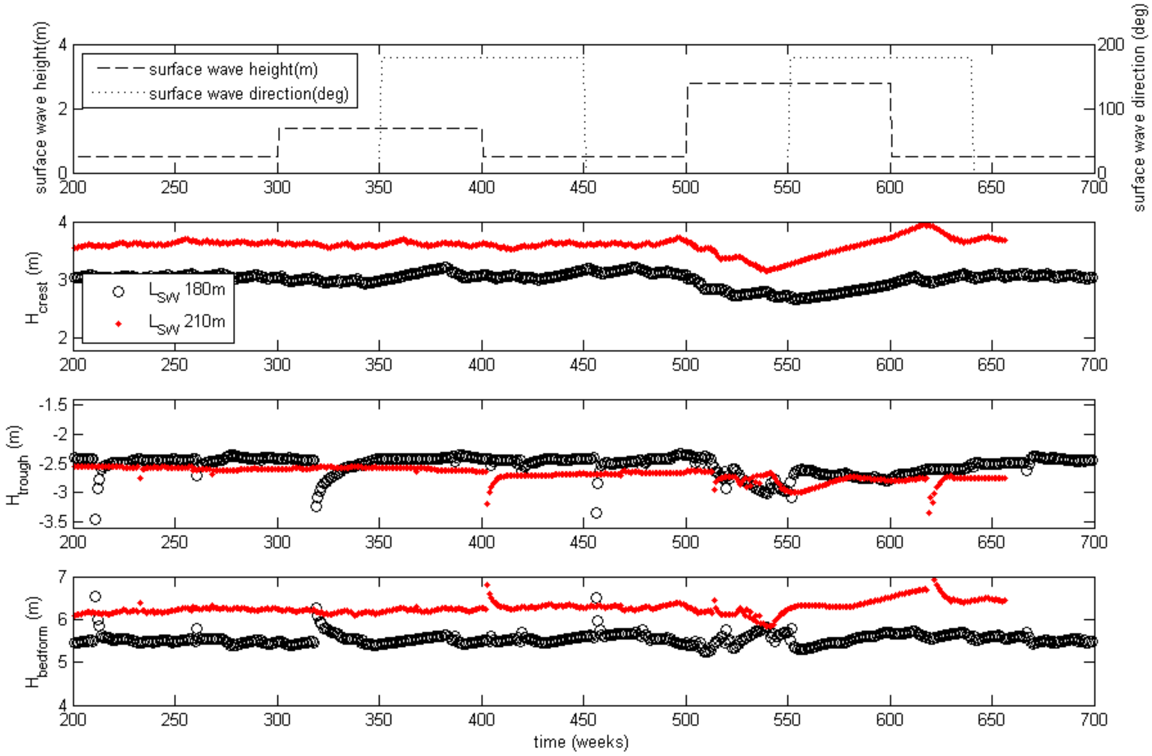

Figure 4.13: Experiment 1 results. 1) Surface wave settings: Height (m) and angle with the tidal axis (degrees). 2) Height of the crest (m). 3) Depth of the trough (m). 4) Ratio of 2) and 3) (-). Note the total height of the sand wave is the sum of Hcrest and H_{trough}. This is about 5.5 metres for this simulation.

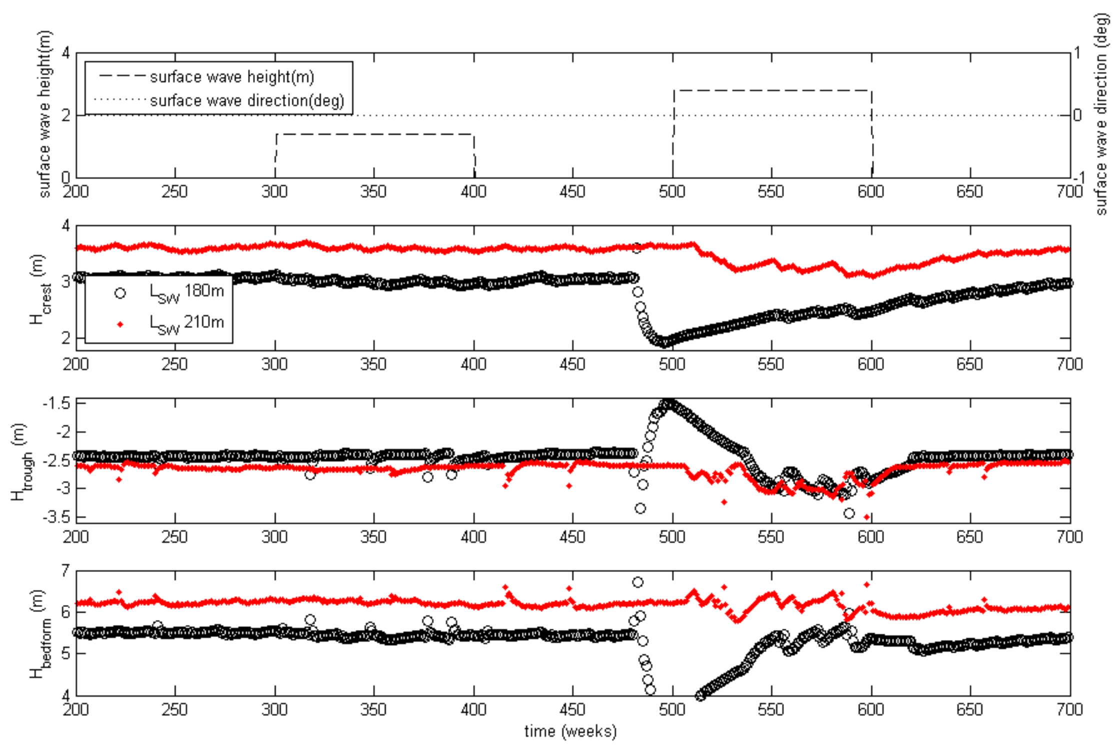

Figure 4.14: Experiment two. The items are the same as figure 4.13, only this time the angle was kept at zero degrees, so collinear with the tidal axis.

The results for experiment one and two for the length of the crest and the length of the stoss side of the sand wave are shown in figure 4.15 and figure 4.16.

L_{trough} is defined as $L_{SW} – L_{crest}$. L_{lee} is defined as $L_{SW} – L_{stoss}$, see chapter 2. As a change in L_{crest} thus means an equal but opposite change for L_{trough}, the results for L_{trough} are not plotted separately. The same relation goes for L_{stoss} and L_{lee}. The results for L_{lee} are therefore also not shown.

L_{crest}

The length of the crests is not significantly affected by the smaller surface waves (t = 300 – 400), but is by the higher waves (T=500 and onwards). The timescale for the adaptation is 50 weeks. After the surface wave height is reduced again, the lengths of the crests gradually reduce back to their initial equilibrium state with a timescale of 100 weeks. In both experiments L_{crest} changes from 92 to 102 m in the L_{SW} 210 simulations. L_{crest} / L_{trough} thus changes from (92 / 118 =) 0.78 to (102 / 108 =) 0.94.
The L_{crest} / L_{trough} ratio of the L_{SW} = 180 simulation changes from 0.84 to 1.00.

<u>Experiment one</u>
The crests lengthen by about 10-12 metres over a period of 50 weeks. For the L_{SW} 210m simulation, the length reverts after 60 time steps, before the forcing is removed. It does not do this for the L_{SW} 180m simulation. Therefore, the effect may not be considered to be caused by the change in wave angle.
<u>Experiment two, L_{sw} 210m</u> shows that the response is closely related to the change in wave forcing. The effect is only reverted when the surface wave height is lowered again.

L_{stoss}

The length of the stoss side of the bed form is almost instantly affected by the height of the surface waves and is changed back when the surface wave height is reduced again. An influence of the angle of the surface waves can not be distinguished.
<u>Experiment one:</u> The L_{SW} 180m simulation only shows a response to the wave height forcing, a influence of wave angle can not be distinguished.
The L_{SW} 210m simulation responds later to the wave forcing than the L_{SW} 180m simulation does and the length of the stoss side is reduced to its fair weather equilibrium state before the wave height is reduced. The effect is probably not due to the change in wave angle as the L_{SW} 180m does not change under changing wave angle.
<u>Experiment two</u> shows that the adaptation to the storm situation and back to the fair weather equilibrium is almost instantly with respect to the surface wave height forcing.

Under influence of the larger surface waves, the ratio L_{stoss} / L_{lee} changes from 1.5 to 2.3 in the L_{SW} 180m simulation. For the L_{SW} 210m simulation the change is from 1.2 to 2.5.

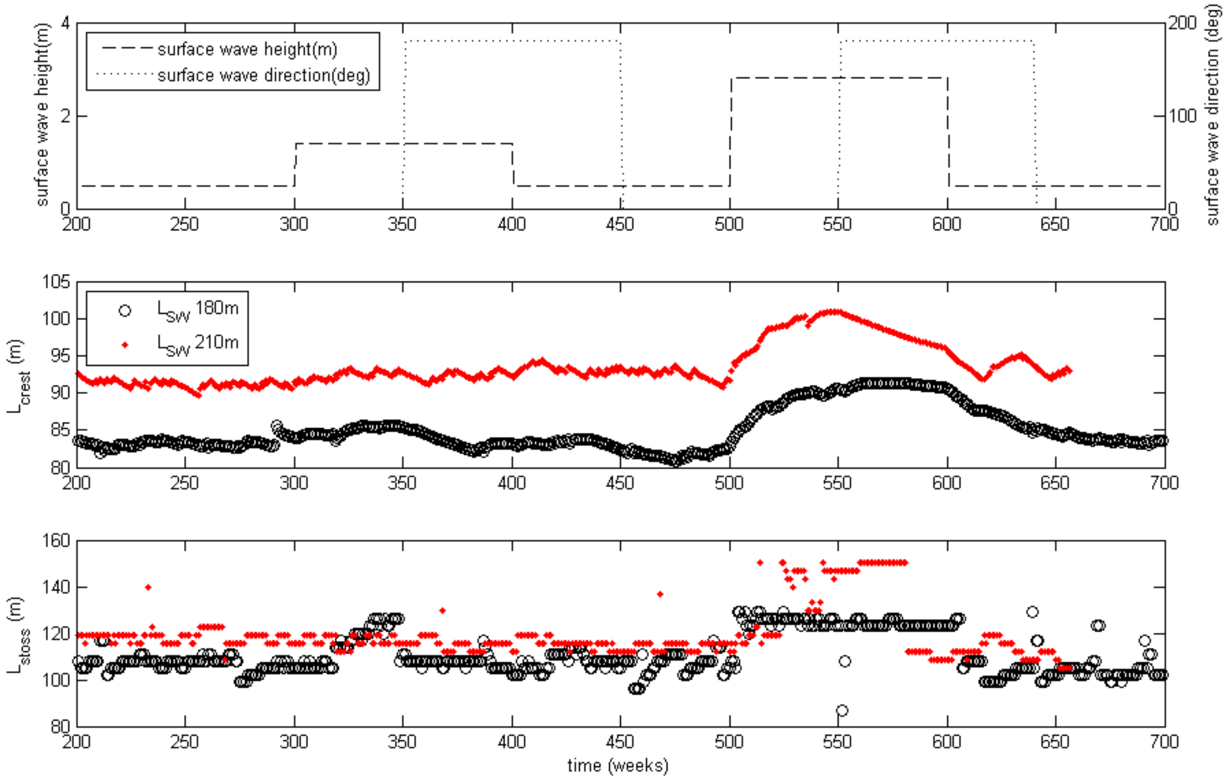

Figure 4.15: Experiment 1. 1) Surface wave climate: Height and direction. 2) Length of the crests (m). 3) Length of the stoss side (m). The x-scale shows the time in weeks. The results for the L_{stoss} are more step like than the results for L_{crest} due to the way they are defined, see chapter 2.

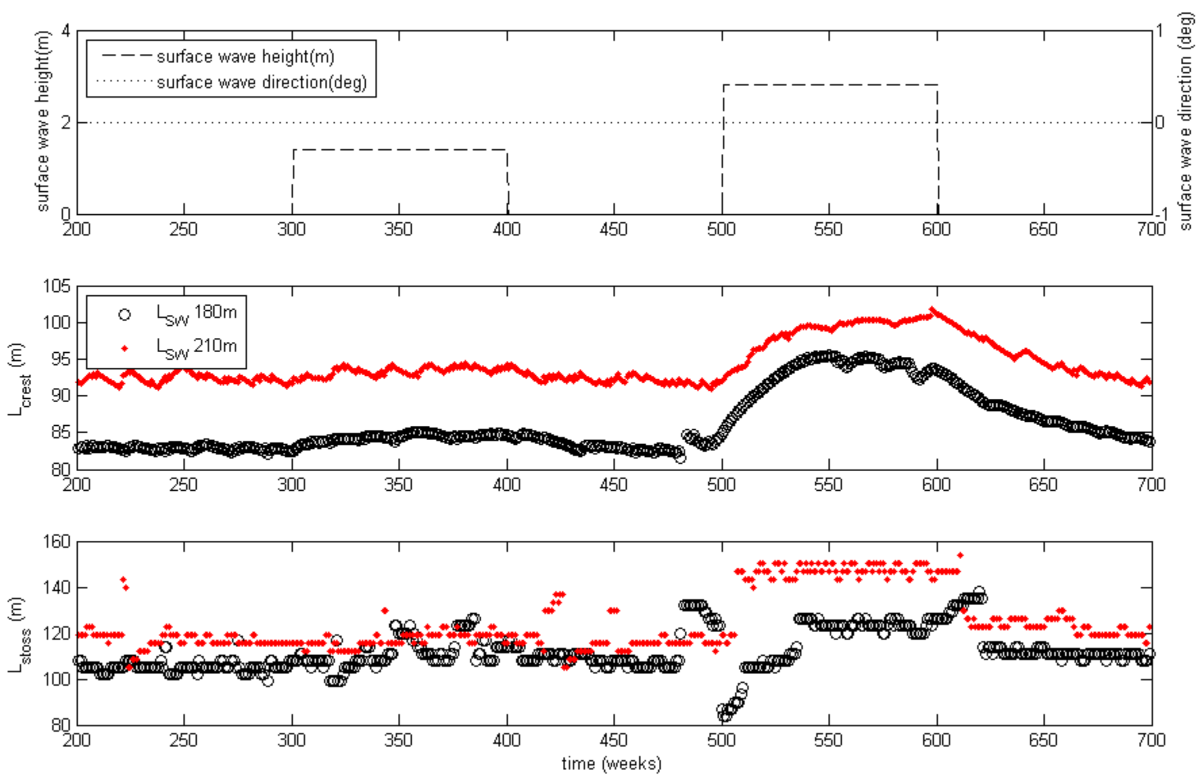

Figure 4.16: Experiment 2. The items are the same as in figure 4.15. Surface wave angle was however kept 0.

Migration rate
The migration and transport rate (see figure 4.17 & figure 4.18) increase as a result of an increase in wave height if the angle of the wave is 0^o with respect to the residual flow direction. If the waves oppose the residual current (angle = 180^o), migration rate and transport rate are reduced to below the rate when the system is simulated with low, fair weather waves. The migration direction however is never reversed.
The effect is instantaneous with respect to the forcing of the surface waves and the effect is larger for higher waves.

(Also see chapter 2.) The migration rate in the simulation results is determined as the average of the 20 previous time step and thus lags somewhat behind the actual change. The reason for this is the fact that the migration rate is determined by the change in x coordinate of the highest point in the domain. Non-zero migration is only recorded when a shift in position of the crest is recorded. The migration rate is equal to:

$$dx \text{ (m/year)} = 52 \text{ (weeks/year)} / \text{time step (weeks)} * (n * nx/SWL)$$

In which n is the number of positions the x coordinate changes, nx the number of horizontal steps (60 in these simulations), SWL the sand wave length. The time step is the number of weeks per time step (1 is this case). In case of small time stepping the x coordinate may change only every now and then. Therefore, the migration rate can be determined when the average amount of coordinate shifts per time is known. Due to the relative large horizontal step size (SWL / nx = 3 m) versus the rate of migration (the minimum found in the simulations is 21 m / year), a change in crest position is estimated to occur every 7 time steps. Therefore, averaging over 20 time steps seems a reasonable choice for a minimum required number of the time steps.

The transport rate can be determined without averaging but shows a comparable result. This transport rate is the rate of the change of area of the transect per length meter. This rate reflects the rate with which the shape changes per length meter of the domain (simulations) or the transect (recordings). The way the transport is determined does not allow for determining the direction of migration, so the two are both considered.

Transport rate
The simulation results (1.8 – 3.0 m^3/m^2*year, see figure 4.17 & figure 4.18) show the rate of transport is affected in the same manner as the migration rate. Both the surface wave height and the surface wave angle affect the rate.

Volume
The volume of the sand waves is 1.0 m^3/m^2 for the L_{SW} 180m simulation and 1.1 m^3/m^2 for the L_{SW} 210m simulation. This difference is interpreted to be a result of the difference in height of the sand waves. These differences in height were interpreted to be the result of the choice in domain length, which via the angle of repose (see chapter 3) limits the height of the saturated bed forms.
For the first experiment the total volume of sand that is mobilized increases under the highest and opposing waves for both simulations. This effect is gradual and has a timescale of 50 weeks. The effect can be seen for both the L_{SW} 180m as the L_{SW} 210m simulation.
The gradual increase in volume is shown for both simulations in the first experiment and is not shown in the second experiment. This may thus be caused by the change in wave angle. The trend in volume change is expressed in the height of the crests (see $\mathbf{H_{crest}}$ above). The combined effect may be that the stirring action of the higher waves mobilizes more sediment, which is not transported due to the waves opposing the current and thus result is an increase in crest height.

The influences of the higher waves in the second experiment are reflected in an increase in variability in the sand wave volume without a significant change in mean volume. The variability reduces again after the wave forcing is removed.

General result
The changes in crest height and trough depth can be attributed to the surface waves. The waves do have to be sufficiently high. The waves of 1.4m are not sufficient to cause a change in the shape of the sand wave, they do however affect the rate of migration and rate of transport.

The combined effect of the higher surface waves on the bed form is that the crests lengthen and flatten. The L_{crest} / L_{trough} ratio and the H_{crest} / H_{trough} ratio becomes less asymmetrical. The L_{stoss} / L_{lee} ratio becomes more asymmetrical.

The combined effect of the lowering of both the crests and the deepening of the troughs is that the bed form height is hardly affected.
The maximum height of the crests and depth of the troughs of the sand waves appear to be a direct consequence of the chosen length of simulation domain. This may be a result of the fixed maximum angle of repose that is a function of the parameter λ (also see chapter 2). In smaller domains, the equilibrium height of a sand wave is lower due to the fact that the angle of repose (given the smaller domain length) is higher than for simulation with a longer domain. In the bed load transport formula we see sediment transport limited by an increasing angle of repose.

The changes to the crest height occur gradually over a period of about 50 weeks, which is a long time span compared to a single storm or even a series of storms during winter.

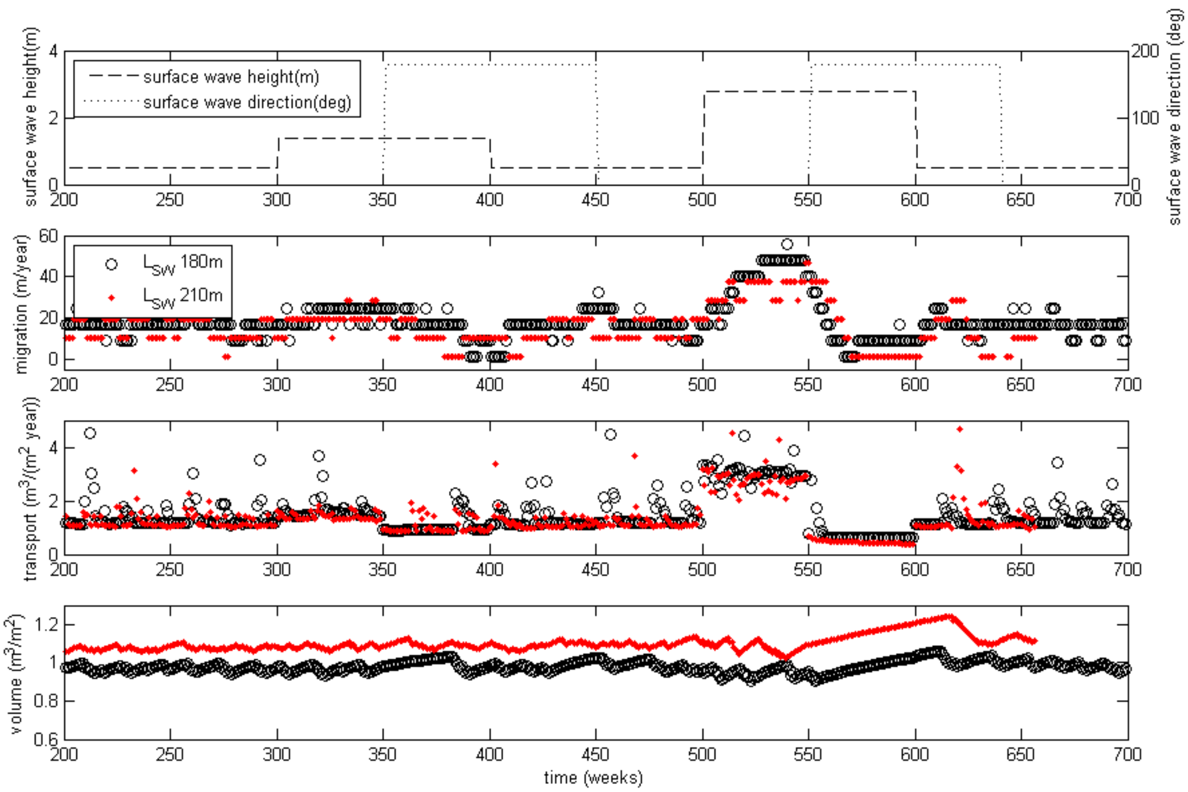

Figure 4.17: Experiment one. The surface wave forcing [1] versus the migration rate (m/year) [2], transport rate ($m^3 * m^{-2} * year^{-1}$) [3] and volume of the sand wave in m^3/m^2 [4]. Notice the simularity with figure 4.13.

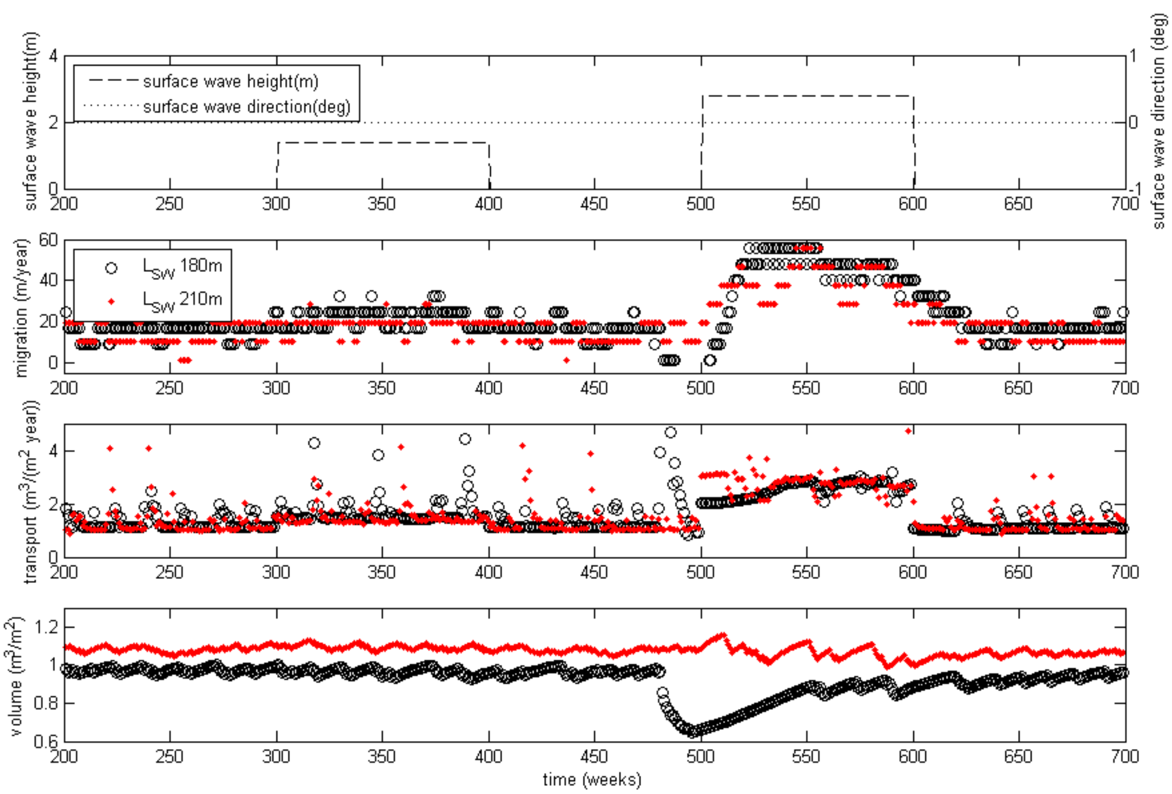

Figure 4.18: Results for experiment two. Items are the same as in figure 4.17.

Comparison between the simulations and the empirical dataset.

Bed form length

The length predicted by the fastest growing mode (210 m) is about a factor 3-4 larger than the bed forms found in the area we simulated, which are around 80 metres.

Bed form height

The predicted sand wave heights are 6m and 5.5m for the L_{SW} 210m and the L_{SW} 180m simulations. The mean sand wave heights in the empirical dataset are between 4.10 – 4.89m and between 3.05 – 3.85m in the pre and post storm respectively. The height is thus overestimated 25 – 50%. In the post storm situation the simulated crest height was reduced 0.4 m, but as this coincided with a lowering of the troughs, the code did not predict a significant bed form height reduction. Under opposing waves the simulation even predicted a bed form height increase due to extra stirring of the sediment which resulted into increase in bed form volume.

Volume

The total volume of sand that is in the simulated bed forms increases when the sand waves are exposed to larger and opposing surface waves. For the simulations with a zero degrees wave angle, no significant change in volume can be seen.
In the empirical dataset the crests of sand waves become longer and flatter after the stormy period. The sand is more dispersed over the crests of the sand wave. As a result, the transects show a reduction of the volume. For the first transect the volume reduces from 0.53 to 0.47 m^3/m^2 between the first and second recording. For the second transect the volume change is from 0.79 to 0.69 m^3/m^2 for the first and second recording.
The sand wave code simulation overestimates the height of the sand wave and thus over predicts the sand wave volume (1.0 – 1.1 m^3/m^2).

L_{stoss} / L_{lee}

The simulated change in the pre and post storm situation is from 1.5 to 2.3 in the L_{SW} 180m simulation. For the L_{SW} 210m simulation the change is from 1.2 to 2.5.
In the empirical dataset that asymmetry changes from 2.0 – 2.7 and 1.3 – 1.9 in the pre and post storm situation for transect 1 and 2 respectively. (The value 2.0 is found if we invert the L_{stoss} / L_{lee} asymmetry of 0.5).

The change in the length of the stoss side of the simulated bed form is almost instantly (3 weeks) affected by the surface wave forcing. This is short compared to the timescale of the crest height modification that takes (unrealistically) long. The higher surface wave first initiates a larger shift in crest position before the sand wave starts to migrate faster as a whole. The change in crests position is therefore a modification of a combined wave current interaction with the sediment. This might explain why the change in L_{stoss}/L_{lee} asymmetry occurs on a smaller time scale than changes in e.g . crest height. Another reason might be that the L_{stoss}/L_{lee} modification only involves modification of the most active and exposed part of the sand wave, the crest.

Migration rate

The migrations rate (20 – 47 m/year) and transport rates (1.0 - 2.1 $m^3/m^2 \cdot year^{-1}$) are similar to the rates found in the empirical data:
Transect 1: 66 – 139 (m/year) and 1.18 ($m^3/m^2 \cdot year^{-1}$).
Transect 2: 22 – 32 (m/year) and 2.44 ($m^3/m^2 \cdot year^{-1}$).

Chapter 5. Results: Eco Morf 3 area

Chapter summary

Bathymetry analysis show sand waves move back and forth in the seasons. The migration is a results of a combined wind/wave driven current and a long term mean residual flow. With an idealized sand wave model we show that the wave direction can not explain the migration direction of the sand waves by itself. Most probably a variable residual flow is needed.
Higher surface waves increase the dynamics of the system as higher waves lower the growth time and increase the transport rate. Sand wave volume increases and crests are flattened and lengthened under the increased stirring action of higher waves. The angle of the waves with respect to the current lowers the horizontal asymmetry.

Description of the area

The Eco Morf 3 area is situated about 50 km of the Dutch coast near Alkmaar, as is shown in figure 5.1.

The bathymetry recordings that are investigated are shown in figure 5.2. The area is 2 by 2.5 km large and has long regular sand waves of up to 2 – 2.5 metres height, with length of about 200 metres. See figure 5.3.
The sea floor ranges between 30 and 25 metres below mean sea level (MSL). The same area was recorded five times between March 2001 and September 2002. The dates the recordings were made and time in between recordings are given in table 5.1.

Figure 5.1: Location of the Eco Morf 3 area

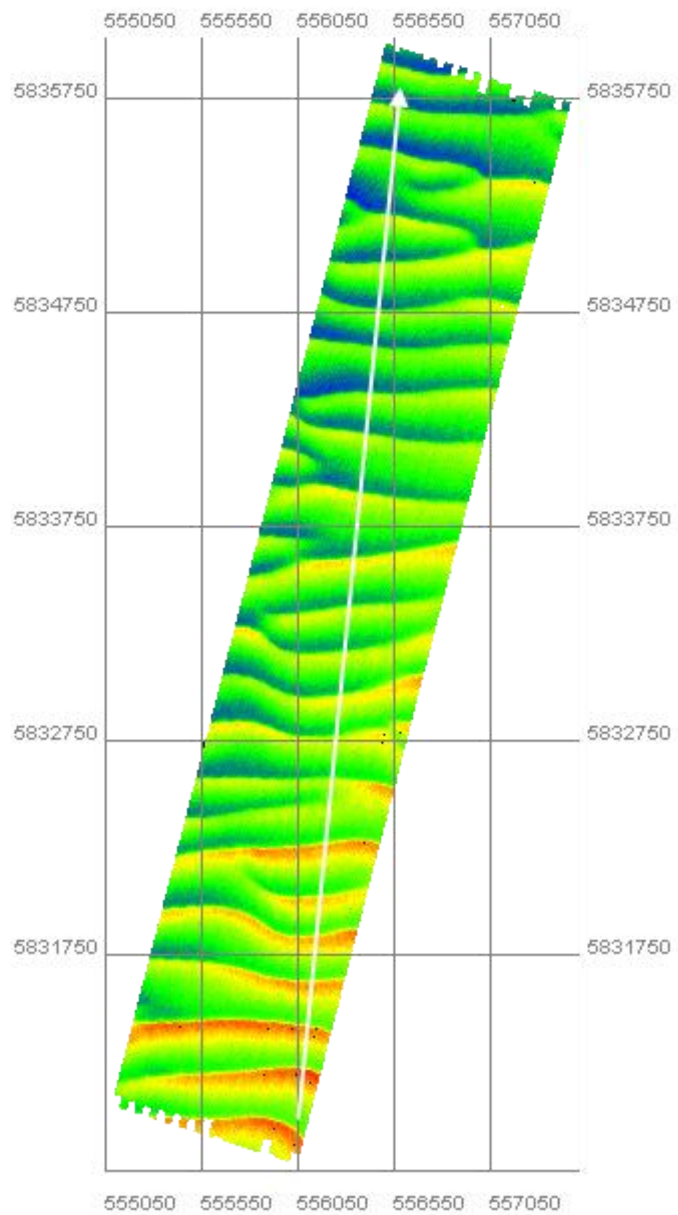

Figure 5.2: Eco Morf 3, March 2001. The location of the transect that were studied, is shown in white . A plot of this transect for the march 2001 recording is given figure 5.3. The orientation of the transect is the same as the orientation of the sand waves; stoss side to lee side, South to North.

date of recording	**dt (days)**
20th of March 2001	
15th of July 2001	105
26th of September 2001	80
15th of July 2001	202
26th of September 2001	135
total:	**522**

Table 5.1: Dates of recording and their time difference in days.

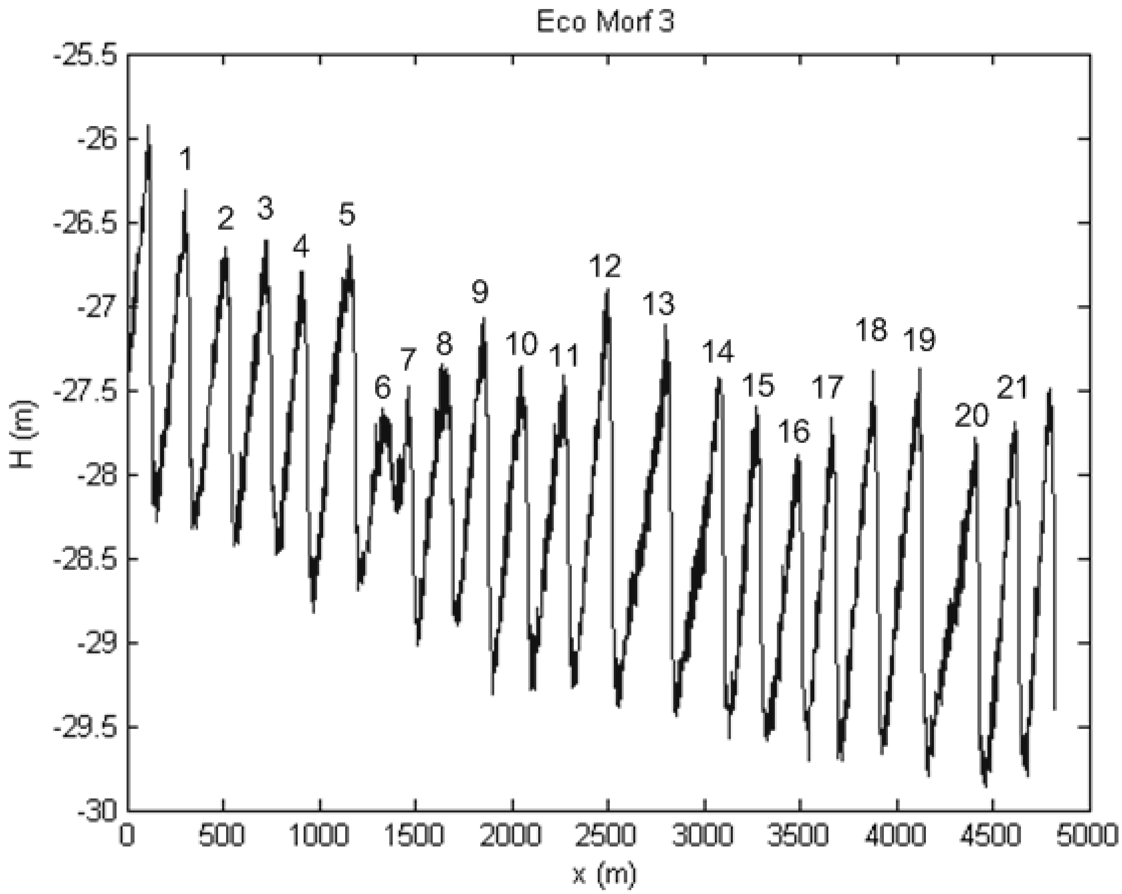

Figure 5.3: Transect of Eco Morf 3 area. Left to right is South to North. The characteristics of the sand wave signal are given in Table 5.2. Notice the bifurcation at 6th and 7th sand wave from the left.

5.1 Morphodynamics

Fourier analysis results

Using the Fourier analysis (see chapter 2), the sand wave signal is extracted from the bathymetry transect data as shown in figure 5.3. The sand wave shape characteristics are then determined. The results of this analysis are shown in table 5.3. The sand waves are more asymmetrical and lower than the sand waves in the Varne area.

characteristics	L	H	Dune Index	Lstoss	Llee	AI
min	174	1.34	100	130	43	2.6
mean	222	1.79	124	174	48	3.6
max	309	2.18	145	261	56	5.7
st dev	38	0.23	14	38	3	0.9

Table 5.2: The minimum, mean, maximum value of the wave length (m), wave height (m), their ratio (-), the length of the stoss side of the sand wave, the lee side and this ration. As no systematic change happened over the period the results are given as the average value for all recording. E.g. the minimum value of 126 for the sand wave length is the minimum for the 20 bed forms in the transect averaged for the 5 recordings of this transect.

The used settings for the Fourier analysis are:

Maximum wavelength	500 m
Minimum wavelength	40 m

The sand waves are found to move at a average maximum rate of 4.5 m/j, see table 5.3. Individual sand wave can be seen to move are a rate of up to 18 m/year. This migration rate is however not supported by the system over a longer period. The standard deviation in the difference between the first and last recording (last column,table 5.2 table 5.3) is a lot smaller than the standard deviation of the recordings that were done with shorter period in between. Also, the mean migration over the long period is a lot smaller than the mean migration in the periods in between. This is interpreted as a large movement back and forth in seasons with adjustment of each bed form to the neighbouring bed forms with a small time independent total movement in Northern direction.
This conclusion is further supported by the correlation in change of neighbouring bed forms. This is illustrated in figure 5.4 and figure 5.5. The figures display the change in crest height and trough depth for each bed form after each period. Neighbouring bed forms tend to change in the same direction and with a similar amount. Note that the bed forms change in opposite direction in the first and second period (the blue and red line). The crests and troughs tend to show the same behaviour in time and place.

dx crests rate (m/y)	20 March 2001 - 15 July 2001	15 July 2001 - 26 September 2001	26 September 2001 - 18 April 2002	18 April 2002 - 3 September 2002	20 March 2001 - 3 September 2002
min	-18.3	-8.0	-3.6	-2.0	-2.6
mean	-1.1	-1.3	2.3	4.5	1.6
max	7.8	4.6	6.8	12.2	3.5
stdev	6.6	3.7	2.8	4.2	1.5

dx troughs rate (m/y)	20 March 2001 - 15 July 2001	15 July 2001 - 26 September 2001	26 September 2001 - 18 April 2002	18 April 2002 - 3 September 2002	20 March 2001 - 3 September 2002
min	-12.2	-6.8	-0.9	-6.8	-1.4
mean	-0.9	2.0	3.5	-0.5	1.3
max	7.0	8.0	7.7	4.7	3.5
stdev	5.0	3.7	2.5	3.7	1.1

Table 5.3: Migration rate in (m/year) as a change in x coordinate along the transect shown in figure 5.2. A positive number means migration approximately Northward. (The transect was taken in the direction 6 degrees to the East.) Note the last column represents the changes between the first and last recording.

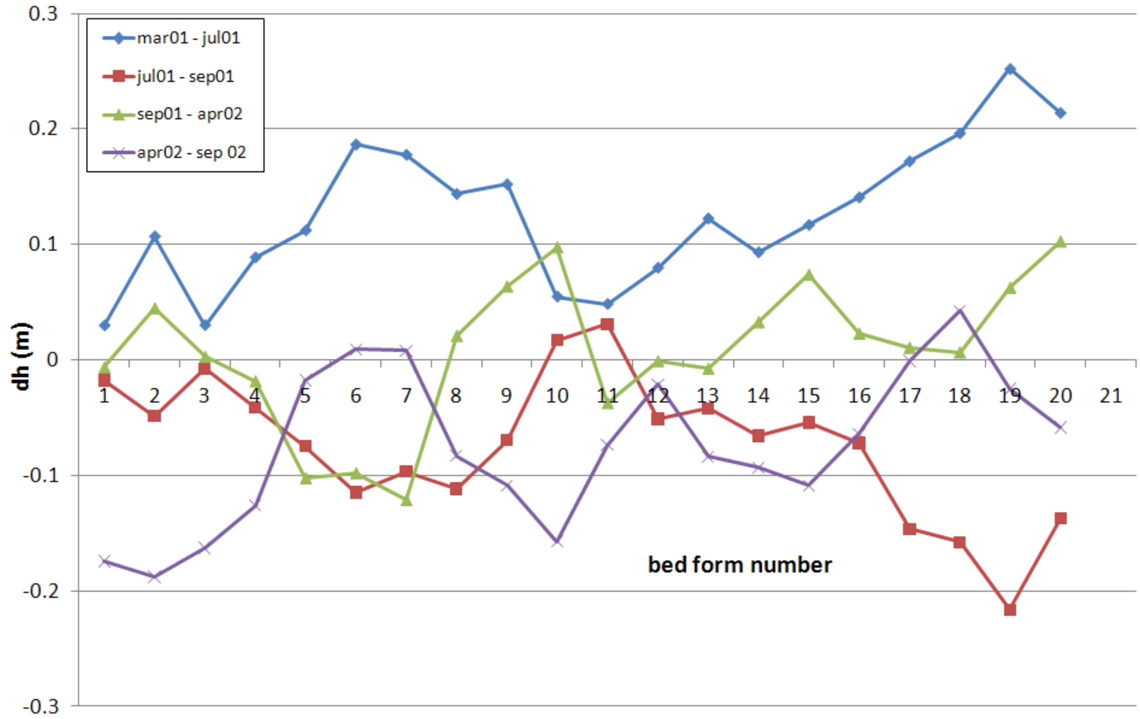

Figure 5.4: Correlation in change in crest height between neighbouring bed forms. The x-axis is the bed form number in the transect left to right. dh represents the change in height of the crests. A negative value means the crest became lower.

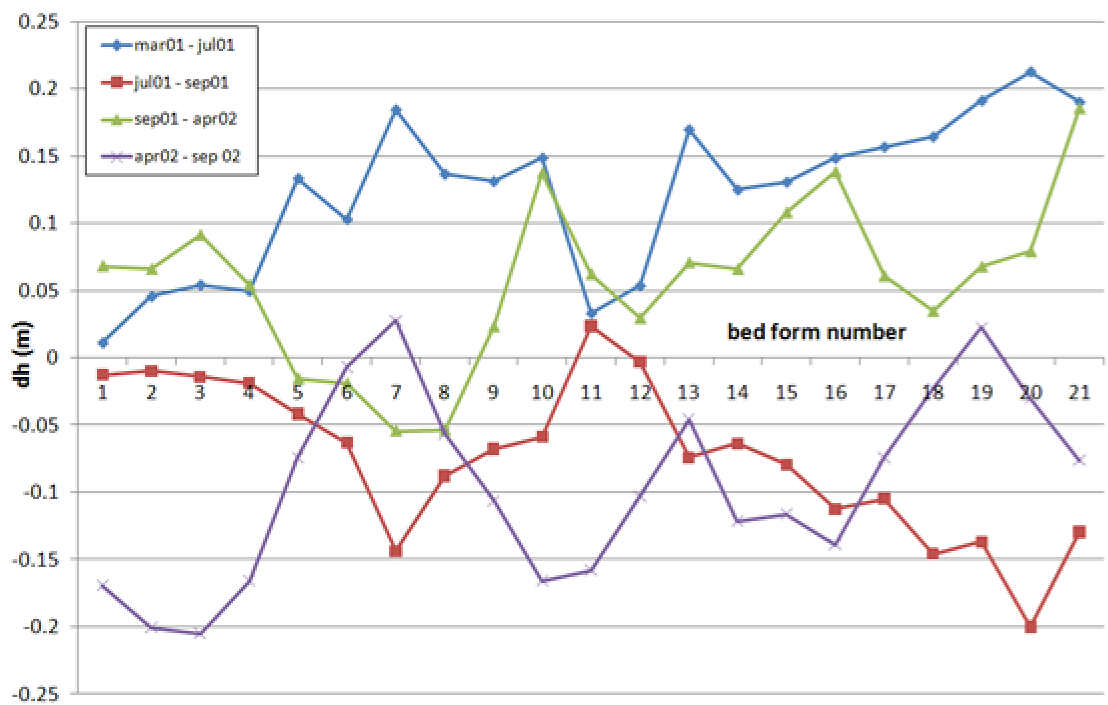

Figure 5.5: in change in trough height between neighbouring bed forms. The x-axis is the bed form number in the transect left to right. dh represents the change in height of the troughs. A negative value means the trough became deeper.

No significant changes in bed form height can be seen when averaging over the entire transect, see table 5.4.

dh crests (m)	20 March 2001 - 15 July 2001	15 July 2001 - 26 September 2001	26 September 2001 - 18 April 2002	18 April 2002 - 3 September 2002	20 March 2001 - 3 September 2002
min	0.0	-0.2	-0.1	-0.2	-0.2
mean	0.1	-0.1	0.0	-0.1	0.0
max	0.3	0.0	0.1	0.0	0.1
stdev	0.1	0.1	0.0	0.1	0.1

dh troughs (m)	20 March 2001 - 15 July 2001	15 July 2001 - 26 September 2001	26 September 2001 - 18 April 2002	18 April 2002 - 3 September 2002	20 March 2001 - 3 September 2002
min	0.0	-0.2	-0.1	-0.2	-0.1
mean	0.1	-0.1	0.1	-0.1	0.0
max	0.2	0.0	0.2	0.0	0.2
stdev	0.1	0.1	0.1	0.1	0.1

Table 5.4: Change in crest height and trough depth (m). Change is with respect to a absolute level, so a negative value for a change in dh_{trough} means the trough has become deeper. For the crests a negative values means the crests has become lower. Note the last column represents the changes between the first and last recording.

Volume and rate of change

The volume of the bed form is equal to 0.26 - 0.25 m^3/m^2, for all time steps. This is half that of the bed forms in the Varne area, that have a volume of 0.50 m^3/m^2. The rate of change of the Varne area sand waves 2.4 $m^3/(m^2.year)$ which is 5 to 10 times the rate of change found in the Eco Morf 3 area, see table 5.5. This difference in volume has to do with the higher bed forms at the Varne area. The difference in rate of change represents the higher dynamics in the Varne area.
Since the volume in the sand waves is constant over time, the rate of change is due to shape change and/or migration. This supports the conclusion of Van Dijk & Kleinhans (2005) that the sand waves here are more or less saturated. The last row shows that the change in volume in between the first and last recording is smaller than the change during in between period. This supports the conclusion that the sand waves moved back and forth.

	20 March 2001	15 July 2001	26 September 2001	18 April 2002	3 September 2002
V [m3/m2]	0.26	0.26	0.26	0.25	0.25
	20 March 2001 - 15 July 2001	15 July 2001 - 6 September 2001	26 September 2001 - 18 April 2002	18 April 2002 - 3 September 2002	20 March 2001 - 3 September 2002
dV [m3/m2*year]	0.10	0.12	0.05	0.09	0.03

Table 5.5: Volume change of the transect in m^3 / (m^2 .year). The rate represents the rate with which the height changes averaged over the length of the transect.

Cross correlation

The migration in the Fourier analysis was determined along a line South to North oriented 6 degrees from the North, perpendicular to the orientation of the crests. By means of cross correlation we verified if the bed forms indeed migrated more or less along this line. The methodology is explained in chapter 2. For this analysis the area was split up in 3 sub areas.

The rate and direction of migration are shown in table 5.6 and table 5.7. In this analysis the effect of the grid size on the cross correlation results was done. The analysis is repeated for two different grid sizes, 1x1 m and 2.5x2.5 m. The point data is spaced about 5 metres apart, so the Kriging interpolation is done with a search radius of 5 metres in order to prevent gaps in the regular grid. The 2.5x2.5 grid appears to be very coarse compared to the migration rate under interest: The smallest dt is 80 days, or about 0.2 years. The maximum (average) rate of migration found in the Fourier analysis was about 1.6 m/year. This makes the grid therefore about $((0.5*2.5) / (1.6*0.2)) \simeq 4$ times too large to accurately find any migration. The 1x1 grid therefore seems to be a more reasonable choice. This grid is however still too large and the grid is interpolated from the same 5 meter spaced original data, making the Kriging radius large with respect to the x and y precision. The discussion at the end of this report handles the uncertainty that is associated with small displacements in terms of angle and distance.

The results in the table are the extrapolated migration rates per year. These rates were obtained by multiplying the displacements with the cell size and by the dividing them by the time in between recordings. For easier comparison the direction of migration are presented as a wind direction. The short term migration is not always large enough to be able to determine a rate of migration. That, or no significant migration occurred. In this case the migration rate is set to zero and the direction was left blank.

The maximum displacement in grid cells is found to be 1 (both x and y) in the 2.5x2.5 grid and 4 and 2 in the x and y direction of the 1x1 grid respectively. The rate of migration is often overestimated in the 2.5x2.5 grid compared to the rate found in the 1x1 grid. This is interpreted as the 2.5x2.5 grid being a bit too coarse to accurately represent migration in the short periods due to the large influence the grid size has on the rate of migration.

The larger migration rate in the period in between supports the back and forth movement found in the Fourier analysis. The rates over the longer period (the last column) also correspond well with the rate found in the Fourier analysis.
The migration direction was often found to be not in line with the direction chosen for the transect as e.g. the directions East, and East North East are almost at a 90^0 angle with the transect line. The high uncertainty in the direction of small displacements (using cross correlation) could well be the reason for this.

	20 March 2001 - 15 July 2001	15 July 2001 - 26 September 2001	26 September 2001 - 18 April 2002	18 April 2002 - 3 Septemer 2002	20 March 2001 - 3 September 2002
area 1					
dx = 1	3	9	2	4	2
dx = 2.5	0	11	6	7	2
area 2					
dx = 1	7	0	4	4	3
dx = 2.5	9	0	5	7	2
area 3					
dx = 1	3	0	6	3	3
dx = 2.5	9	0	5	7	2
Fourier analysis					
crests	-1.1	-1.3	2.3	4.5	1.6
troughs	-0.9	2.0	3.5	-0.5	1.3

Table 5.6: Rate of migration (in m/year) using cross correlation [rows 1-3] and the mean value found in the Fourier analysis [4] (table 5.3). The direction of migration is listed in table 5.7.

	20 March 2001 - 15 July 2001	15 July 2001 - 26 September 2001	26 September 2001 - 18 April 2002	18 April 2002 - 3 Septemer 2002	20 March 2001 - 3 September 2002
area 1					
dx = 1	W	E	N	NE	NE
dx = 2.5		E	NW	E	N
area 2					
dx = 1	E		NNE	NW	ENE
dx = 2.5	E		N	E	NE
area 3					
dx = 1	E		ENE	N	ENE
dx = 2.5	E		N	E	NE
Fourier analysis					
crests	S	S	N	N	N
troughs	S	N	N	S	N

Table 5.7: Direction of migration using cross correlation [rows 1-3]. The direction was calculated as an angle in degrees to the North, but is presented as a wind direction for easy comparison. The direction derived from the Fourier analysis is shown in row [4]. A positive number in table 5.6 corresponds with a Northward migration, a negative number with a Southward migration as the transects were taken oblique to the North (a 6 degrees angle). A zero migration rate is listed as a blank value.

5.2 Wind, Waves & Current data

To link changes in the bathymetry to changes in the surface wave direction we discuss the wave data from the www.waterbase.nl website. The wave height and wave direction measured in the period between 2001-2002 is plotted in figure 5.6. The direction indicates where the waves traverse towards. As higher waves are more effective in mobilizing sediment, we transformed the wave height and wave angle into an energy flux, using the formulas described in Chapter 2. The results of this is shown in figure 5.7.

In figure 5.6[2] and figure 5.7[3] we see that the surface waves are generally oriented towards the East. Variation exists in the orientation North East or South East. The periods between recordings 1 and 2 appear to have a predominant direction towards the South East and a mixed North Eastern / South East direction in the second two periods. This means the waves are oriented about 90^o with respect to the direction in which we took the transect for the Fourier analysis. The sign (S or N) of the direction found in the Fourier analysis does correspond with the variation SE or NE in the wave direction, see table 5.7 [4]. It might therefore be that the bed forms moved in the direction of the wave/wind forcing.

To estimate the effect of the waves over the entire period between recordings, we made direction distribution plot of the wave energy, shown in figure 5.8. It can be seen that in the first two periods the waves towards the South East add most to the total wave energy transported. In the second two periods, waves directed towards the NE add most to the wave energy transport. The amounts are shown in table 5.8.

period		(N) 310^o – 30^o	(SW) 180^0-270^o
20 March 2001 -	15 July 2001	0.6	0.3
15 July 2001 -	26 September 2001	0.6	0.3
26 September 2001 -	18 April 2002	0.2	0.6
18 April 2002 -	3 September 2002	0.4	0.5
20 March 2001 -	3 September 2002	0.4	0.5

Table 5.8: Wave energy transport from the NE (310^o – 30^o) and the SW (180^o - 270^o) in percentage

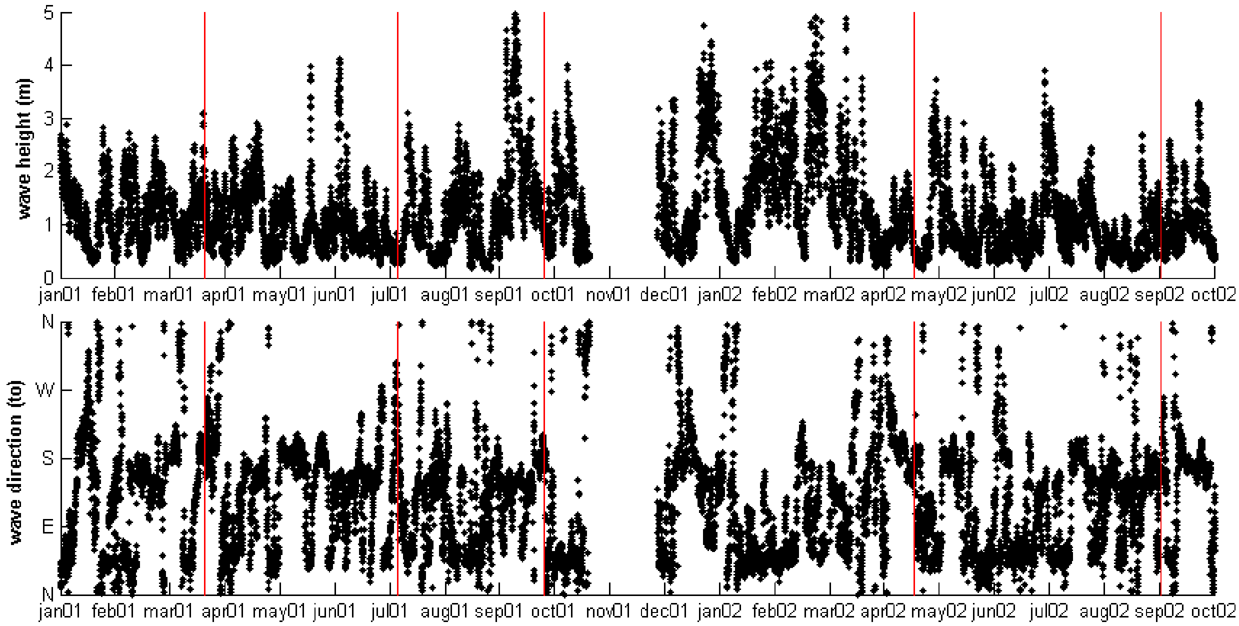

Figure 5.6: Wave height and direction the waves travel towards. The red lines indicate when the bathymetry was recorded.

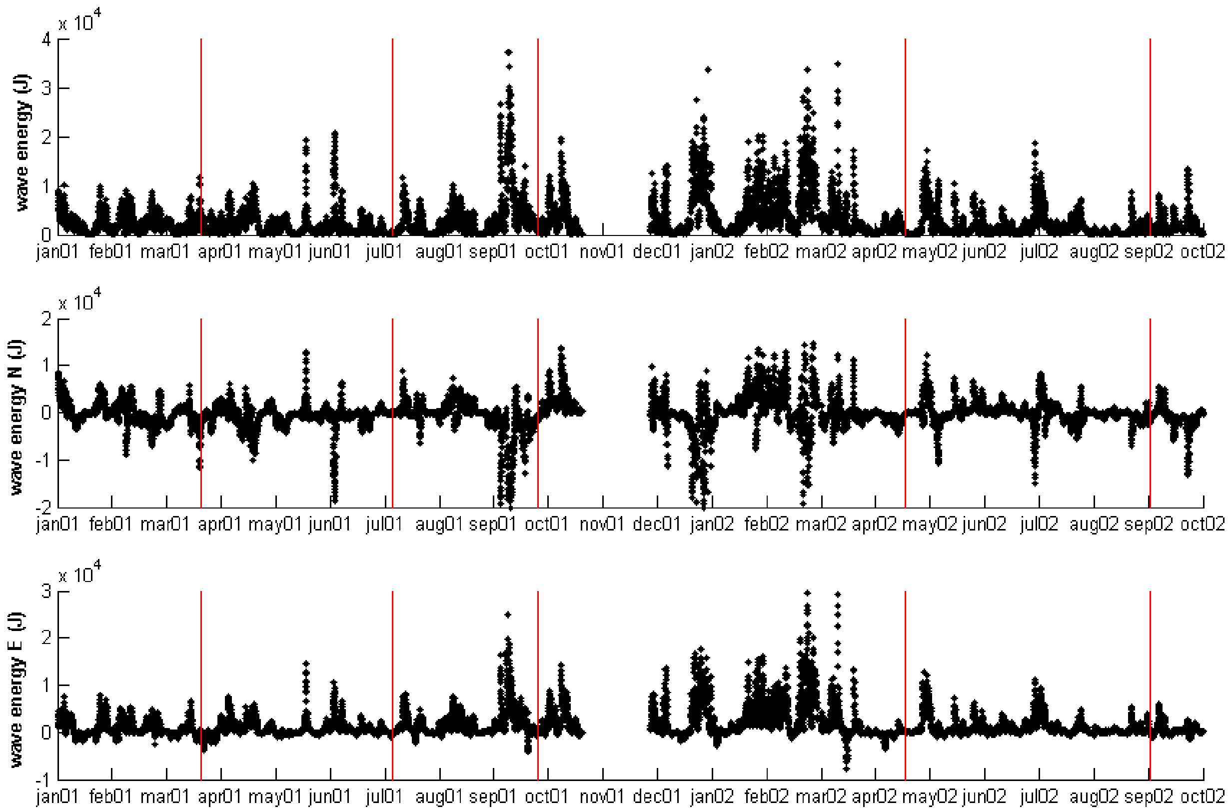

Figure 5.7: [1] Wave energy as a function of wave height (figure 5.6[1]) and transport in Northern [2] and Eastern [3] direction when [1] is multiplied by the angle (figure 5.6[2]). A negative number means transport in Southern [2] and Western [3] direction.

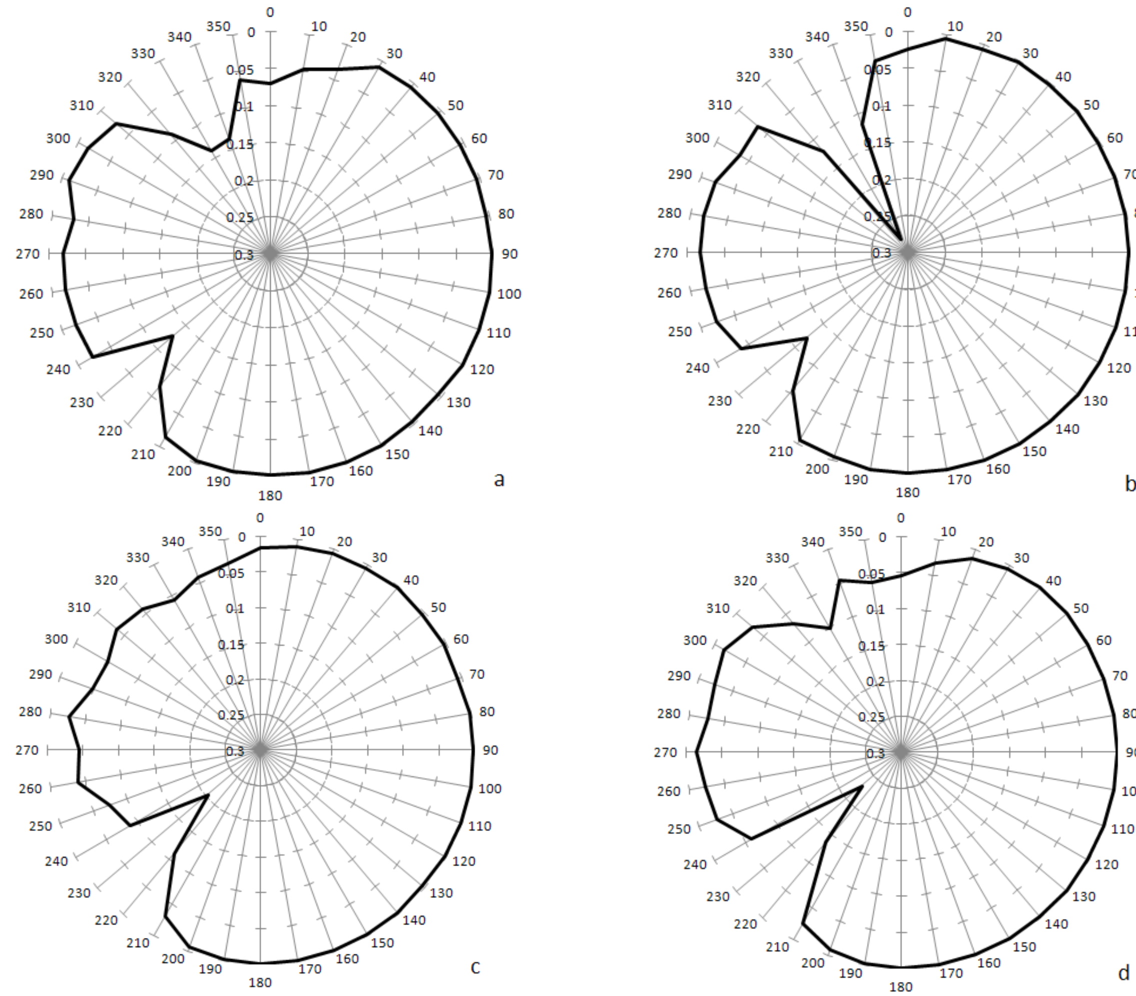

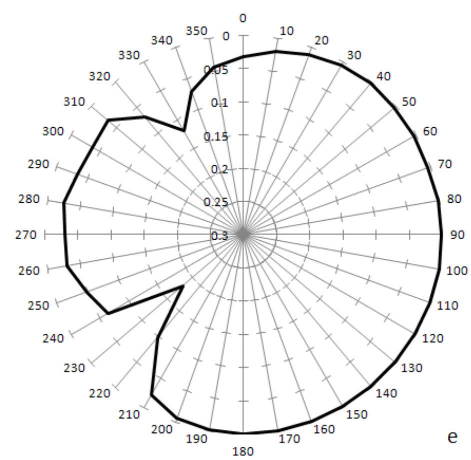

Figure 5.8: Wave energy flux distribution IJmuiden monition depot per period indicated by the red lines in figure 5.6. Indication of the direction the flux came <u>from</u>.
Periods:
[a] 20 March 2001 – 5 July 2001
[b] 5 July 2001 – 25 September 2001
[c] 25 September 2001 – 17 April 2002
[d] 17 April 2002 – 2 September 2002
[e] 20 March 2001 – 2 September 2002 (all data)

The general difference between the first two and second two periods is summed up in figure 5.9. A conclusion from this image could be that the migration direction is both influenced by the long term mean residual flow and the short term wind/wave driven flow.

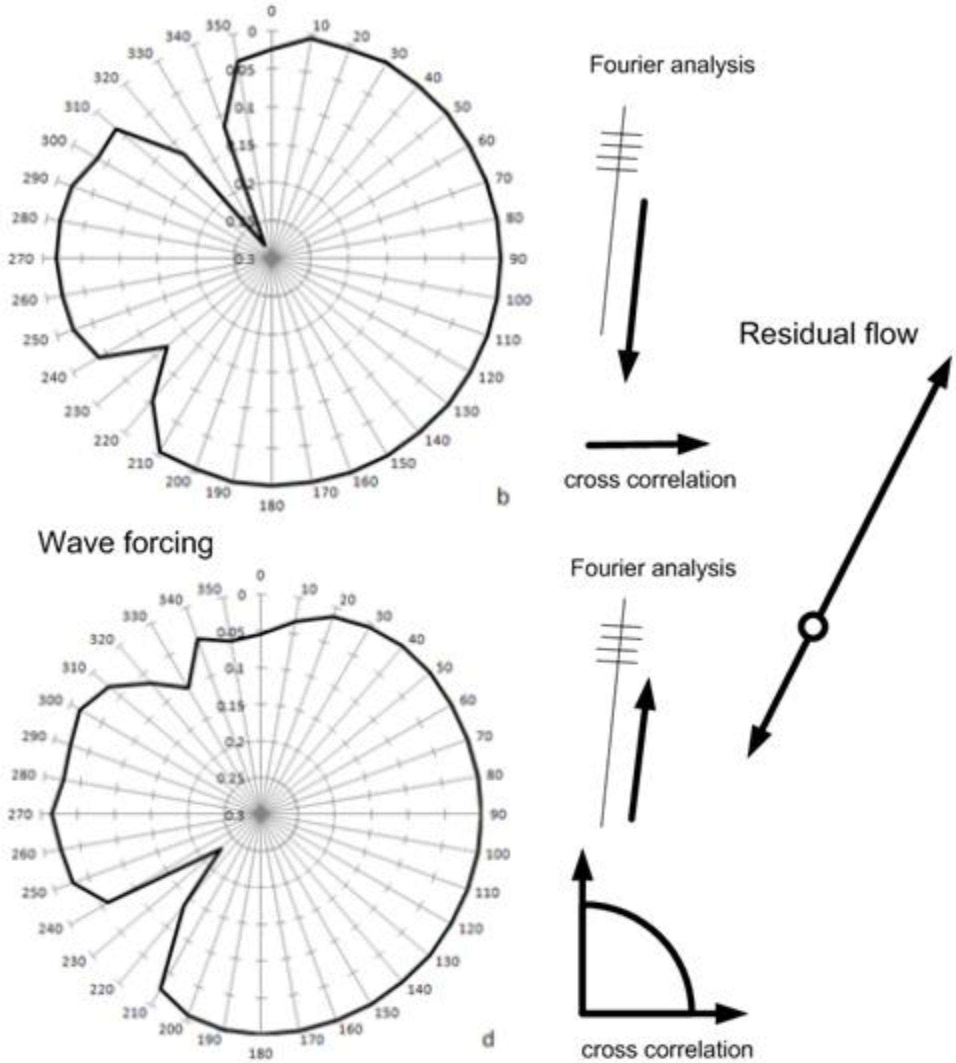

Figure 5.9: Wave forcing direction- frequency distribution, the found migration using cross correlation and the Fourier analysis and the long term mean residual flow.

The question we now need to answer is if the wave direction is independent from the flow direction in this area.

The MATROOS dataset did not include flow data from the 2001- 2002 period. Therefore, a comparison is done with the 2006 data, see figure 5.10. For the year 2006 both flow and wave data is available.
The flow direction is the direction vector of the 12 hour average Northward flow velocity and the 12 hour average Eastward flow velocity. The 12 hour average was taken to mean out the M2 (dominant) tidal flow signal. What was left is the flow that can be considered the residual flow.

There is a clear relation between peak flow rates and the transport of wave energy. The relation in their direction can be seen as well.
The average of the Northern and Eastern vectors combined is 0.05 m/s to wards the North East, but under large waves (interpreted as being caused by strong winds during storms) the residual flow can be up to 4 times this velocity.

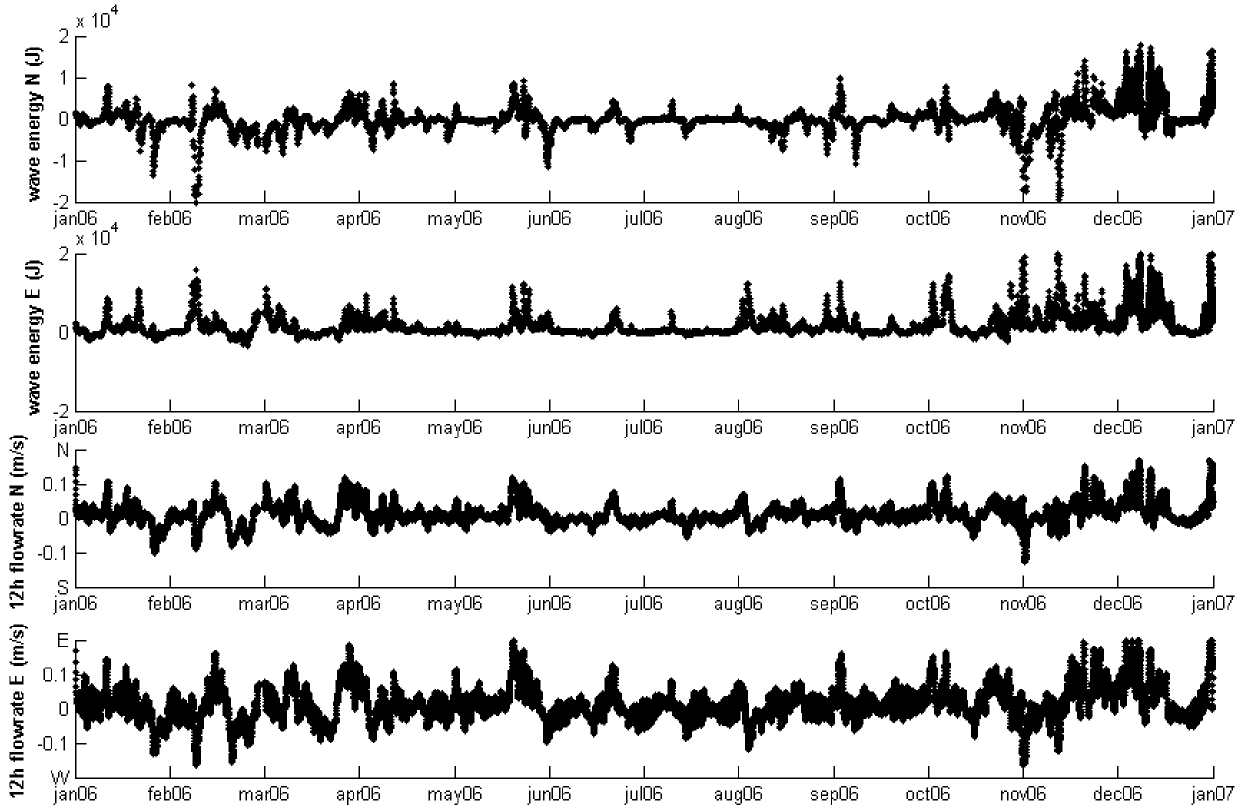

Figure 5.10: [1] Surface wave energy towards the North (J). [2] surface wave energy towards the East. [3] 12 hour average flow rate towards the North (m/s). [4] 12 hour average flowrate towards the East (m/s). The data used for plot [1] and [2] is from www.waterbase.nl. The data represented in plot [3] and [4] are made with data from MATROOS.

For this area we can conclude that residual flow and (wind induced) surface waves are not independent. It is a save assumption to make that the strong relation between the wave height and direction and flow velocity and direction also holds for the period in which the bathymetry was recorded.

The effect of the residual flow on the asymmetry, migration rate and direction of sand waves is already known from field data and simulations done in chapter 4. What is still interesting to discover is what part of the effects on sand waves can be attributed to the surface wave stirring and the effect of the angle of the surface waves with respect to the current.

5.3 Eco Morf 3 SWC simulations

To investigate the wave induced (non flow related) part of the migration direction, migration rate and asymmetry, the area described in pervious paragraph is modelled using the SWC (see chapter 3). Contrary to the simulation in chapter 4 (Varne area), in these simulation the wave angle and height are varied under continuous circumstances.

Tidal flow settings

The tidal velocities and direction have been studied for MATROOS data for the IJmuiden ammunition depot from January 2008. In our SWC, the tide is modelled as a combination of a symmetrical M2 tide and a steady residual current. The representation and measurements are shown in figure 5.11. Higher harmonics and interactions are not taken into account, but are considered to be represented accurately enough by this idealized description.

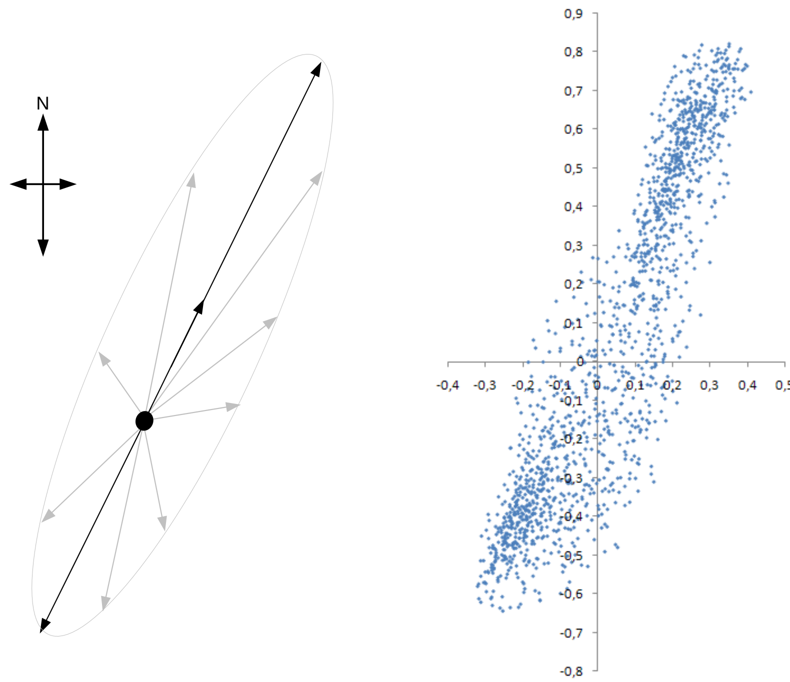

Figure 5.11: a) Schematization of the tidal flow ellipse. The SWC assumes a combination of the symmetrical tide with a smaller residual current. b) Tidal flow measurements taken from MATROOS for January 2008. Velocities in northward and eastward directions in m/s

Surface wave settings

The surface wave angles of attack (figure 5.12) are transformed to be relative to the chosen direction of the tide in the SWC. The angle of the peak displayed at 230 degrees with the tidal current in the model is therefore (230 – 203 =) 27^{o}, which means the waves and current are nearly collinear. The second (smaller) peak at 340 degrees, makes an angle with the residual current of (340 – 203 =) 137^{o}. An angle between 90^{o} and 270^{o} means the waves are opposing the direction of the residual current. As the wave forcing is symmetrical in the tidal axis, only simulation with wave angle between 0^{o} and 180^{o} were done.

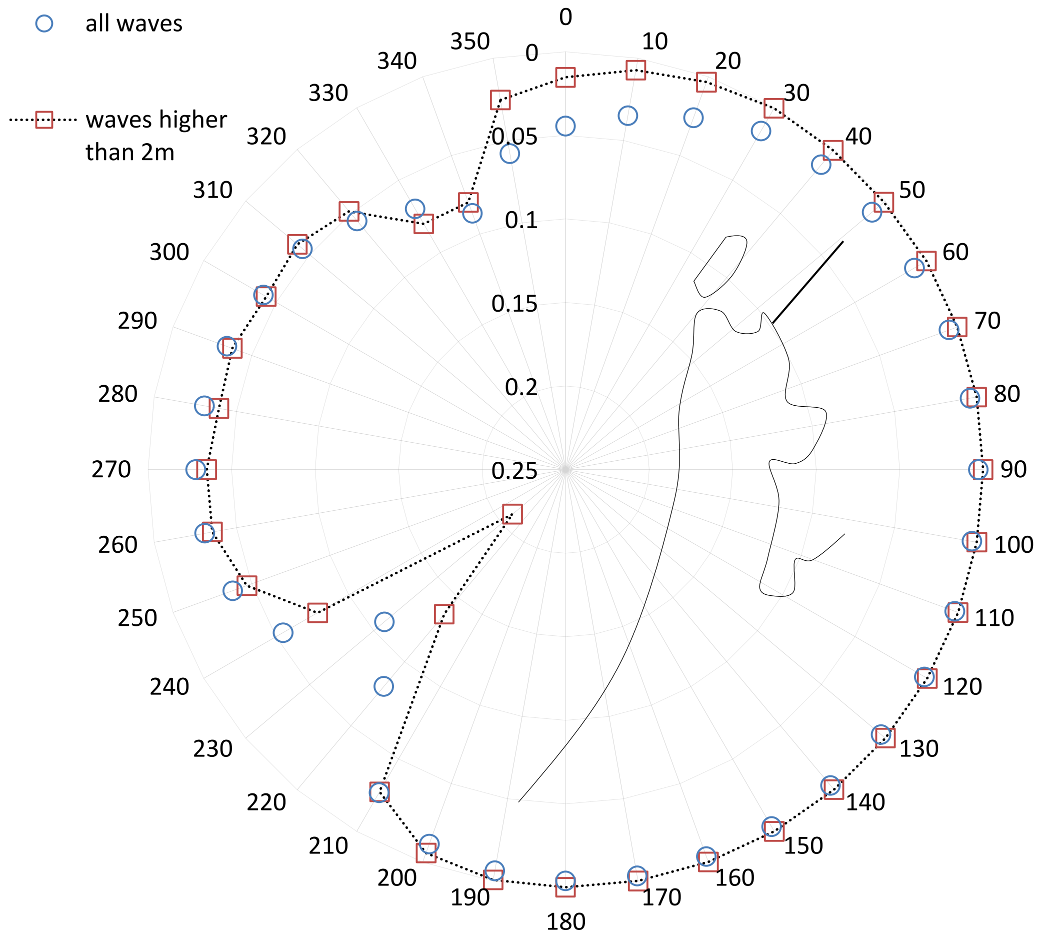

Figure 5.12: Wave attack angle frequency distribution in 10^{0} classes in degrees from the north at the IJmuiden munition dump site in the North Sea, data source: www.waterbase.nl, data period: 1990-2009. 230^{o} is the dominant direction the waves come from. They thus migrate towards the North East.

The different surface waves (see table 5.9) from the different angles are simulated under continuous circumstances. As increasingly higher surface waves have an exponentially lower frequency of exceedence, more "truthfulness" should be given to the simulations with lower wave heights.
To be able to discuss the relative effects of the results, the situation without waves is also studied. In order to say something about the minimum and maximum potential rate of migration the direction exactly collinear with and opposing the residual flow are also simulated. A simulation with and without residual current was done to separate the effect of waves and current.

wave height (metres)	wave period (seconds)	probability of exceedence (%)
1,00	5,30	50%
2,40	7,00	10%
4,20	8,90	1%
5,50	10,7	0,1%

Table 5.9: Wave height probability distribution near Ijmuiden after De Leeuw (2005)

Parameters settings
The residual tidal velocity component is chosen 0.00 or 0.05 m/s and the symmetrical tidal velocity is chosen 0.50 m/s.

A_v and S settings
Using the typical North Sea settings written in Nemeth (2003) for calculating the FGM, a sand wave length of 280 m is found. The average actual sand wave length is found to be 215 metres long on average (Table 5.2). To compare both the height and asymmetry of the bed forms with the actual sand wave shape, the simulation domain is chosen to be equal to the average length of the measured sand waves.
The most important reason to do this has to do with the fact that due to the slope term described earlier, the maximum height of the bed form is partly determined by its length. This effect is shown in the Varne simulation in chapter 4. The correct FGM may be accomplished by changing e.g. A_v and S until the correct FGM was found. However the A_v and S parameter are very difficult to estimate and it is unknown what the effect on the simulations is outside the known values. These parameters are therefore kept at the values of Nemeth (2003). The domain is set at 220 m. At this domain length, dans wave simulation is still possible as the growth rate of bed forms of this length shows positive in the FGM plot, see figure 5.13

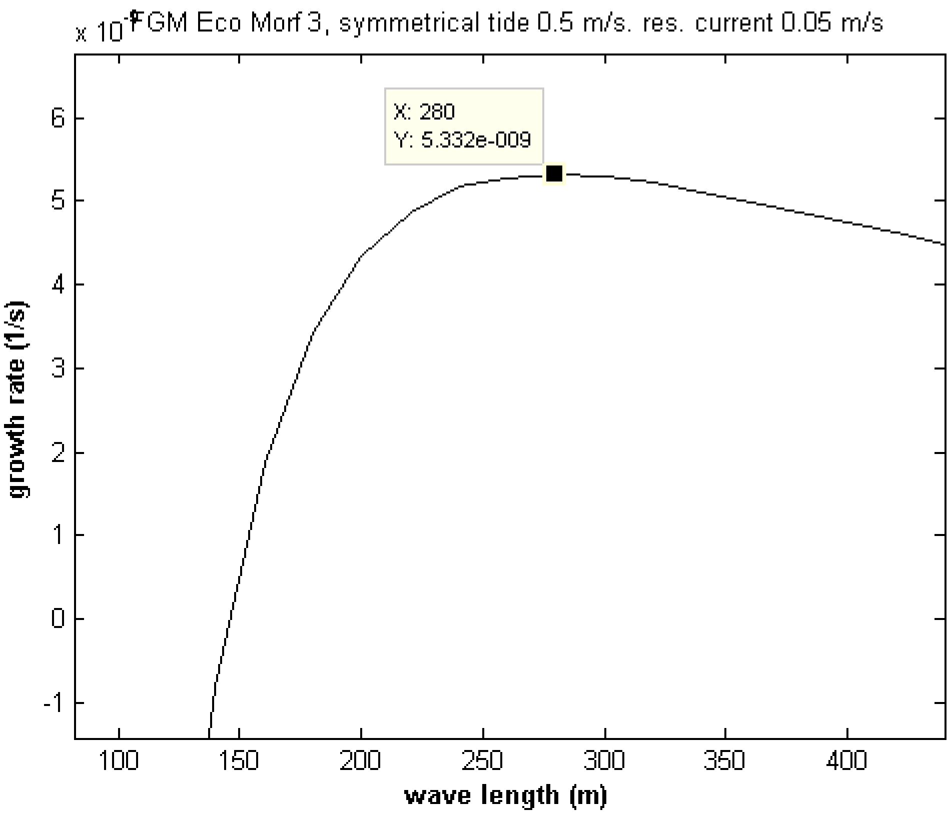

Figure 5.13: FGM for the Eco Morf 3 area. Symmetrical tide 0.5 m/s. residual current 0.05 m/s.

Simulation results
The definitions of the geometric properties given in these results are further explained in chapter 2.

When the results speak of accuracy, this is meant as the stability of the found value of the parameter under influence and not the "correctness" of the found value. The accuracy is expressed by the standard deviation. All attributes (except for the T90) are averaged over the time steps 600 to 700. The mean and the standard deviation are given in the results figures. E.g. the simulation bed form height [h1.0m 137 degrees, no residual current] shows a large standard deviation of 2m.

Bed form height (figure 5.14)

General result

The bed form height is most significantly influenced by the presence of absence of a residual flow and or waves that are high enough (4.2 m and 5.0 m simulation). A strong relation between the bed form height and the bed form volume (figure 5.15) exists.

No waves

The bed form height without waves is very accurate for both the situation without a residual current (H 12 m) and with a residual current (H 8.5 m).

No residual current

The presence of the waves, in the situation without residual current, leads to a lowering of the bed form height by about 2 meter to 10.0 metres for the 1.0 m and 2.4 m waves. A lowering of 3 metres to a 9 m bed form height can be seen for the situation with waves that are 4.2 m and 5.5 m high.

Residual current

In the situation with residual current the bed forms become a meter higher under increasing surface wave height. The change is most significant between the 2.4 m and 4.2 m waves.

Wave angle

A clear relation of the influence of the wave angle on the predicted height can not be seen. The bed form height loses accuracy for simulations with extreme waves in the direction of the residual current. Under the larger two wave categories, without a residual current, the predicted bed form height increases if the waves are more perpendicular (80^0) to the direction of the tidal axis.

The simulated bed form height (8 – 12 m) is over predicted with respect to the measured bed form height of 1.72 m (table 5.2). The increase in bed form height under larger waves might well be caused by the increase in volume of sand that is stirred by the surface waves and is thus made available for the bed form to grow.

The increase of the bed form height under waves more perpendicular to the tidal axis might be caused by the fact that the wave induced bed load transport is sufficiently large, but has a smaller component parallel to the tidal axis. This reduces the lowering effect of the waves, thus allowing the bed forms to become higher. This conclusion is supported by the bed form net transport (figure 5.16): The higher two waves induced transports show a reduction in transport as the surface waves make an angle that is increasingly perpendicular to the tidal axis. This is true for the situations with and without residual current.

Bed form volume (figure 5.15)

The bed form volume generally increases with increasing surface waves under residual current. The relations discussed in the bed form height are all valid for the bed form volume as well. The volume of the simulated bed forms is between 1.2 – 2.0 m^3/m^2. The volume of the measured transects is 0.25 m^3/m^2 for all recordings, see table 5.5. The over prediction of the sand wave volume by a factor 5 – 8 is equal to the overestimation of the height of the sand waves by a factor 4 – 6.

Bed form net transport (figure 5.16)

The transport figure shows that waves of 1.0 height are not sufficient to add to the amount of sediment transported. Under higher surface waves, the sediment transport increases. A break in the trend can be

seen in the simulations [0 and 27 degrees, 2.4m waves]. In these simulations the sand waves did not show a shape change (transport rate zero) and did not migrate (figure 5.17).
Under increasingly perpendicular angle wave angle, the sediment transport and the migration rate decrease. This is probably due to the lowering of the transport component parallel to the tidal axis described above.

Migration rate (figure 5.17)
The migration rate (logically) shows a similar behaviour as the sediment transport with the exception that the migration rate can show the direction in which sediment is transported. When the waves oppose the direction of the residual current, the migration rate decreases. The "no residual current simulations" show that the bed forms can even move in the opposite direction, if the waves are sufficiently high and if the angle of the waves is approximately perpendicular or larger. In the simulations with residual current, the rate is only lowered and does not become negative.

The migration and transport rate result for simulation [h 5.5 m, angle 80, 137 and 180] show a minimum that is closer to 80 degrees than it is to the 180 degrees angle. This is interpreted as a direct result of modeling the wave induced contribution to the transport as a function of the velocity component parallel to the tidal axis.
The empirical magnitude of the migration was 1.5 m/year over the long run. Individual waves can be seen to move up to 12 m/year over shorter periods. The continuous simulations accurately predict the migration for two categories with lower waves: 4-11 m/year for the residual currents and 0-2 m/year for the simulation without a residual current. For the higher waves the migration is overrated, but these waves in reality have a frequency of occurrence of 1% and 0.1% respectively and can thus only be extrapolated to short term values.

L_{stoss} / L_{lee} (figure 5.18)
As to be expected the L_{stoss} / L_{lee} ratio is 1.0 for the simulation without a residual current and waves. A value of 1 means both side are equally long. For this simulation this means the length is 220 / 2 = 110m. Upon increasing wave angle, the stoss side shortens a bit bringing the ratio just below 1 for the waves opposing the current. The simulations with a residual current accurately predict the mean value measured in the bathymetry data, 3.5, for the lower wave categories. (See Table 5.2)
The L_{stoss} / L_{lee} asymmetry in the Varne area is given in table 4.2 and table 4.3.
, the values are between 1.23 and 2.57. The asymmetry in the simulations (without waves) is 1.33. The lower the L_{lee} / L_{stoss} asymmetry might be due to the higher symmetrical tide velocity (1.0 vs. 0.5 m/s) in this area and in the simulations.

Ratio L_{crest} / L_{trough} (figure 5.19) and Ratio H_{crest} / H_{trough} (figure 5.20)
Increasing surface wave height lengthens the crests and decreases the height of the crests for the simulation with a residual current. For the no residual currents simulations a relation can not be seen. The pre storm situation in the Varne area showed narrow short crests with long troughs that were transformed in lower broader crests after a storm. Unfortunately these two ratio's cannot be determined in the Fourier methods, so a quantitative comparison can not be made.

T90 (figure 5.21)
The growth rate to 90% of the height of the final bed for is 20 and 45 year for the situation with and without residual current respectively. Under stormy situations the T90 decreases to 7 – 13 years.

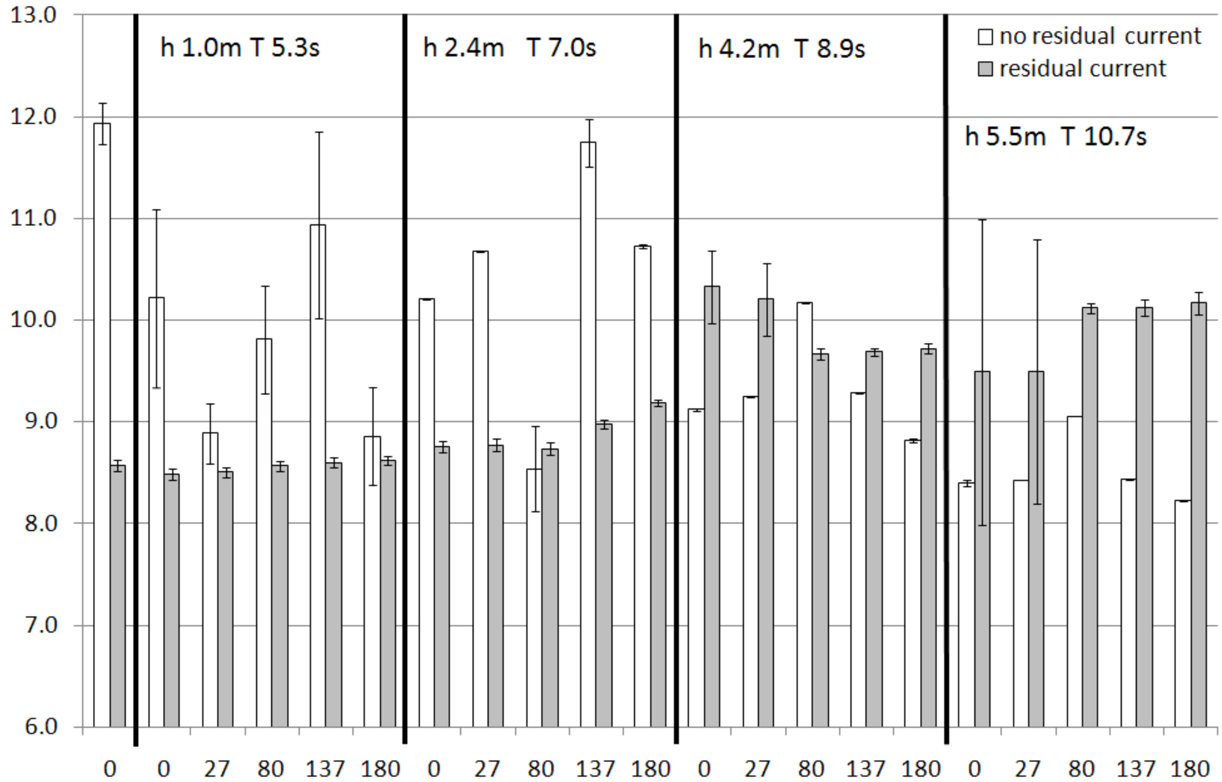

Figure 5.14: SWC bed form height (m) as function of the surface wave height and angle. Note the height of the sand wave starts at 6.0 m. The left two bars represent the simulation without waves (h 0m). Errors bars indicate the mean value ± standard deviation.

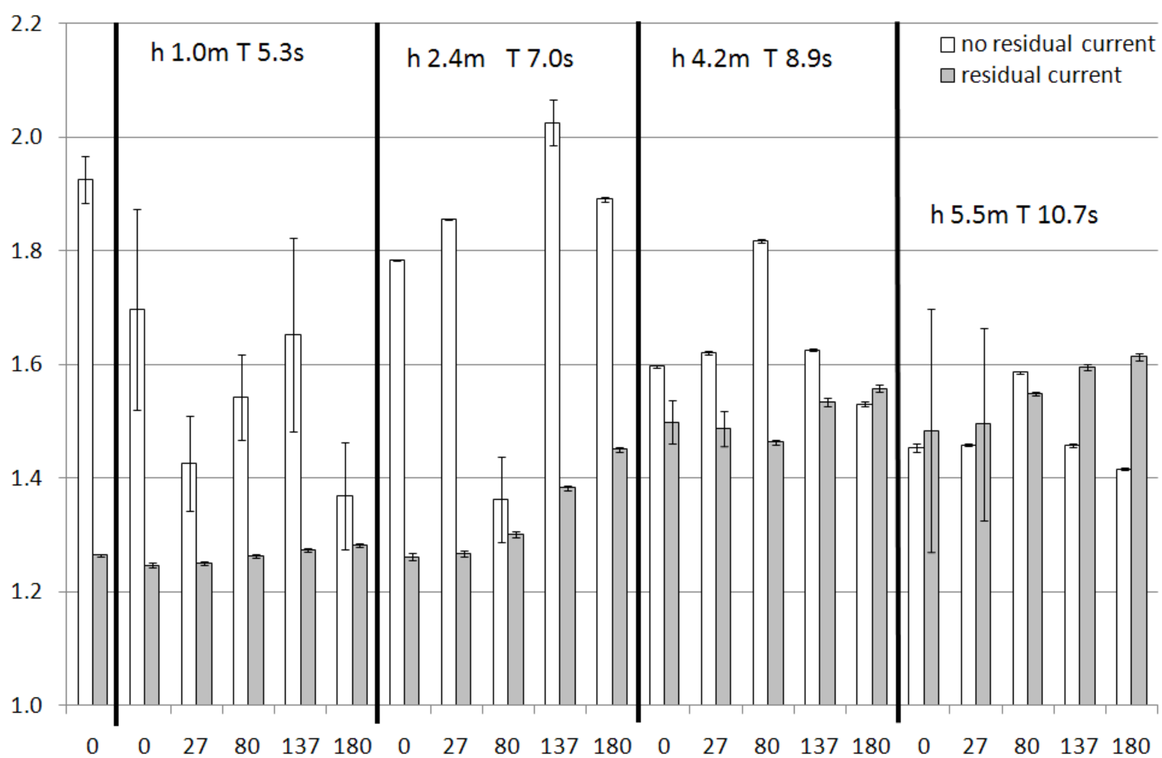

Figure 5.15: SWC bed form volume (m3 / m2) as function of the surface wave height and angle. The left two bars represent the simulation without waves (h 0m). The error bars indicate the mean ± the standard deviation.

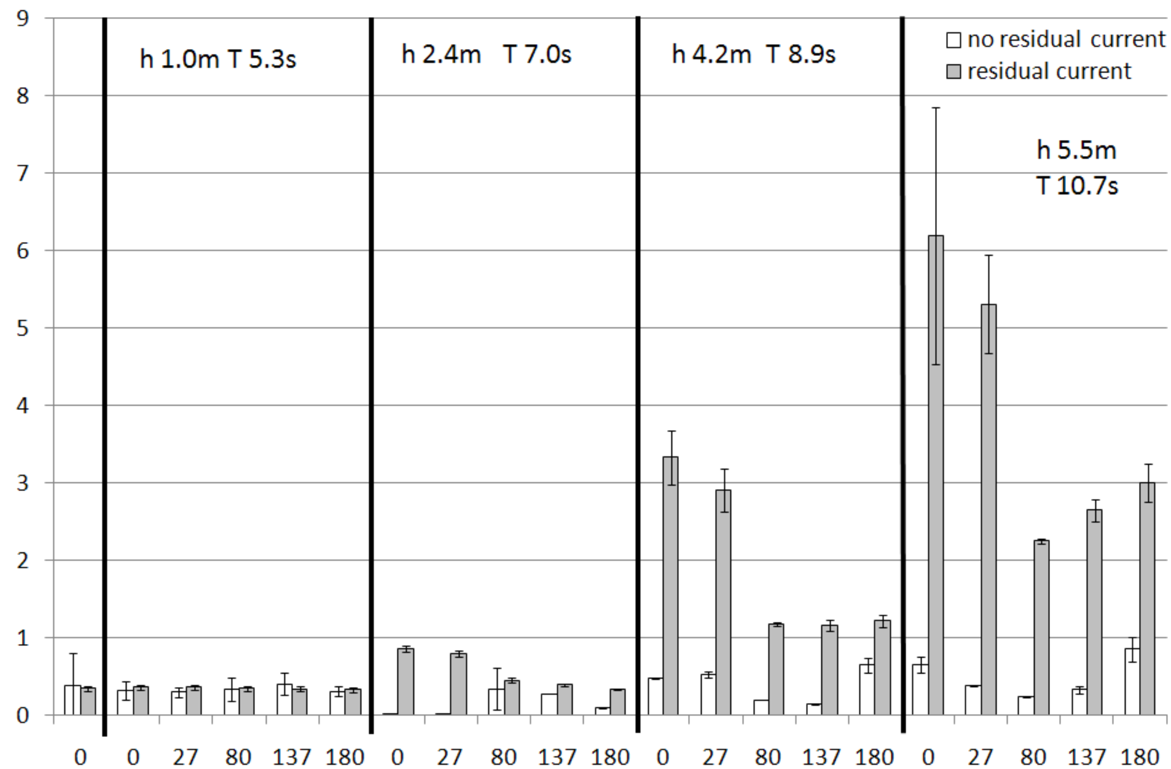

Figure 5.16: SWC transport volume (m3 / m2 * year) as function of the surface wave height and angle. The left two bars represent the simulation without waves (h 0m). The error bars indicate the mean ± the standard deviation.

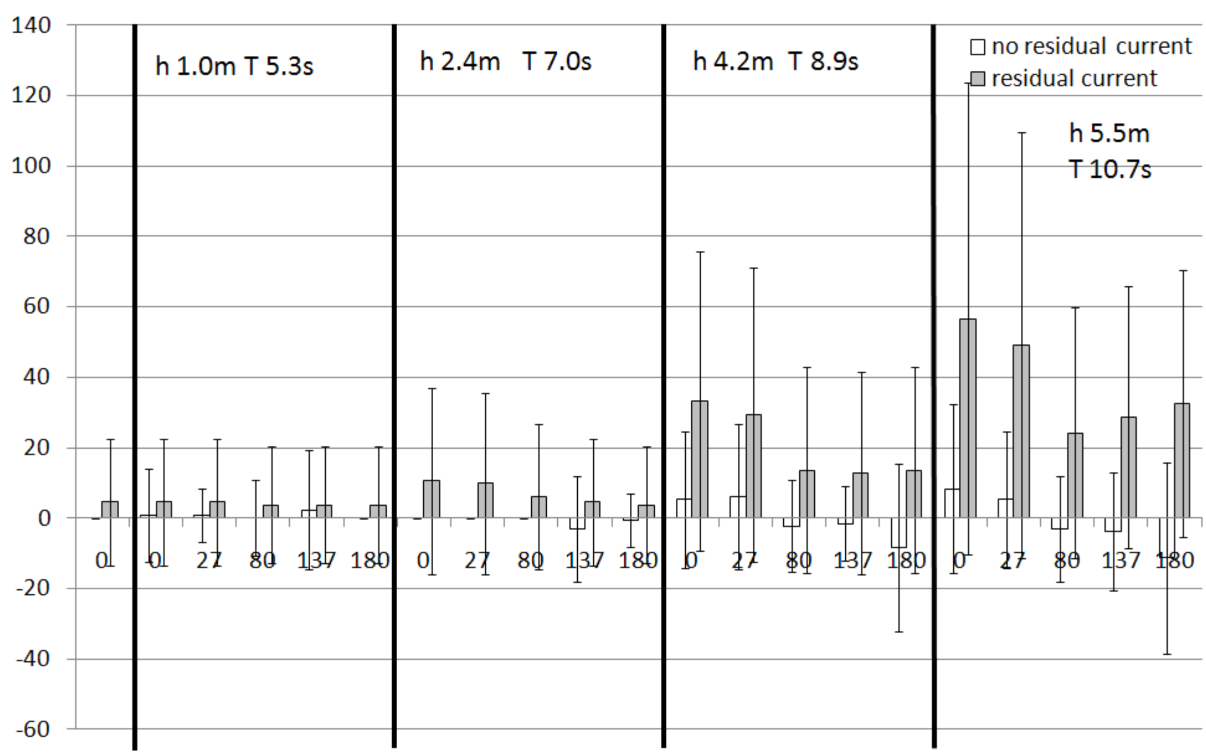

Figure 5.17: SWC (crest) migration rate (m/ year) as function of the surface wave height and angle. The left two bars represent the simulation without waves (h 0m). The error bars indicate the mean ± the standard deviation.

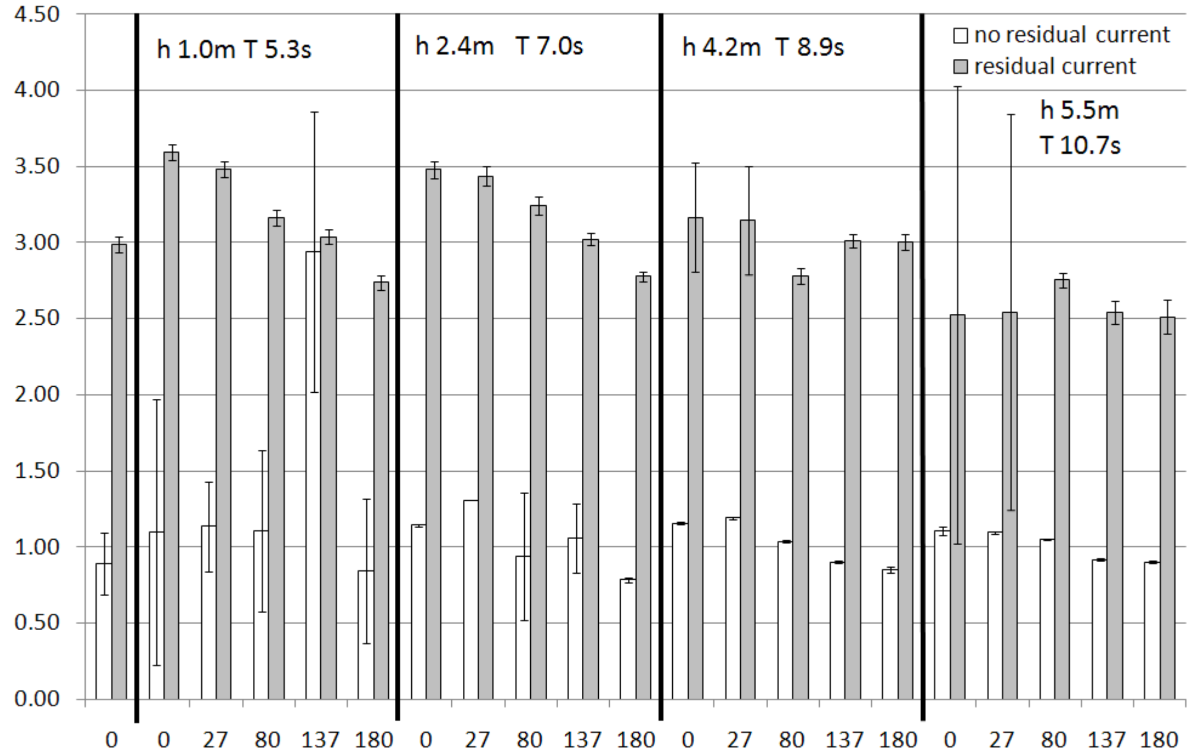

Figure 5.18: SWC L_{stoss} / L_{lee} (-) as function of the surface wave height and angle. The left two bars represent the simulation without waves (h 0m). Errors bars indicate the mean value ± standard deviation.

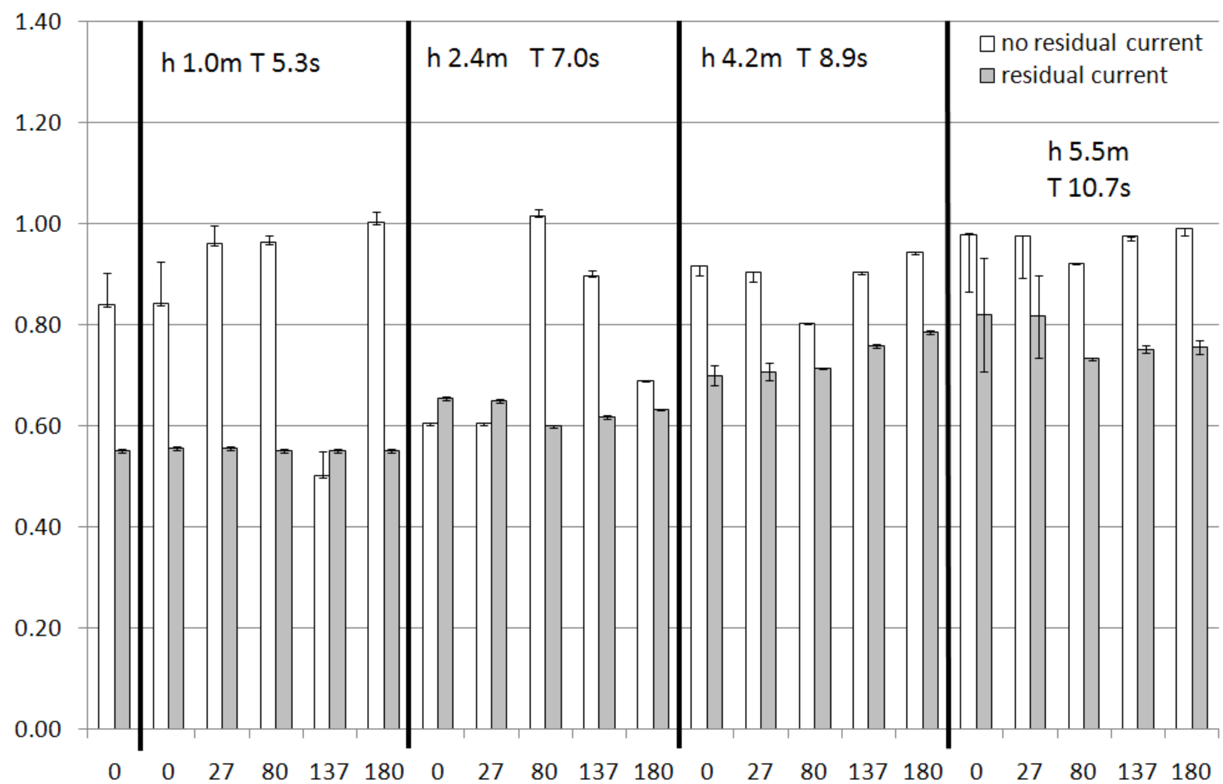

Figure 5.19: SWC L_{crest} / L_{trough} (-) as function of the surface wave height and angle. The left two bars represent the simulation without waves (h 0m). Errors bars indicate the mean value ± standard deviation.

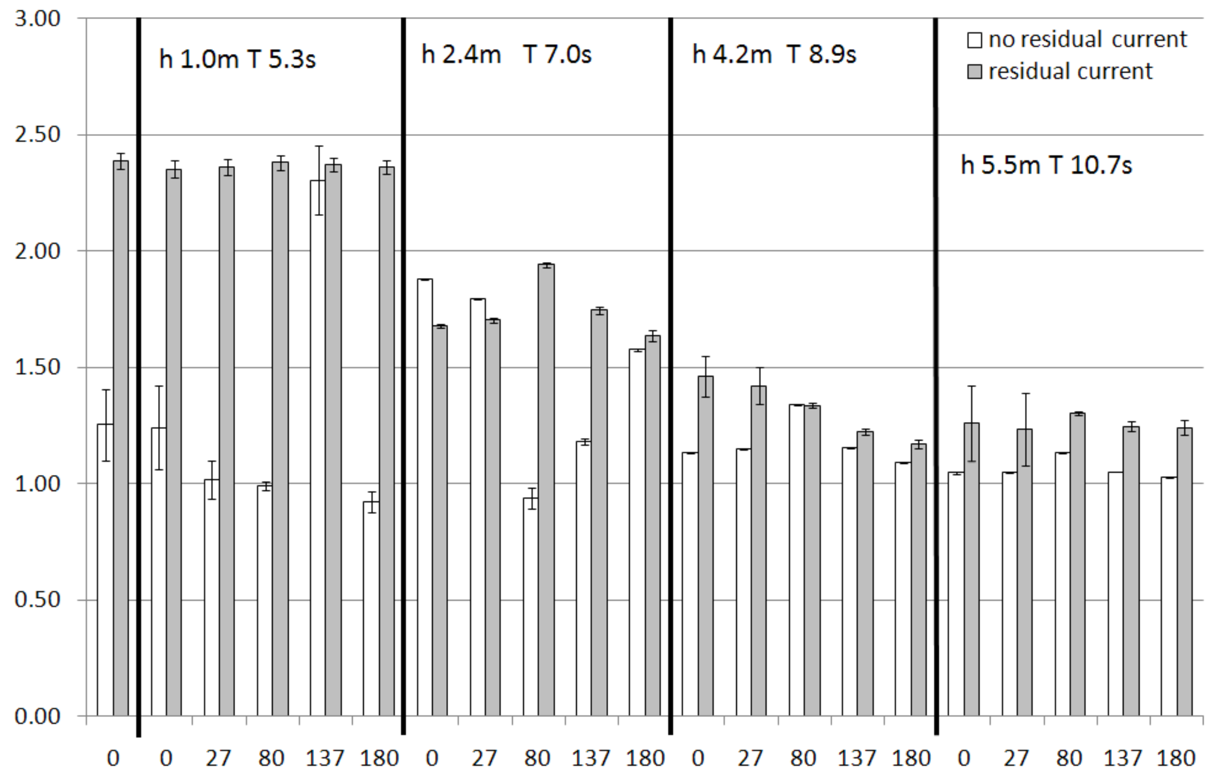

Figure 5.20: SWC H_{crest} / H_{trough} (-) as function of the surface wave height and angle. The left two bars represent the simulation without waves (h 0m). Errors bars indicate the mean value ± standard deviation.

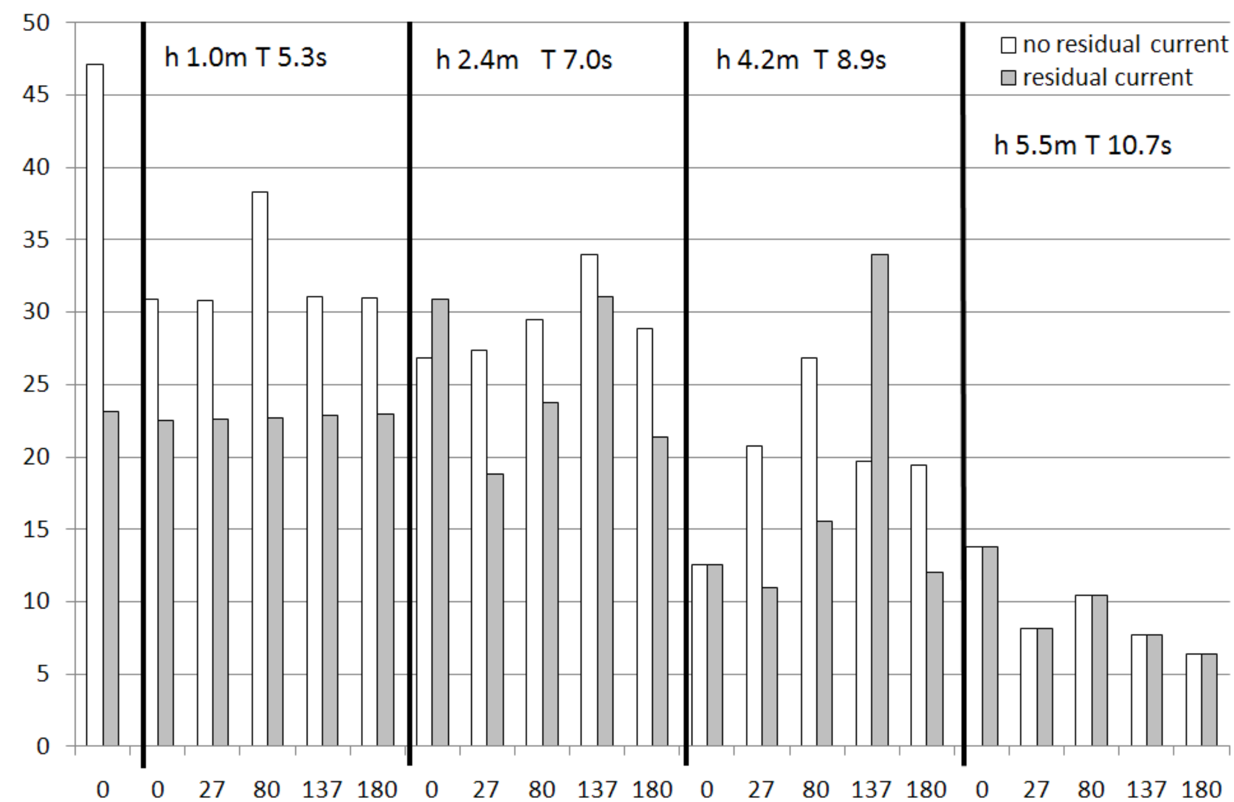

Figure 5.21: SWC T90 (years) as function of the surface wave height and angle. The left two bars represent the simulation without waves (h 0m).

Comparison between the empirical dataset and the simulation results.

In this comparison, the results from the empirical data are compared to the results for the most "truth like" simulation. The simulation chosen has 1 metre waves attacking with an angle of 27°. This is the third bar in the result plots in the previous section.

Bed form length
The fastest growing mode of 280 metres compares fairly well with the average length of the measured sand waves of 214 metres. Since the sand wave code also showed a positive growth for a length of 220 metres, this length was chosen for the length of the simulation domain. In a longer domain the sand waves might become higher than they are now. In the simulations for the Varne area, the 210 metre simulation resulted in a larger sand wave height than the simulation with a 180 metre domain length. This is probably partly controlled by the balance between the slope uphill and the fact that sand is more easily transported downhill.

Bed form height
The simulations predict a bed form height of 8.5 metres, while the recordings show an average bed form height of 1.47 metres.

Volume
The measured volume is 0.25 m^3/m^2. The modelled volume is equal to 1.1 m^3/m^2. The overestimation by a factor 4 is comparable to the overestimation in sand wav height.

Migration rate
The migration rate found in the recordings of between 2 and 11 metres / years was also found in the simulations: 10 metres/year.

L_{stoss} / L_{lee}
The model is able to predict the correct asymmetry. It was measured at 3.6 (-) and was simulated at 3.5 (-).

Chapter 6. Discussion

Discussion on simulation results

Crest modifications

The time span in which most modifications of the sand wave shapes are expressed due to wave influences are 50 to 20 weeks. These simulation time spans are long compared to the rate at which changes took place in the Varne area, 66 days. Also, the continuous conditions imposed in the model are hardly realistic when we consider the fact that these waves have an actual frequency of occurrence of 1% or less. Finally, the results when only waves are varied are limited compared to observed changes even though the morphological (build up) time scale is significantly shortened when higher waves are included.

A possible explanation is given by Tonnon *et al.* (2007). They use a full process sand wave model with neap-spring variations, a surface waves propagation model and both a bed-load and suspended load transport modes. In their outcomes they find that sand waves grow under weak tidal current and low surface waves. This is when bed load transport is dominant. The sand waves decay when suspended load is dominant. This transport mode is dominant under strong tidal current and storm waves. The explanation they give is that under suspended load sand wave particle are able to be transported beyond the crest, which leads to a flattening of the crests. It might be that the suspended sediment should be added to increase the effect sorted by surface waves. According to Sterlini (2009) however, the suspended sediment is very small for the grain sizes in the observed research area, 25 mm.
In this modelling effort, suspended sediment was not included as the complex interaction between suspended sediment and surface waves might prove to complex for the time available in this study. This is left for future work.

Another interesting aspect about the observed sand wave modification due to the storms is difference in water depth between the two transects. The water depth of the first transect is between 23 and 29 metres. The water depth of the second transect is between 18 and 27 metres. If the sand wave height reduction is caused by surface waves, it would be logical to presume that the height reduction in the second profile is substantially larger due to the greater exposure to surface waves. Yet both profile show the same height reduction, 1 metre. This remarkable outcome was also found in the pre and post storm survey of the Middelkerke Bank, as described by Houthuys *et al.* (1994). Houthuys finds no difference in large dune height reduction (1.2 metres) even though the two areas surveyed differ significantly in local water depth.
The small distance (1km) between the transects in this study makes it likely the two transect are exposed to the same conditions. The measurements are however located North East of the Varne sand bank. It could very well be that the second transect, which is situated more southerly, is less exposed to flow and waves from the South West due to shielding by the Varne bank. This was not further investigated.

Domain length

The discrepancy in the length of the predicted fastest growing mode and the actual wave length found in the Varne area could maybe be resolved by changing the Av and S, as for these parameters the model is very sensitive. Németh (2003) and Sterlini (2009) did sensitivity analysis for (among others) these parameters. It could be that modification of these parameters within the valid range applicable for the Varne area could improve the domain length prediction. Sterlini (2009) also showed that suspended sediment may cause a shortening of the fastest growing mode.

Varne Lee- Stoss asymmetry.
The Fourier methodology, as described in chapter 2, assumes the analysis of a particular bed form starts with the stoss side, meaning the stoss side should have a lower x-coordinate than the lee side of the same bed form. Knowing the residual current to be in North Eastern (NE) direction, as well as the dominant direction of migration, one would expect to see transects showing the -generally longer- stoss side on the South Western (SW) side of each bed form. The data analysis however showed the bed forms are generally longer on the North East side and have their mega ripples most often on the North East side of the sand wave. It may be that the proximity to sand bank (just to the South West of the area under interest) causes the discrepancy in the length of the sand wave slopes.

Comparison
The simulations for the Varne and the Eco Morf 3 area were performed under the same parameter value that were shown to be of importance by Németh (2003) and Sterlini (2009), such as H, A_v, S and magnitude of the residual current. The only parameter that was significantly altered between both simulations was the rate of the symmetrical tide. This was 1.0 m/s for the Varne region and 0.5 m/s for the Eco Morf 3 area. The water depth was also slightly different. The effect of this is thought to be minimal. In the Eco Morf 3 simulations, we chose a lot more different wave heights and angles, so this comparison is made with the simulation considered closest to the Varne simulation, "h2.4m; 0 angle; with residual current". See Table 6.1.

	Simulated results	
	Varne	Eco Morf 3
Waterdepth (m)	30.0	28.2
surface wave height (m)	2.8	2.4
residual current (m/s)	0.05	0.05
H_{SW} (m)	6	8.5
L_{sw} (m)	210	220
Volume (m^3 / m^2)	1.25	1.1
Transport (m^3 / m^2 year)	3	0.9
Migration (m/year)	40	10
L_{stoss} / L_{lee} (-)	1.33	3.5
L_{crest} / L_{trough} (-)	0.91	0.65
H_{crest} / H_{trough} (-)	1.17	1.7

Table 6.1: Comparison between the Varne and the Eco Morf 3 area simulation results.

Under the higher symmetrical part of the tide the sand wave height diminishes as a result of the higher flow velocity. The flow velocity also greatly increases the sand wave migration rate and the sand wave transport. The volume is a little bit less; probably less sediment is moved by the lower maximum flow velocities. Striking is the fact that the sand wave volume in the Eco Morf 3 simulation is lower, while the sand wave is higher.
Due to the relatively larger asymmetrical tide, the L_{stoss} / L_{lee} asymmetry is larger in the Eco Morf 3 area. The asymmetry is well predicted.

Discussion on methods

Cross correlation

The cross correlation allows us to see in what direction the sand waves migrate. As we showed, this is not necessarily in the direction perpendicular to the crests. The results are however very sensitive to the grid size of the regular grid. Preferably the grid size is small with respect to the migration of the area. The reason for this is illustrated in figure 6.1. If the migration is over a small distance, the uncertainty of the actual migration distance and angle increases severely.

E.g. if the maximum correlation is found at displacement 2,3 (dx,dy units), the calculated displacement is $\sqrt{2^2+3^2} = \sqrt{13} \simeq 3.6$ units. The uncertainty in the displacement is $\sqrt{1^2+1^2} = \sqrt{2} \simeq 1.4$ units. The relative uncertainty in displacement is therefore 1.4 / 3.6 = 0.4 (or 40%). The calculated direction of migration in this example is $34^{o}\pm11^{o}$. In this $\pm11^{o}$ is the uncertainty in actual direction of migration.

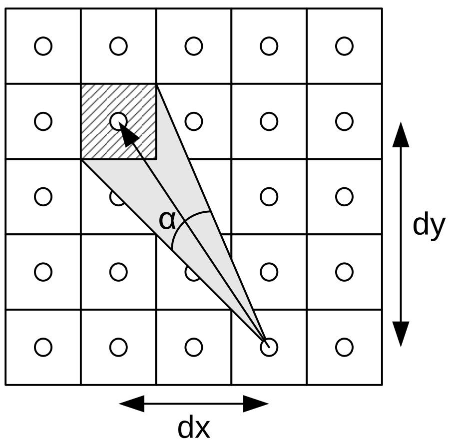

distance (-)

offset y direction						
5	0.2	0.2	0.2	0.2	0.2	0.2
4	0.3	0.3	0.3	0.3	0.3	0.2
3	0.3	0.4	0.4	0.3	0.3	0.2
2	0.5	0.6	0.5	0.4	0.3	0.2
1	1.1	1.0	0.6	0.4	0.3	0.2
0	-	1.1	0.5	0.3	0.3	0.2
offset x direction	0	1	2	3	4	5

angle (+/- degrees)

offset y direction						
5	6	7	7	7	6	6
4	8	8	9	8	7	6
3	11	11	11	9	8	7
2	18	17	14	11	9	7
1	45	27	17	11	8	7
0	-	45	18	11	8	6
offset x direction	0	1	2	3	4	5

Figure 6.1: Uncertainty in migration distance (as percentage of the found displacement) and displacement angle uncertainty. For small migrations the uncertainty in distance and angle is significant.

In the Eco Morf 3 area, maximum migration was approximately 2 metres, or 2 grid cells. The uncertainty in displacement is therefore 50% in distance and $\pm14^{o}$ in angle. The uncertainty in migration in the Varne area is 5 – 10 % in distance and $\pm3^{o}$ in angle.

Chapter 7. Conclusions

This research was started with the following research questions:

1) How did the observed sand waves change shape and migrate over time?
3) What relations between the observed bathymetry changes and changes in environment data can be seen?
4) To what extend are the morphodynamic responses we see in the empirical dataset supported by our idealized model simulations?
5) Are the time scales in which the model predicts changes, if any, realistic compared to the changes we find in the bathymetry dataset?

1. *How did the observed sand waves change shape and migrate over time?*

A summary of the bathymetry data studies is presented table 7.1.

Varne area

In the Varne area we see that the sand wave reduce their crest height by a meter between a pre- and post storm situation (from 4.9 m & 4.0 m to 3.9 m & 3.0 m). The data shows the crests and trough migrated in to the North Eastern direction with a to yearly values extrapolated rate of between 22 and 139 metres / year. The troughs of the first transect however move in the direction of the South West with a rate of 66 m/year.

Before and after the storm the volume of the sand waves was reduced from 0.53 [m^3/m^2] to 0.48 [m^3/m^2] for the first transect and from 0.80 [m^3/m^2] to 0.72 [m^3/m^2] for the second transect. This result supports the conclusion of a collapse of the sand wave in this period.

The L_{stoss} / L_{lee} asymmetry inverted from 2.7 to 0.5 (-) for the first transect and increased from 1.3 and 1.9 (-) for the second transect.

The most striking about this result is the fact that the sand waves (except for the second recording of the first profile) have their longest side on the North East side of the sand wave, while the long term mean residual current is towards the North East as is the direction of migration and the wave/wind forcing. Based on these properties we would expect the longest side to be on the South West side of the sand wave.

Eco morf 3

The eco morf 3 area sand waves are found to be stable in height and asymmetry. Migration varied in the direction North East and South East. Long term migration rates (2 m / year) were found to be significantly lower than short term migration rates (up to 4.5 m/year). This is interpreted as a seasonal back and forth movement.

	Observed results		
	Varne		Eco Morf 3
	transect 1	transect 2	
H_{SW} (m)	3.9 – 4.9	3.0 - 4.0	1.47
L_{sw} (m)	92 - 96	86	214
Volume (m^3 / m^2)	0.48 - 0.53	0.72 - 0.8	0.25
Transport (m^3 / m^2 year)	2.44	1.77	0.03 - 0.12
Migration (m/year)	66 - 139	22 - 32	2 – (11)
L_{stoss} / L_{lee} (-)	2.0 - 2.7	1.3 - 1.9	3.6

Table 7.1: Summary of the bathymetry changes in two empirical datasets.

3. *What relations between the observed bathymetry changes and changes in environment data can be seen?*

Varne Area

High, narrow crested sand waves were formed in a period of at least 2 month without waves higher than two metres. In a period with a lot of subsequent storm, the crests were found to be a metre lower than in the pre storm situation. This result is also supported by the reduction found in the volume of both transects.

The short term, high migration rate were found not to be supported in the long period between recording of the second transect. This indicates that most of the observed migration in the first transect may partly be caused by a change in shape rather than a migration of the sand wave as a whole.

Migration in this period was in the direction of the residual flow, as was the (continuously) dominant direction of the surface waves. An exception to the migration direction are the troughs in the first recording of the transect. The troughs moved towards the SW. Again this migration may even be a combine effect of migration and shape change.

Eco Morf 3

The back and forth movement of the sand waves in the Eco Morf 3 area was found to coincide with the direction distribution of the wave energy. In the first two periods the sand wave migrated South and the wave energy was also directed towards the South. In the third period both sand wave migration and wave energy was directed North.

The fourth period is inconclusive in this trend, as it does show a migration of the sand waves towards the North, but the wave energy is as frequently from the North as it is from the South West.

4. *To what extend are the morphodynamic responses we see in the empirical dataset supported by our idealized model simulations?*

Higher surface waves also increase the migration rate and transport rate of the sand waves more. If the waves are however opposing the residual current, the rates drop to below the rates found in absence of waves. This effect increases with increasing angle with respect to the residual current.

Varne area
The lowering and broadening of the crests, as well as the increase in L_{stoss} / L_{lee} asymmetry were supported by the model simulations. The asymmetry in the model increased from 1.3 to 2.5 in the pre- and post storm situation. The bathymetry data showed a pre and post storm asymmetry of 2.7 to 0.5 (transect 1) and 1.3 – 1.9 (transect 2). The striking difference is that in the simulations the stoss (or longest) side of the sand wave is on the upstream side of the sand wave with respect to the residual current. The Varne sand waves have their longest side on the lee side of the sand wave.

The sand wave volume in the Varne area shows a reduction in volume of 10 – 20% for the pre and post storm situation. Also, the (fair weather) narrow crested sand waves with long troughs collapsed reduced their crest height a metre under stormy situations. This reduction in volume was not found in the simulations. Under increasing wave height and opposing wave directions, the sand wave volume was even found to increase 10% due to the strirring of extra sediment by the waves.
The reduction in crest height was seen, but an equally large lowering of the troughs (not seen in the empirical dataset) made that the total bed form height did not change in the model, while it did in the recorded data.

Eco Morf 3
The sand waves in the Eco Morf 3 area showed a back and forth movement in seasons. The direction in which the bed forms moved corresponded well with the wave energy direction in the period that the changes occurred.
In the simulations however, even the highest waves opposing the residual current are not able to cause a negative migration.
Therefore, when the empirical data showed migration against the direction of the long term average residual current, this is thought to be the result of short term fluctuations in the residual flow rate and direction itself. This process may however be supported by the wave action as increased wave action lowers the time in which sand wave form, the T90, by almost 50%.

The overestimation of the sand wave volume in the Eco Morf 3 area is comparable to the overestimation in bed form height. The link between the sand wave height and the domain length found in the Varne simulations is not supported by the empirical dataset as the Varne sand waves are higher, while the eco morf 3 waves are longer.

We showed that the short term residual flow rate and direction have a very strong relation with the height and direction of the wind waves, as was found by Bowden (1956) for the Varne area. In short: Strong winds induce both high waves and a residual current, both in the same direction. The analysis done here only changes the angle of the waves and keeps the residual current collinear with the symmetrical tide. Also, the magnitude of the residual current is not varied with increasing wind strength. As a recommendation for future modifications, the code could be adjusted to link the angle of the wave and the angle of the residual flow. It would be interesting to see if the constant variation in wave and residual current directions and magnitude result in a general lowering of the bed forms.

5. *Are the time scales in which the model predicts changes, if any, realistic compared to the changes we find in the bathymetry dataset?*

Varne
Modification of the L_{stoss} / L_{lee} ratio we found to occur within several weeks according to the model. This makes it realistic to believe that in term of this asymmetry parameter, waves do play an important role. The hypothesis is that residual current is the dominant factor in the rest of the changes.

The model is more or less able to predict the correct sand wave height (6 metres simulated, actual height 4 metres), but the bed form length found in the field data shows a negative growth rate in our linear stability analysis. Simulations for the Varne area were done with a domain length of 210 metres, which overestimates the actual length (80 metres) by a factor 3.

Eco Morf 3
The highest categories of wave (4.2 m and 5.5 m) have a frequency of occurrence of only 1% and 0.1% of the time. The simulations of the highest category are thus only to be used to show the equilibrium the bed forms tend to under stormy conditions. The equilibrium under continuous stormy situations may never be reached for those effects of which the time scale is an order scale longer than the duration of storms. E.g. the time scale for height adjustments of the crests (in the Varne simulations) was found to be about 50 weeks.

The combined effect of flow and waves is however apparent. The surface waves lengthen and flatten the crests, even though the volume of the entire bed form increases due to the extra wave stirring. The high waves also adjust the rate with which the sand waves reach their equilibrium height, T90. The surface waves thus significantly affect the dynamics of the system. When waves oppose the residual current, they lower the L_{stoss} / L_{lee} asymmetry and the rate of migration and transport.

Chapter 8. Recommendations

[1] The main recommendation is to modify the model to be able to investigate the effect of an angle of a residual current with respect to the direction of the symmetrical tide - and with that the sand wave - as well. The reasons for this:
[1a] The surface waves and residual current were found to be very strongly correlated in magnitude and direction in both empirical datasets we studied. [1b] The wave induced modifications of the bed form shape characteristics (other than the L_{stoss} / L_{lee} asymmetry) were found to take place on time scales that are not comparable with the rate of these changes in the empirical dataset. This, even though the model is able to predict a lot of other modification time scales within accurate values; e.g. the T90, migration rate, rate of transport and bed form volume. [1c] The simulated amount of change (in e.g. crest height) was found to be limited with respect to actual changes observed in the field data, even though [1d] the simulations were done under extreme and continuous wave conditions. [1e] Negative migration rates (as observed in the back and forth movement in the Eco Morf 3 area) were not found in the model unless the residual current was absent.
Our expectation is that placing the residual current under the same angle as the surface waves will help bring the characteristics closer within the observed timescales and magnitudes. With respect to observation [1a] this will bring the system a bit closer to realistic attributes, while still being able to vary and thus study the magnitude of each of the processes.

Chapter 9. Appendices

9.1 Xcorr 2D plane correlation software example

An example of the Xcorr program is shown in figure 9.1. In this example two 280x193 grids are compared with each other. The user defines a box size (in this example 201x114) that contains the area that is compared and a starting position. In our case we made sure the box was in the centre of the data, since we did not know the direction of migration. The software finds the direction and displacement by itself. In the second grid the box is shifted over the entire second grid. The data that fall into the box of the second grid are cross correlated with the data that are in the box of the first grid. In this example the box can move 40 places in each direction. Therefore it calculated 80x80 = 6400 cross correlations of underlying data from the second grid with the area that is in the (stationary) first grid. Note that this method thus correlates a 201x114 grid size area of the first grid with the entire 280x193 grid size area of the second grid. This means that only 42% of the data in the first grid is used in the analysis. (201x114 / (280 * 193) = 0.42).

The correlation is displayed in the top right figure. Red indicated high correlation. The highest correlation is presumed to be on the place the sand waves shifts to. Repetition in high correlation is shown when e.g. the box has shifted one wave length in the direction perpendicular to the sand wave crest (not seen in this example). High correlation along a crest can be seen in data with regular sand waves as a shift oblique to the sand wave crest will compare more or less the same pattern (see example). Specific sand wave features, such a bifurcations in sand wave crests, are physically maintained over longer time and result in the highest correlation on that particular location, thus resulting in correctly identifying the migration of the features.
The area size and the size of the box determine the calculation time and the maximum distance in which migration can be found. The choice for these sizes should be made based on an upper boundary of what possible migration still makes sense considering the time in between recordings and the resolution of the data.
In the example shown, the maximum displacement can be 40 cells in each direction. The lack of periodic repetition in the higher correlation shows that the maximum shift that is assessed in smaller than one sand wave length. The correlation in this shift is however high (0.88) and this highest correlation is found away from the edges of the dataset, making it likely that this is indeed the displacement of the bed forms. A visual inspection shows us that the contour plots resemble each other properly.

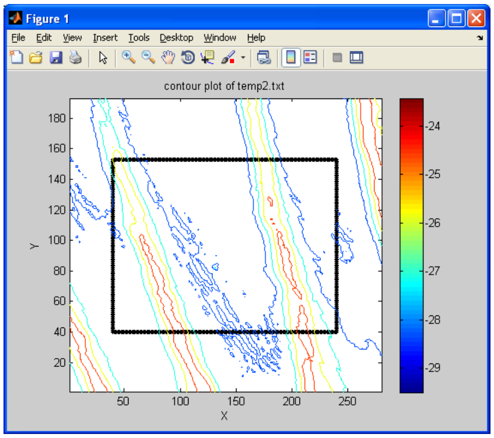

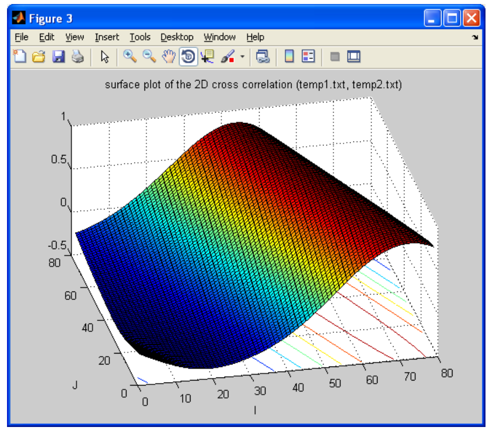

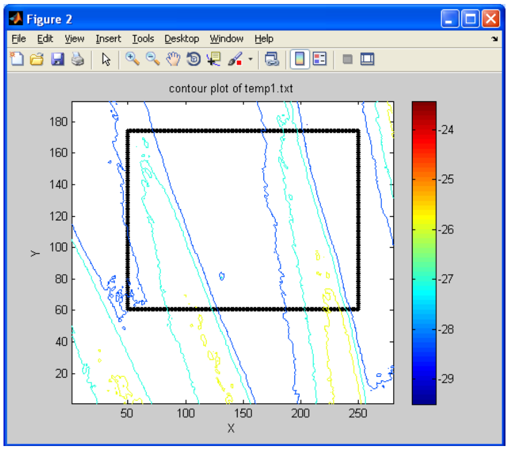

Figure 9.1: Xcorr cross correlation matlab code. (top left, and bottom left): Contour plot of the two bathymetries. X and y indicate the cell number in both horizontal directions. The color bars indicated the water depth in metres below MSL for each recording. The dotted box shows location of maximum correlation of the second boxed area with respect to the first. (Top right): correlation plot. Red indicates high correlation. The I and J coordinate represent the shift of the second box. As the box is shifted 2*40 places in the x (left-right) and y direction (up-down), the size of the cross correlation box is 80x80. The contours in the I,J plain are the 2D contours of the 3D cross correlation plot.

Bibliography

Besio, G. *et al.*, “On the modeling of sand wave migration”, *JOURNAL OF GEOPHYSICAL RESEARCH*, VOL. 109(C04018, doi:10.1029/2002JC001622) 2004

Bowden, K.F., “The Flow of Water through the Straits of Dover, Related to Wind and Differences in Sea Level”, *Royal Society Publishing*, 1956

Buijsman, M.C. and H. Ridderinkhof, “The relation between current and seasonal sand wave variability as observed with ferry-mounted ADCP”, *PECS, Astoria, OR-USA*, 2006

Carruthers, J.N., “J. Cons. int Explor. Mer, 5, 167”, *no title*, 1930

De Leeuw, C.J., “Model predictions of wave-induced sediment transport on the shoreface”, *Msc thesis, University of Twente, The Netherlands*, 2005

Harris, P.T., “Sandwave movement under tidal and wind-driven currents in a shallow marine environment: Adophus Channel, northeastern Australia”, *Continental Shelf Research*, 9(11):981-1002 1989

Houthuys, R. *et al.*, “Storm influence on a tidal sandbank's surface (Middelkerke Bank, southern North Sea)”, *Marine Geology*, p. 23-41, 1994

Hulscher, S.J.M.H., “Tidal-induced large-scale regular bed form patterns in a threedimensional shallow water model”, *Journal of Geophysical Research 101*, p. 727–744, 1996

Knaapen, M.A.F. and S.J.M.H. Hulscher, “Regeneration of sand waves after dredging”, *Coastal Engineering*, 46:277-289 2002

Komarova, N.L. and S.J.M.H. Hulscher, “Linear instability mechanisms for sand wave formation”, *Journal of Fluid Mechanics*, 413:219-246 2000

Lanckneus, J. and G. De Moor, “Evolution of large dunes. Sediment Mobility & Morphodynamics of the Middelkerke Bank”, *University of Gent*, 1993

Mei, C.C., “The applied dynamics of ocean surface waves”, *Advanced Series on Ocean Engineering*, World Scientific Publishing Co Pte Ltd 1999

Morelissen, R. *et al.*, “Mathemetical modelling of sand wave migration and the interaction with pipelines”, *Coastal Engineering*, 48:197-209 2003

Németh, A.A., “Modelling offshore sand waves”, *Ph.D. Thesis*, p. 2803, 2003

Németh, A.A. *et al.*, “Modelling sand wav migration in shallow shelf seas”, *Continental Shelf Research*, 22(2795-2806):18-19 2002

Németh, A.A. *et al.*, “Simulating offshore sand waves”, p. 53, 265-275, 2006

Prandle, D. *et al.*, “Tidal Flow through the Straits of Dover”, *Proudman Oceanographic Laboratory*, 1992

Sterlini, F., “Modelling Sand Wave Variation”, *Ph.D. Thesis*, 2009

Tonnon, P.K. *et al.*, “The morphodynamic modelling of tidal sand waves on the shoreface.”, *Coastal Engineering*, 54:279–296 2007

Van den Berg, J. and D. Van Damme, “Sand wave simulation on large domains”, *River, Coastal and Estuarine Morphodynamics*, REM2005:991-997 2006

Van der Veen, H.H. *et al.*, “Seabed morphodynamics due to offshore wind farms”, *River, Coastal and Estuarine Morphodynamics: RCEM*, 2007

Van Dijk, T.A.G.P. and P.J.P. Egberts, “The variability of sand wave migration in the North Sea”, *Marine and River Dune Dynamics*, 2008

Van Dijk, T.A.P.G. and M. Kleinhans, “Processes controlling the dynamics of compound sand waves in the North Sea, Netherlands”, *JOURNAL OF GEOPHYSICAL RESEARCH*, VOL. 110, F04S10, doi:10.1029/2004JF000173 2005